LANGLEY GRANT
IN-76-CR

FINAL REPORT

NASA GRANT NAG1-972

31901 4
P. 115

MORPHOLOGICAL STABILITY AND KINETICS IN CRYSTAL GROWTH FROM VAPORS

Period of Performance
1/20/89 through 7/19/90

Principal Investigator

FRANZ ROSENBERGER

Center for Microgravity and Materials Research
University of Alabama in Huntsville
Huntsville, Alabama 35899

Table of Contents

1. Introduction

The original proposal submitted to NASA under this title entailed a comprehensive research program for 36 months duration. In view of the fundamental nature of the proposed investigations, NASA elected to support only a revised program for one year and, thus, provide the PI with a better starting position for seeking support for the remainder of the program from other funding agencies, such as the National Science Foundation. Consequently, the activities reported here should be viewed as start-up for ensuing research rather than a rounded program.

The Revised Statement of Work for the one year effort contained five tasks:

Task 1: Design and assembly of a state-of-the-art high resolution storage and processing system for microscopy images.

Task 2: Vapor growth kinetics and morphology study with carbon tetrabromide.

Task 3: Design and assembly of a photothermal deflection setup for vapor concentration measurements during crystal growth.

Task 4 : Bridgman growth of iodine single crystals to be used in task 3.

Task 5: Concentration distribution measurements during iodine crystal growth from the vapor.

2. Work Performed

In the following we will briefly outline the results obtained under the above tasks. Overall, the work performed considerably exceeds the initial projections. In addition, we have obtained a breakthrough in the modelling of vapor growth morphologies resulting under pronounced anisotropy in attachment kinetics, an activity of great importance for the experimental work pursued here, but not planned under the original proposal.

2.1 Microscopy image storage and processing system

A system was to be developed for the state-of-the-art storage, digitization, processing, display and printing of images from an existing Leitz microscope-interferometer vidicon setup.This task has been completed: the system has been designed, assembled and tested. All components have at least 1024 x 1024 lines of resolution. In addition to the Dage MTI Hr-2000 high resolution monitor, that was already available in our Center, the system consists of the following components and software packages:

Compaq Deskpro 286, 640K Ram, 40 Mb Hard Drive, with two 1.2Mb, 1/4" floppy drives

Compaq VGA high resolution monitor and high resolution Logitech mouse

Univision UDC 2600-12M display board

Tecon DVX 1024 frame grabber

Dage MTI precision 81 high resolution TV camera

Pasecon video tube

Dage 207233-1049/30 sync generator

Grundig BK224H high resolution video recorder

Image Pro II Software (IP2UDC)

Customized software for freeze-frame video to capture high resolution 1024 image.

The TECON corporation, from which we purchased the majority of the components, has been invaluable in the design of this system. They have also assembled and tested the system according to our specifications prior to shipment to our Center.

With this system we are able to video-record (in real time) microscopic images of crystal growth morphologies obtained in a growth chamber on the microscope table. These images can be recalled in their analog form for the identification of crucial events. Selected images are then saved in digital form in the host computer. These data are available for image analysis and processing. The overall performance of this system is such that, in combination with the Linnik microscope interferometer, a depth resolution of about 50 Angstroms can be obtained. In addition, features which are hardly discernable on the original low contrast image, can be enhanced for ready recognition.

Features of the ImagePro software enable us to perform several types of image analysis and processing, such as intensity histograms (256 grey scales), line distance and angle measurements, spatial frequency filtration as well as contrast changes through stretching and sliding of intensity distributions.

In view of the high resolution of the system and the high cost of high resolution printers, we have opted for photographic recording of the (as recorded or processed) monitor images. For the cataloging of images we are using HP laserjet prints with 300 dots per inch.

The total cost of the system (without high resolution monitor) is about $31,000, of which $21,000 were provided by this grant. The remainder was provided in about equal parts by NASA

grant NAG8-711 and by the State of Alabama through the Center for Microgravity and Materials Research.

2.2 Growth kinetics and morphology study with Carbon Tetrabromide

We have investigated the surface kinetics and morphology of CBr_4 during its growth from the vapor by high resolution microscopy and interferometry. Temperatures were chosen to include the transition from the low temperature monoclinic to the high temperature cubic phase. Rounding of corners and edges as well as the development of new facets has been observed with increasing temperature at fixed supersaturation on approaching, but distinctly below the transition. The rounding temperatures of crystallographically equivalent corners are equal, and different for corners formed by different index faces. As the supersaturation is increased the rounded corners and edges resharpen. Such a rounding/sharpening behavior can be alternatively induced with successively increasing temperature and supersaturation, respectively. We have interpreted this behavior in terms of surface roughening theory and computer simulations (see also Monte Carlo modelling below).

With respect to the polymorphic phase transition of CBr_4 we have found that the high temperature phase begins to form at grain boundaries and other macroscopic defects at temperatures distinctly below that of the bulk phase transition. The new phase grows partly at the expense of the old one, leading to surface depressions around the new growth locations. The growth rate of the new phase during the transition increases dramatically with temperature and exceeds by far the growth rates observed on the monoclinic and cubic phase alone. These high growth rates have been experimentally determined to result from simultaneous deposition from the vapor and redistribution of solid material via surface diffusion. This rapid growth is associated with morphological instabilities.

This material will be presented at the 1991 March Meeting of the American Physical Society and in a major publication to be submitted to the Journal of Crystal Growth (see Sect.2.6).

2.3 Photothermal deflection vapor growth setup

The vapor concentration measurement cell developed earlier under NASA Grant NAG1-733 was to be improved optically and equiped with a better crystal growth tip. This task has been completed. A new design, consisting of an optical quality fluorimeter cell cemented to Pyrex glass tubes, was developed. In addition we have improved the flow conditions through the upstream iodine reservoir to ensure saturation of the carrier gas at low pressure differentials.

2.4 Bridgman growth of iodine single crystals

A melt growth technique was to be developed for single crystals of iodine to be used as seeds for the concentration field measurements. This task has been completed. Originally we had planned to grow a boule, cleave a seed and mount it to a flat coldfinger. This, however, entails considerable handling of the (soft) crystal and thus has the potential for introducing high structural defect densities and chemical impurity levels. To circumvent these drawbacks we have configured the coldfinger (with a seed selection capillary) as an integral part of the melt growth system. After growth of a single crystal from a small volume of melt in and onto the coldfinger, it is transferred to the vapor concentration probing setup.

2.5 Concentration field measurement during growth

The concentration field about growing iodine crystals was to be determined in three dimensions at various vapor temperatures, supersaturations and inert gas flow velocities. Concurrent photographic records of the crystal morphology were to be made. This task was begun and preliminary, encouraging results were obtained. Under growth conditions, concentration measurements can be made with a concentration resolution of 0.2 torr of iodine in one atmosphere of nitrogen and a spatial resolution of better than one millimeter in three dimensions. At low inert gas flow velocities (twice the diffusion velocity) and high wall temperature gradients, we see clear evidence for variations in the concentration distribution due to convection rolls. These rolls were also confirmed with flow visualization. At higher flow velocities and lower wall temperature gradients the concentration profiles closely resemble solutions to the one-dimensional transport equation with the crystal forming an appropriate sink.

2.6 Monte Carlo Modelling of Growth Morphology with Anisotropic Surface Kinetics

In addition to the tasks outlined in the Revised Statement of Work (see Sect. 1) we have very successfully become involved in the theoretical treatment of the interplay between vapor transport (task 5) and anisotropic growth kinetics (task 2) through Monte Carlo modelling. The model combines nutrient transport, based on a modified diffusion-limited aggregation process, with anisotropic surface kinetics and surface diffusion. Through a systematic variation of the simulation parameters (temperature, bond strength and supersaturation), the whole range of growth morphologies from fully facetted to side-branched dendritic growth is recovered.

The diffusion in the bulk nutrient and the anisotropy in the interface kinetics are seen to be morphologically destabilizing and stabilizing, respectively. It is found that for a given set of simulation parameters and symmetry of the lattice, there is a critical size beyond which a crystal cannot retain its stable, macroscopically facetted growth shape. This critical size scales linearly

with the mean free path in the vapor. Since both thermal and kinetic roughening reduce the kinetic anisotropy, the critical size decreases as either temperature or supersaturation is increased. Surface diffusion is seen to stabilize facetted growth on the shorter scale of the mean surface diffusion length.

In simulations with a uniform drift superimposed on the random walk nutrient transport, crystal faces oriented towards the drift exhibit enhanced morphological stability in comparison to the purely diffusive situation. Rotational drifts with periodic reversal of direction are found to be morphologically stabilizing for all faces of the crystal.

These efforts, which have also been supported by the State of Alabama through the Center for Microgravity and Materials Research, have lead to five publications (some invited) and several (invited) presentations, which are listed in the following section.

3. Presentations and Publications of Results obtained under this Grant

- Rong-Fu Xiao, J. Iwan D. Alexander and Franz Rosenberger, *Morphological Evolution of Crystals Growing in the Presence of a Uniform Drift: A Monte Carlo Simulation*, Phys. Rev. A **39**, 6397-6401 (1989) **attached.**
- Rong-Fu Xiao, J. Iwan D. Alexander and Franz Rosenberger, *Growth Morhology with Anisotropic Surface Kinetics,* J. Crystal Growth **100,** 313-329 (1990) **attached.**

- R.-F. Xiao, J.I.D. Alexander and F. Rosenberger, *Simulation of Surface Morphologies in Crystal Growth from Vapor*, J. Crystal Growth (in print) **attached.**

- R.-F. Xiao and J.I.D. Alexander and F. Rosenberger, *Growth Morphology of Crystal-Vapor Interfaces*, Phys. Rev. (in print) **attached.**

- F. Rosenberger, R. -F. Xiao and J.I.D. Alexander, *Morphological Stability of Interfaces with Strong Anisotropy in Growth Kinetics*, in **Lectures on Crystal Growth**, ed. by H. Komatsu, (in print) **attached.**

- F. Rosenberger, *Morphological Stability of Interfaces with Anisotropic Growth Kinetics*, invited seminar, Forschungszentrum Jülich, Germany, Division for Solid State Physics, September 18, 1990.

- F. Rosenberger, *Morphological Stability of Interfaces with Anisotropic Growth Kinetics*, invited seminar, University of Osnabrück, Osnabrück, Germany, Department of Physics, September 21, 1990.
- Rong-fu Xiao, *Simulation of 2D Crystal Surfaces Growing from the Vapor,* Bull. Am Phys. Soc. **35**, 308 (1990).
- Rong-fu Xiao, *Simulation of 3D Crystal Surfaces during Growth,* Bull. Am Phys. Soc. **35**, 684 (1990).
- Rong-fu Xiao, *Simulation of Surfaces Morphologies in Crystal Growth from the Vapor,* invited paper at Eighth American Conference on Crystal Growth, Vail, CO, July 1990.
- Rong-fu Xiao, *Simulation of Crystal Growth Morphologies,* poster at the Gordon Research Conference on Fractals, Plymouth State College, NN, August 1990.

Morphological evolution of crystals growing in the presence of a uniform drift: A Monte Carlo simulation

Rong-Fu Xiao, J. Iwan D. Alexander, and Franz Rosenberger
Center for Microgravity and Materials Research, University of Alabama in Huntsville, Huntsville, Alabama 35899
(Received 20 December 1988)

A Monte Carlo model is used to simulate the morphological evolution of crystals growing under the influence of a uniform drift in the nutrient phase. The model combines nutrient transport (via a biased random walk) with anisotropic surface attachment kinetics and surface diffusion. It is found that the crystal morphology closely depends upon the imposed drift, growth temperature (or bond strength), and supersaturation. Facets facing the drift direction exhibit enhanced morphological stability as compared with the no-drift situation.

The growth morphology and morphological stability of a crystal is an extremely complex problem, involving, in general, an interaction between the effects of nutrient transport and surface kinetics.[1-7] Recently, the collective effect of nutrient diffusion, based on a modified diffusion-limited-aggregation[8,9] (DLA) model, and surface kinetics on morphological evolution has been investigated by a Monte Carlo (MC) simulation.[10,11] A variety of conditions, ranging from kinetic- to diffusion-controlled growth were examined, and successive transitions from compact faceted (surface kinetics limited case) to open dendritic morphologies (nutrient diffusion limited case) were obtained.

However, in reality, a condition of pure diffusion in the nutrient is rarely found. The trajectories of particles in the system are inevitably perturbed in some preferential direction in the presence of some external field. Such bulk flow may, for instance, be due to buoyancy or surface tension gradients. There is considerable evidence[12,13] for the influence of a fluid flow on growth morphology. In particular, the morphological stability of the interface may be altered by the presence of a fluid flow.

Although progress has been made, the theoretical study of the influence of a flow on the morphological stability has been limited by the difficulties associated with the highly nonlinear governing equations coupled with moving boundary conditions. So far, only a few cases of crystal growth from the melt with simple boundary conditions have been solved.[6,14-21] For instance, Delves[6] has shown that a forced flow parallel to the interface helps stablize the interface against a Mullins-Sekerka instability.[3] In addition, it has been shown that coupling between morphological and convective (thermosolutal) modes of instability can occur in the presence of nonparallel flow.[18-21]

For more complex situations, a microscopic approach, e.g., the tracking of individual growth units by MC simulation[22] appears more promising. In 1983, Meakin,[23] for the first time, investigated the drift effect on pattern formation by applying a MC method. In his approach, a drift was superimposed on the random walk of a DLA model. A crossover was found from the DLA fractal on short length scales to a uniform structure on larger length scales as a drift was applied. However, lacking realistic elements of attachment kinetics, Meakin's model cannot give insight for a crystal growth system. In addition, his computational algorithm cannot readily be shown to correspond to a known formulation of macroscopic transport.

In this communication we use a MC model, based on our previous work,[10,11] to study the morphological change of a crystal that grows in response to a chemical potential gradient. We examine the effect of a nutrient drift, and also account for nutrient diffusion and surface kinetics. We use a uniform drift velocity superimposed on a random walk, in contrast to real systems where the bulk velocity depends on the local (viscous) flow configuration. Consequently, the result of our formulation, though providing physical insight, can be considered at best qualitative.

We consider a crystal growth system which consists of two basic processes, e.g., nutrient transport and surface kinetics. We assume that the motion and aggregation of growth units take place on a 2D square grid, and restrict our study to a physical system with the following properties. (1) The nutrient phase is gaseous. (2) The nutrient phase consists of two components; component A, the growth species, is highly diluted in an inert gas B, which randomizes the motion of A. (3) The system is isothermal, i.e., heat conduction is rapid compared to mass diffusion, thus the latent heat released during crystallization can be ignored. (4) The chemical potential is taken to be a linear function of the growth species concentration. This results in a Fickian transport equation and thus, a random walk may be used to describe diffusion in the nutrient phase.[10,11,24] (5) There is a macroscopic as well as microscopic drift acting on the individual growth unit in the nutrient.

Under purely diffusive conditions the nutrient transport can be described by a simple random walk with an isotropic jumping probability.[10,11] However, if there exists an externally imposed drift, the individual jumps of the random walk will be biased. This is schematically depicted in Fig. 1, where the dashed circle is the source from which growth units are released. The vector **a** is an unbiased random walk with equal jumping probability to

pied nearest neighbors of site i, and ϕ is the interaction energy of a molecule with a nearest neighbor.

If the particle does not stick onto the site i, it will jump to one of its unoccupied neighbor sites. The jump probability from site i to a neighboring unoccupied site j (on the surface or in the nutrient) is[10]

$$P_{i\to j}=\frac{\beta^{(n_i-n_j)}}{\sum_{j=1}^{c'}\beta^{(n_i-n_j)}}, \tag{8}$$

where c' is the number of unoccupied nearest neighbors of site i. Clearly, larger n_i results in a higher probability that a molecule will jump to site j on the interface.

The combination of Eqs. (7) and (8) contains the essential physics of the surface kinetics for a crystal growing from a vapor. It should be realized that the crystal anisotropy has already been taken into account implicitly in Eqs. (7) and (8), since n is an anisotropic factor.

Based on the preceding formulation, we carried out the simulation by following the previous procedure including the multiple registration technique to reduce the noise.[10,11] In this simulation, a larger size of growth pattern (10^4 particles) with stable morphology was obtained by increasing the mean free path to 10 lattice units. The source boundary was chosen at $r_s=r_{\max}+50$, where $r_{\max}$ is the radius of gyration of the growing cluster. The simulation was implemented on a CRAY X-MP/24 and typical cpu times used for each simulation were around 2000–5000 sec. To show the time sequence of the growth patterns, we divided the total growth particles into four groups of 2500 each and indicated the morphology associated with each group by a line.

For comparison, results without a superimposed drift ("diffusion only") are presented in Fig. 2. This figure shows the effect of bond strength or growth temperature, i.e., ϕ/kT on the growth pattern for a constant supersaturation ($\gamma=2.0$ or $\Delta\mu/kT=0.69$). One can see that with increasing temperature (or decreasing bond strength) the crystal morphology changes. At low temperature, despite an appreciable supersaturation, the crystal is still able to retain a compact faceted form [Fig. 2(a)]. At higher β's a branched pattern with four main protrusions results [Figs. 2(b) and 2(c)]. Finally, at the highest value of β, it becomes dendritic. The formation of these different growth morphologies has been explained by consideration of the collective effect of nutrient diffusion and surface kinetics.[10,11]

Figure 3 shows the effect of a drift on growth morphologies at a fixed drift magnitude ($\delta=50$ lattice units), and otherwise the same conditions as Fig. 2. One can see that as a drift is applied, asymmetric growth patterns appear. The sites facing the drift grow much faster than those opposite to the drift. Although the drift affects all cases, the response of growth morphology increases with decreasing bond strength or increasing temperature [Figs. 3(a)–3(d)]. In addition to modifying the growth rate, the drift is also seen to stabilize the faceted growth in comparison to the "no-drift" case. Whereas, e.g., the no-drift patterns of Figs. 2(b) and 2(c) show deep depressions in the middle of the facets, the corresponding drift cases [Figs. 3(b) and 3(c)] exhibit much smoother facet surfaces on which the flow impinges. The flow causes a stronger increase of the mass flux to the center of a facet, as compared to the edges. This can even lead to the overgrowth of a depression [see the "hole" in Fig. 3(d)] that remains open in the corresponding no-drift case [Fig. 2(d)].

Figure 4 shows the effect of changes in drift direction [Figs. 4(a) and 4(b), $\delta=50$] and magnitude [Fig. 4(c), $\delta=25$; Fig. 4(d), $\delta=16$]. One can see that the growth pattern depends closely on the characteristics of the drift. As the drift direction changes the crystal changes its shape accordingly. The morphologically stabilizing effect of the drift on the faceted growth morphology is again well illustrated in the sequence a,c,d of Fig. 4. Note that, here, the supersaturation and the bond strength and/or temperature correspond to those of the no-drift case of

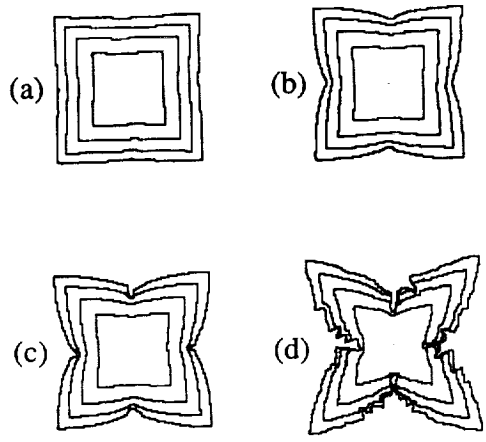

FIG. 2. No-drift case ($V=0$). Effect of bond strength and temperature on growth pattern with $\Delta\mu/kT=0.69$. (a) $\phi/kT=4.60$, (b) $\phi/kT=3.90$, (c) $\phi/kT=2.30$, (d) $\phi/kT=0.69$.

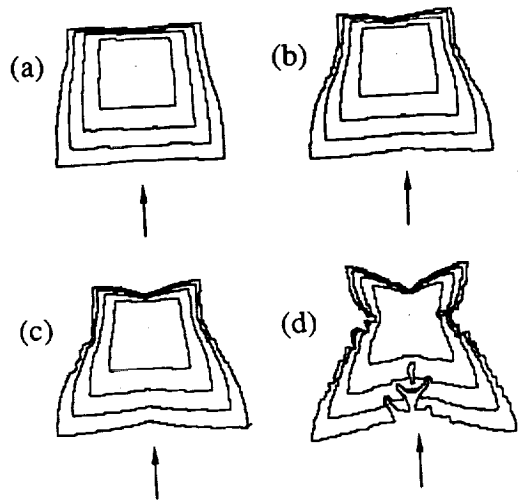

FIG. 3. Effect of drift on growth morphology with $\delta=50$, and conditions otherwise the same as Fig. 2. The arrow indicates the direction of the drift.

Current Physics, edited by K. Binder (Springer-Verlag, Berlin, 1986).
[23]P. Meakin, Phys. Rev. B **28**, 5221 (1983).
[24]C. C. Lin and L. A. Segel, *Mathematics Applied to Deterministic Problems in the Natural Sciences* (Macmillan, New York, 1974).
[25]D. W. Heermann, *Computer Simulation Methods in Theoretical Physics* (Springer-Verlag, Berlin, 1986).

Journal of Crystal Growth 100 (1990) 313–329
North-Holland

GROWTH MORPHOLOGY WITH ANISOTROPIC SURFACE KINETICS

Rong-Fu XIAO, J. Iwan D. ALEXANDER and Franz ROSENBERGER

Center for Microgravity and Materials Research, University of Alabama in Huntsville, Huntsville, Alabama 35899, USA

Received 15 August 1989; manuscript received in final form 20 November 1989

A Monte Carlo model is used to simulate the morphological evolution of crystals growing from an incongruent vapor phase. The model combines nutrient transport, based on a modified diffusion-limited aggregation process, with anisotropic surface kinetics and surface diffusion. Through a systematic variation of the simulation parameters (temperature, bond strength and supersaturation), the whole range of growth morphologies from fully facetted to side-branched dendritic growth is recovered. The diffusion in the bulk nutrient and the anisotropy in the interface kinetics are seen to be morphologically destabilizing and stabilizing, respectively. It is found that for a given set of simulation parameters and symmetry of the lattice, there is a critical size beyond which a crystal cannot retain its stable, macroscopically facetted growth shape. This critical size scales linearly with the mean free path in the vapor. Since both thermal and kinetic roughening reduce the kinetic anisotropy, the critical size decreases as either temperature of supersaturation is increased. Surface diffusion is seen to stabilize facetted growth on the shorter scale of the mean surface diffusion length. In simulations with a uniform drift superimposed on the random walk nutrient transport, crystal faces oriented towards the drift exhibit enhanced morphological stability in comparison to the purely diffusive situation. Rotational drifts with periodic reversal of direction are found to be morphologically stabilizing for all faces of the crystal.

1. Introduction

The characterization of the conditions under which a growing crystal is capable of preserving its shape, i.e. is morphologically stable, is both scientifically challenging and technologically important. Morphological stability is necessary for the growth of homogeneous single crystals that are needed for numerous device applications. To adequately describe the growth morphology and morphological stability of a crystal, however, is an extremely complex problem, involving, in general, an intraction between nutrient transport and interface kinetics [1–3].

Two basic approaches to the morphological description of crystal growth have been adopted. The first is the macroscopic approach which involves the solution of a continuum transport equation coupled with moving boundary conditions [4]. The second is the simulation of microscopic processes by tracking the individual growth units [5].

The continuum approach has lead to significant insight into the morphological evolution of essentially isotropically responding, i.e. atomically rough and, hence, macroscopically non-facetted [3] interfaces, such as prevail in many melt growth systems. Morphological stability conditions are well established for a variety of simple geometries [4,6–9], including systems with weakly nonlinear [9–12] and highly nonlinear isotropic response [13–15]. In addition, the coupling between morphological and hydrodynamic instabilities has been examined [16–22]. Continuum models have also been developed for the morphological stability of non-facetted interfaces with anisotropies in surface tension and growth kinetics (e.g., refs. [23–26]). One of the most important results of these treatments is the insight that anisotropies can stabilize otherwise unstable closed growth forms up to a certain critical size. For atomically smooth interfaces, however, that prevail in most vapor and solution growth systems, and on which strongly anisotropic (facetted) growth occurs via atomic layer spreading, the necessary conditions for morphological stability are only partly understood. Several workers have proposed an isotropic continuum formulation for morphological stability in

0022-0248/90/$03.50

interface via diffusion and convection in the nutrient. The actual transport kinetics will, in general, be determined by the interaction of growth units (or their precursors) and other species that form the nutrient. Second, when a growth unit reaches the interface, typically it does not become immediately incorporated into the growing crystal. It will adsorb and diffuse on the interface in an attempt to find an energetically favorable "final" attachment site, or it will even return to the nutrient before it finds such a site. The latter happens, for instance, when the growth unit is misoriented and cannot form stable bonds with the crystal. Alternatively, the growth unit may impinge onto a site with too few neighbors to prevent it from being dislodged by thermal vibrations before it becomes adsorbed. Or, a growth unit may even become dislodged after having arrived at an energetically favorable ("final") site. The probability of all these steps is determined by the local configuration (number of bond-forming neighbors) of the interface sites that the unit happens to visit during its (short) residence time. At molecular length scales, the crystal symmetry will inevitably be reflected in the anisotropy of the attachment kinetics. This underlying symmetry will also be manifested at macroscopic length scales unless the atomic roughness of the crystal interface is high enough to allow diffusion in the nutrient phase to control the evolution of the growing shape. Though a complete model of such complex scenarios is not practical at this point, we will formulate a Monte Carlo model which retains the essential physics of both nutrient transport and interface kinetics, including surface diffusion.

2.1. Mass transport in the nutrient

We assume that the gaseous nutrient phase consists of two components: a growth species A, highly diluted in an inert gas B, such that the B concentration is essentially uniform and A–A interactions can be ignored. Component B randomizes the motion of A, though both components may be subjected to a uniform drift. In addition we assume that heat dissipation is rapid compared to mass diffusion; thus the latent heat released during crystallization can be ignored and isothermal conditions prevail. The chemical potential is taken to be a linear function of the growth species concentration. This results in a Fickian transport equation and, thus, a random walk may be used to describe diffusion in the nutrient phase [47–60].

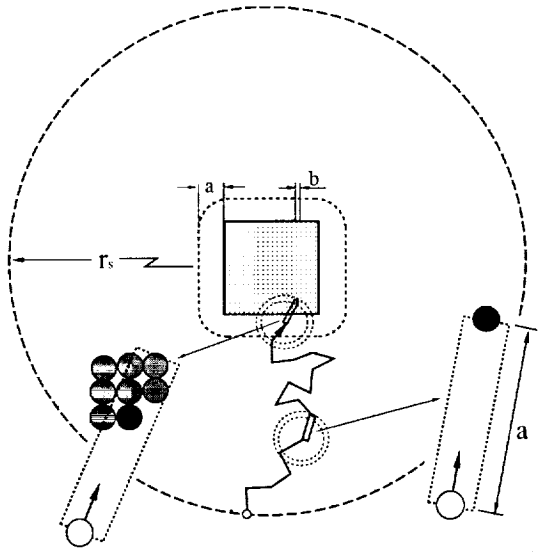

Fig. 1. Schematics of 2D random walk at a large mean free path. Dashed circle: source. Dotted central region: growing crystal. Concentric dotted circles: contain possible landing points (with automatic rounding, i.e. $|a| \pm 0.5b$). The two small collision zones have been enlarged to illustrate the different collision behavior in the bulk and the interface.

These assumptions are consistent with the following Monte Carlo model. The motion of a given growth unit in the nutrient is described by a simple random walk on a discrete lattice of spacing b, with equal jump length, $|a|$, in all directions, unless a (uniform) drift is superimposed on the random walk. This is schematically depicted in fig. 1. The large dashed circle of radius r_s is the source from which walkers are released. After release, a random walker jumps with equal probability to all grid points within the annular region given by $|a| \pm 0.5b$ (with automatic rounding to a nearest grid point if the chosen jumping site is not exactly on a grid). The jump length $|a|$ represents a physical distance on the order of the mean free path of molecules. The grid spacing b, on the other hand, represents a lattice unit of the crystal which is denoted by the dotted central area. In a real crystal–vapor system the mean free path of a

a random walk process, the chemical potential of the source does not appear explicitly in our model. The $\Delta\mu$ in eq. (4), therefore, is governed by the difference between the bulk transport-dependent vapor concentration at the interface and the equilibrium concentration at the same temperature. For a more detailed discussion, see ref. [58].

After impingement on the surface, growth units can either remain at the original site, return to the vapor (evaporate) or continue to wander to an unoccupied neighboring site (surface diffusion). The rates of both the evaporation and surface diffusion processes are sensitive to the local configuration of the site from which a unit is to be dislodged. Hence, following Gilmer and Bennema [46], we cast the evaporation rate into the site-dependent form

$$K_i^- = \nu \exp(-E_i/kT), \tag{5}$$

where ν is a lattice vibration factor and E_i is the product of the pair interaction (bond) energy ϕ of a unit with a nearest neighbor and the number of occupied neighbor sites of site i, n_i.

The probability that a growth unit sticks onto a specific site is then $P_i = K^+/(K^+ + K_i^-)$. In order to relate K_{eq} and ν we assume local equilibrium, and equate impingement and evaporation rates at equilibrium and obtain [58]

$$P_i = \gamma\beta^{n_0-n_i}/(1+\gamma\beta^{n_0-n_i}), \tag{6}$$

where n_0, the number of nearest neighbors in a kink site, is 2 for a square lattice and 3 for a triangular lattice, and $\gamma = \exp(\Delta\mu/kT)$ and $\beta = \exp(-\phi/kT)$.

If the growth unit does not stick onto the site i, it will jump to one of its unoccupied neighbor sites. The jump probability from site i to a neighboring unoccupied site j (on the surface or in the nutrient) is assumed to be [58–60]

$$P_{i\to j} = \beta^{n_i-n_j}\left(\sum_j^{c'}\beta^{n_i-n_j}\right)^{-1}, \tag{7}$$

where c' is the number of unoccupied nearest neighbor sites of site i. Clearly, a larger n_j results in a higher probability that a molecule will jump to site j on the interface.

The combination of eqs. (6) and (7) contains the essential physics of the surface kinetics for a crystal growing from a vapor. It should be realized that the crystal anisotropy has already been taken into account implicitly in eqs. (6) and (7), since both n_i and n_j are anisotropic.

The strength of surface diffusion (described by eq. (7)) is characterized by the diffusion time or diffusion length on the surface. An exact calculation of surface diffusion length is difficult. In our model we estimate the average surface diffusion length $\bar{\lambda}_s$ according to

$$\bar{\lambda}_s \sim \sqrt{\bar{n}_t}\, b, \tag{8}$$

where $\bar{n}_t$ is the average (residence) "time" (actually the number of MC steps) for a random walker to diffuse on the interface (see section 2.3).

2.3. Simulation procedure

A summary of the steps involved in the MC simulation is presented in fig. 2. Initially, a small

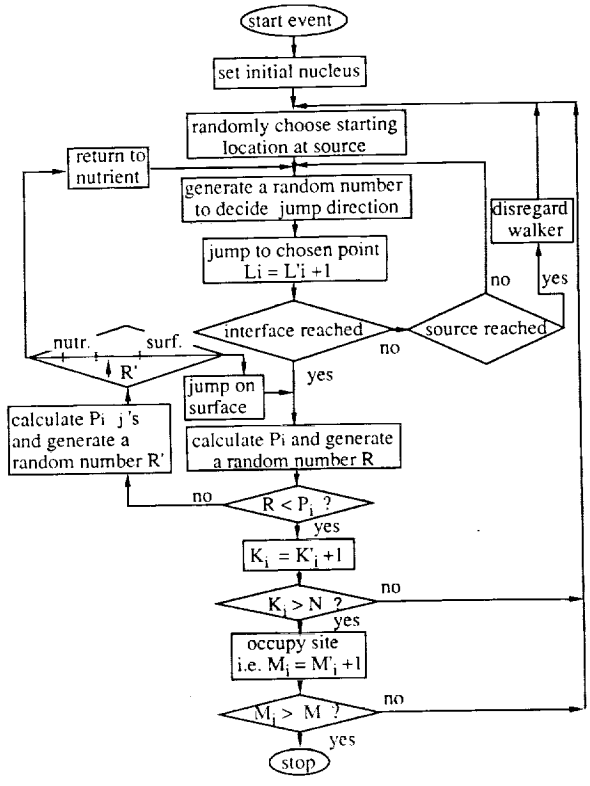

Fig. 2. Flowchart of simulation steps.

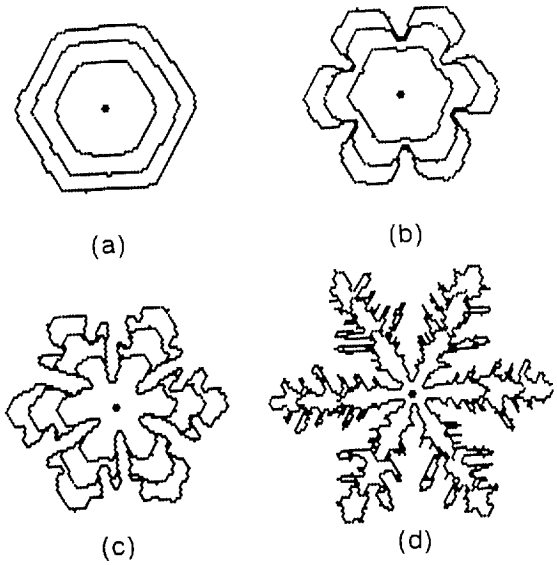

Fig. 3. Effect of bond strength and temperature on growth patterns of a crystal (triangular lattice) at a fixed (normalized) supersaturation ($\Delta\mu/kT = 0.69$): (a) $\phi/kT = 3.91$; (b) $\phi/kT = 2.30$; (c) $\phi/kT = 0.69$; (d) $\phi/kT = 0.36$.

under these or even lower ϕ/kT conditions, leads to the evolution of "macroscopic" depressions (figs. 3b and 4b). On further increase of the temperature, this transition occurs at even smaller

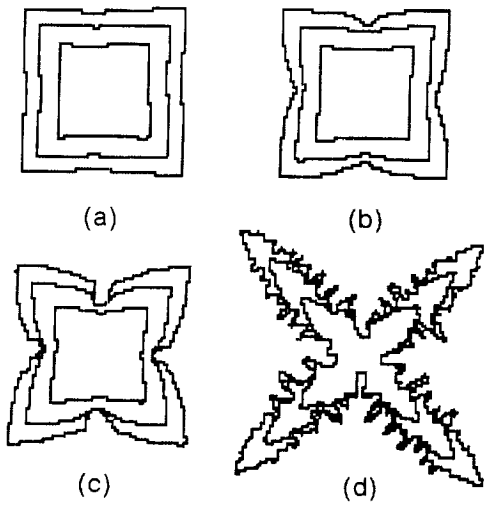

Fig. 4. Effect of bond strength and temperature on growth patterns of a crystal (square lattice) at a fixed supersaturation ($\Delta\mu/kT = 0.69$): (a) $\phi/kT = 4.60$; (b) $\phi/kT = 3.91$; (c) $\phi/kT = 2.30$; (d) $\phi/kT = 0.69$.

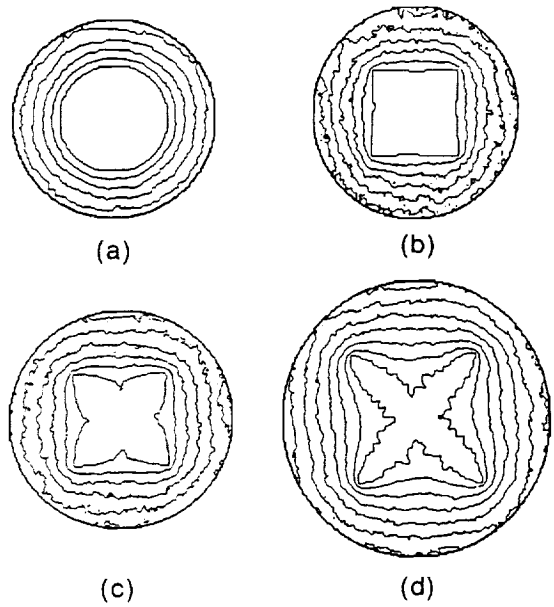

Fig. 5. Nutrient concentration distribution (iso-concentration lines) around growing crystals. (a) circular crystal; (b), (c), (d) growth conditions corresponding to the terminal sizes of figs. 4a, 4c and 4d, respectively.

sizes and dendritic growth occurs (figs. 3c and 4d) which subsequently exhibits extensive side-branching (fig. 3d).

The concentration distributions about a circular growth pattern and the terminal crystal shapes of figs. 4a, 4c and 4d are presented in figs. 5 and 6. The iso-concentration lines in fig. 5 are spaced by constant concentration increments. Hence, more closely spaced lines indicate steeper concentration gradients. This is further illustrated in fig. 6 by the corresponding concentration profiles along the radius vector through a corner and center of a facet, respectively. As expected, for the round pattern (test case for our algorithm) the concentration distribution is circular, with the concentration gradient decreasing with increasing distance from the growing interfaces. For the "crystals", however, one sees that both concentration and concentration gradient are significantly higher in the corner regions than at the center of the facet (or what used to be a facet at smaller crystal size), in agreement with numerous experimental findings [62–64]. These differences increase as the growing crystal takes on a more

shape preservation for facetted crystals [36] and its adaption by Kuroda et al. [37]; see also ref. [42]. The stabilizing effect of the increase in step density as the face center depression increases was expressed in terms of kinetic coefficients ($\beta(p)$ in ref. [36] and $B(p)$ in ref [42]), where p is the local slope of the vicinal surface segment (local tangent to the depression). The growth rate normal to the macroscopic face (fictitious singular surface), V_n, is then related to the nonuniform, normalized supersaturation, σ, in the form

$$V_n = \beta(p)\sigma. \tag{9}$$

It is interesting to re-examine the microscopic morphologies assumed to be relevant in these works, which postulate equivalence of the kinetic effect of microscopic depressions (fig. 7a) and protrusions or hillocks (fig. 7b). Depressions are thought to prevail at higher supersaturations, where 2D nucleation in the corner regions is likely to form the dominant source for growth steps. Protrusions, on the other hand, are thought to prevail at lower supersaturation, where defects, such as screw dislocations (that supposedly form more readily in the center region) supply the growth steps. These features have been well characterized for stable growth from a more uniform nutrient field. It is not clear, however, how an initially shallow hillock, in order to become kinetically more active, can increase in central height when, as growth proceeds, the nutrient supply progressively dwindles in the center region. Our simulations, as well as numerous growth-morphology investigations of actual crystals [67], do not lead to protrusions at face centers.

The above simulations also show, for the first time, the destabilizing effect of an increase in the growth temperature. This is revealed explicitly in figs. 3 and 4 which present a transition from facetted to non-facetted shapes as the temperature is increased. At low temperatures the morphology is controlled by surface kinetics while at higher temperatures volume diffusion is seen to be shape-determining. Fig. 8, which has been computed from (6), shows that at a fixed supersaturation an increase in temperature results in reduction in the anisotropy of the sticking probability.

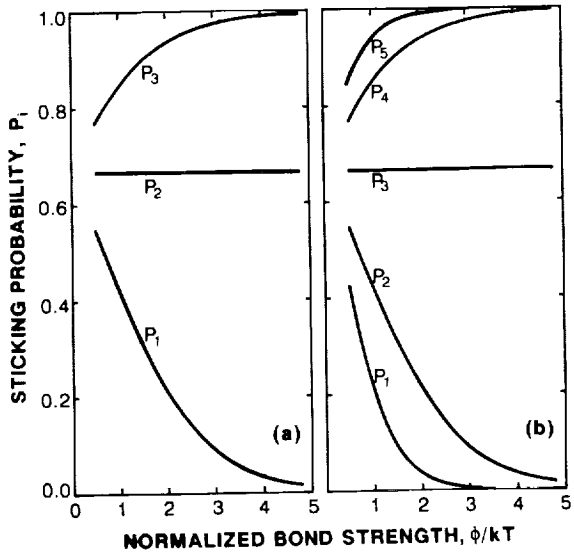

Fig. 8. Dependence of sticking probability P_i (eq. (6)) on normalized bond strength/temperature and number of occupied neighbor sites at fixed $\Delta\mu/kT = 0.69$ for (a) square lattice ($n_0 = 2$) and (b) triangular lattice ($n_0 = 3$).

The temperature (or bond strength) independence of P_2 in fig. 8a (P_3 in fig. 8b) results from the assumption of local equilibrium underlying (6), where the vapor–crystal equilibrium is with respect to the kink site. This reduction in the differences between the P_i's causes the growth pattern to become more isotropic, more dependent on the concentration distribution, and thus more volume diffusion controlled. Note that this transition is, loosely speaking, analogous to thermal roughening [68,69]. The latter, however, is associated with equilibrium conditions and is formally based on minimization of the crystal's total surface free energy under the constraint that the volume be constant. This constraint is not applicable to the dynamic growth conditions considered here.

Furthermore, a comparison of figs. 3 and 4 shows that a decrease in symmetry of the lattice decreases the ability of the crystal to retain a facetted growth form. For instance, facetting prevails at $\phi/kT = 3.91$ on the triangular lattice (fig. 3a). Yet, the perimeter of the square crystal shows macroscopic depressions at the same normalized temperature and supersaturation (fig. 4b); a fully facetted form only appears at significantly higher values of ϕ/kT (fig. 4a). This difference in stabil-

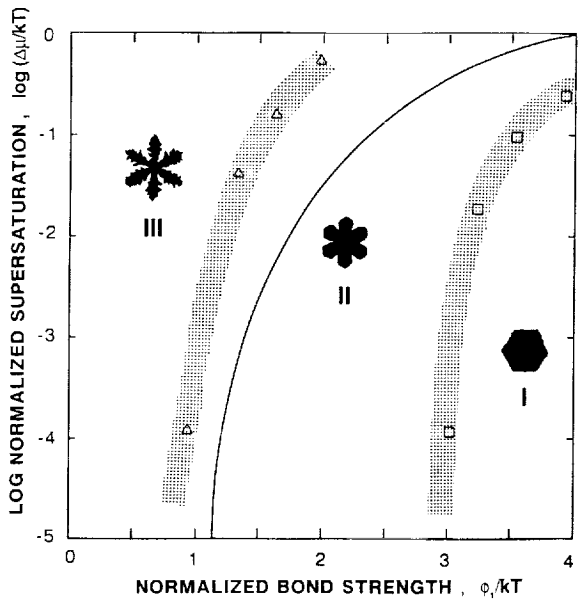

Fig. 10. Crystal-growth morphology as a collective effect of supersaturation and bond strength (or temperature) for triangular lattice, $M = 3 \times 10^3$ and mean free path of one lattice unit. In region I crystals acquire compact-facetted forms; in region II compact branched with six-fold symmetry; in region III dendritic with multiple sidebranches. Symbols: Monte Carlo results judged as "boundary cases". Solid line: Temkin's boundary between facetted and non-facetted growth for a simple cubic lattice [78]. For more details, see ref. [58].

son for this is that nutrient diffusion was not taken into account by Temkin. As pointed out above, nutrient diffusion is always a destabilizing factor and reduces the range over which facets can exist.

It should be emphasized, that the specific locations of the boundaries between the different morphology regions presented in fig. 10 are only representative for growth patterns containing $M = 3 \times 10^3$ particles. For smaller sizes the transitions will occur at higher supersaturations, and/or lower bond strength (higher temperature). For larger sizes, on the other hand, loss of morphological stability would set in at combinations of lower supersaturations and higher bond strengths than in fig. 10. Hence, there is some scaling between the overall size of a growth pattern and its critical size. Thus, even under most favorable growth conditions, any system will eventually reach a size where the destabilizing bulk diffusion will cause loss of morphological stability, i.e. under bulk diffusion-controlled conditions, any macroscopically facetted growth form will become unstable beyond a certain M.

3.2. Changes in growth morphology with increase of mean free path

The above results are all based on the assumption of a mean free path equal to one lattice unit, i.e. $|a| = b$. In this section we increase the mean free path and simulate growth patterns containing 10^4 particles. To show the time sequence of growth shapes, the total particles are divided into four groups of 2500 each.

Fig. 11 shows the effect on morphology of bond strength or temperature at a constant normalized supersaturation,a nd a mean free path of 11 lattice units with otherwise the same growth conditions (i.e., β and γ) as fig. 4. It can be seen that the critical size of a facetted crystal has increased dramatically. In fig. 4b the crystal has lost its macroscopically facetted form at a size less than 3000 particles, but in fig. 11b the facetted crystal remains up to around 6000 particles. In fig. 4d the crystal has become a dendrite with many

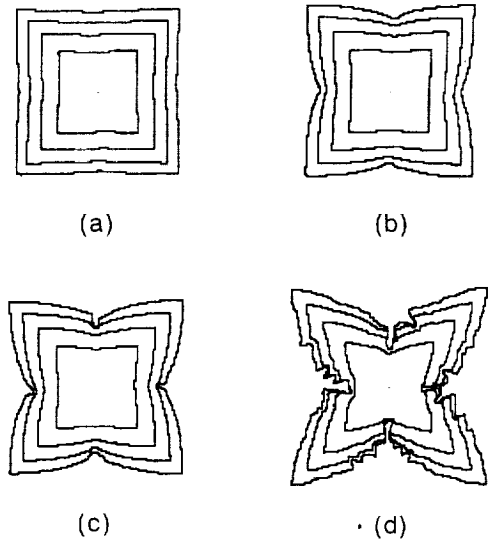

Fig. 11. Effect of bond strength and temperature on growth patterns at a large mean free path ($|a| = 10$ lattice units). The growth conditions (γ and β) are the same as in figs. 4a–4d. Contours correspond to addition of 2500 particles each.

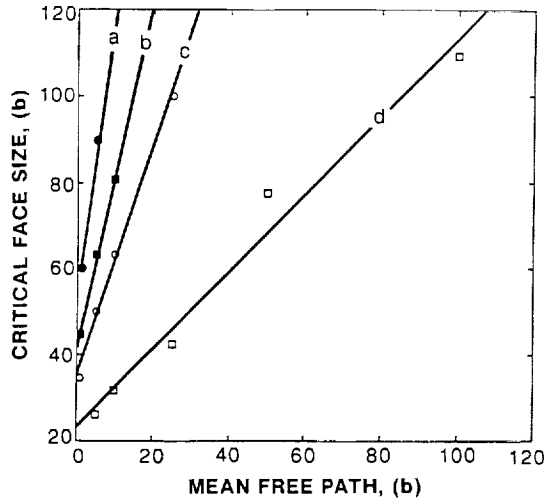

Fig. 14. Dependence of critical size on mean free path at $\delta\mu/kT = 0.69$: (a) $\phi/kT = 4.60$; (b) $\phi/kT = 3.91$; (c) $\phi/kT = 2.30$; (d) $\phi/kT = 0.69$.

simulation of critical crystal sizes determined experimentally [31–35]. However, fig. 14 encourages us to scale linearly to these sizes. For instance, Nanev and Iwanov [33] have found a critical size of 120 μm for a Zn crystal ($b = 1.38$ Å) growing from the vapor phase consisting of a Zn partial pressure of approximately 0.1 Torr in 150 Torr of hydrogen. The mean free path of H_2 at this pressure and temperature is about 1.2 μm. In order to obtain a critical size for a relatively large ϕ/kT system, such as the above Zn experiment, we have run fig. 11a beyond the terminal size shown. "Macroscopic" loss of face stability was observed at a size of $130b$, i.e. with $b = 1.38$ Å at 1.8×10^{-2} μm. Remember, that fig. 11a is based on $|a| = 10b$, i.e. a mean free path of 1.4×10^{-3} μm was assumed. Hence, it is not surprising that the critical size of a face obtained from our MC simulation is three to four orders of magnitude smaller than the experimental finding.

3.3. Surface diffusion and facet stability

The effect of surface diffusion on growth morphology has been studied both theoretically [1,46,58,81] and experimentally [81]. As might be expected, it was found that surface diffusion can smooth the growth morphology on the scale of the average surface diffusion length $\bar{\lambda}_s$. This can be explained as follows: Wherever the surface has a high curvature the nutrient concentration and its gradient are also high. This is shown in figs. 5 and 6. When surface diffusion is permitted, the concentration gradient along the interface is the driving force for surface flow from a protuberance to a depression. This makes the protuberance less stable, while stabilizing the original facet.

The contribution of surface diffusion to face and facet stability is a function of the surface diffusion length λ_s. For the stability of the entire face, surface diffusion is important only when λ_s is comparable to the face length. Hence, the effect of surface diffusion is particularly evident in our simulations when $|a| = b$. However, as a crystal grows larger, the size of faces eventually exceeds $\bar{\lambda}_s$. Surface diffusion will then continue to play a stabilizing role only for terraces or facets with sizes less than or on the order of the average surface diffusion length. We have found that even for the dendritic growth, surface diffusion still has a noticeable effect on primary branch thickening [58].

The above trends can clearly be deduced from figs. 3, 4, 11 and 12. For a quantitative evaluation, however, one must take into account that the surface diffusion length decreases with increasing temperature (decreasing bond strength) and supersaturation, while being insensitive to changes in the mean free path. Consequently, as can be seen from figs. 11 and 12, the terrace size decreases in response to an increase in temperature, but remains approximately constant as the mean free path is increased. The connection between the temperature dependence of $\bar{\lambda}_s$ and face stability is further illustrated in fig. 15, which shows a dramatic decrease in the average surface diffusion length on loss of the planar growth morphology. Therefore, particularly at low temperature (high bond strength) and low supersaturation, surface diffusion must be taken into account in stability considerations.

3.4. Changes in crystal morphology in the presence of a drift

With an externally imposed drift, i.e., $\boldsymbol{d} \neq 0$ in (1), the individual jumps of a random walker will

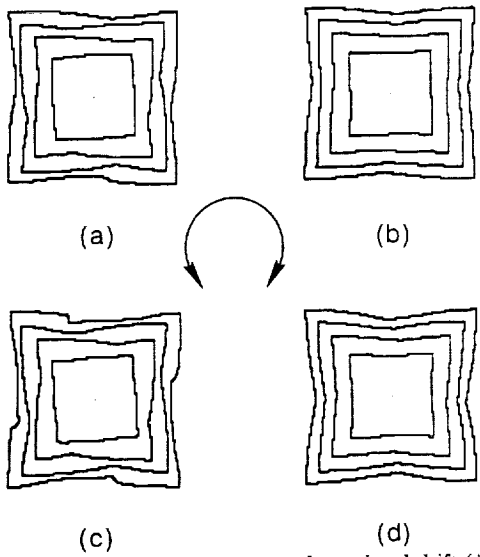

Fig. 18. Effect of periodically reversed rotational drift ($|\boldsymbol{d}| = 2b$) on growth morphology: (a), (b) $\Delta\mu/kT = 0.69$, $\phi/kT = 3.91$; (c), (d) $\Delta\mu/kT = 0.69$, $\phi/kT = 2.30$. The rotational direction is reversed after every 2500 particles in 9a) and (c), and 500 particles in (b) and (d).

ing morphological changes under an influence of a uniform nutrient rotation of $|\boldsymbol{d}| = 2b$ at $|a| = 10b$; the growth conditions are otherwise the same as in figs. 11 and 16. The center of rotation coincides with that of the crystal. One an see that the rotational drift causes the depressions to be shifted away from the center of the facet against the direction of the drift. This is, for instance, observed in solution growth where uni-directional rotation causes depressions and "veiling" (occlusion of mother liquor) behind the leading edges of the crystal; see, e.g., fig. 39 in ref. [83], and ref. [84].

Fig. 18 shows the morphologies obtained after the rotational drift has been periodically reversed. The growth conditions (γ and β) of figs. 18a and 18b correspond to fig. 11b and figs. 18c and 18d to fig. 11c. The rotation direction is changed after the addition of each set of 2500 growth units in figs. 18a and 18c, while in figs. 18b and 18d the direction is reversed after every 500 particles. One can see immediately that crystals with stable morphology result when to rotation is reversed more frequently (figs. 18b and 18d), whereas in the corresponding no-drift cases (figs. 11b and 11c) deeply depressed morphologies result. This is in agreement with the common observation of the benefits of frequent rotation reversal in solution growth [83,85,86].

Acknowledgements

The authors are grateful for the support provided by the Microgravity Science and Applications Division of the National Aeronautics and Space Administration under Grant No. NAG1-972. This research has also been supported by the State of Alabama through the Center for Microgravity and Materials Research at the University of Alabama in Huntsville, and the Alabama Supercomputer Network. Stimulating discussions with Professors I. Sunagawa and A.A. Chernov have been essential for the development of this paper.

Note added in proof

Most recently, Saito and Ueta have obtained similar growth shape evolutions from a Monte Carlo model with anisotropic attachment and evaporation kinetics features, using a DLA technique which launches many walkers at once [87].

References

[1] R.L. Parker, in: Solid State Physics Vol. 25, Eds. H. Ehrenreich, F. Seitz and D. Turnbull (Academic Press, New York, 1970) p. 151, and references therein.
[2] A.A. Chernov, in: Modern Crystallography III: Crystal Growth, Springer Series in Solid State Sciences, Vol. 36, Eds. M. Cardona, P. Fulde and H.-J. Queisser (Springer, Berlin, 1984), and references therein.
[3] F. Rosenberger, in: Interfacial Aspects of Phase Transformations, Ed. B. Mutaftschiev (Reidel, Dordrecht, 1982) p. 315, and references therein.
[4] J.S. Langer, Rev. Mod. Phys. 52 (1980) 1.
[5] H. Müller-Krumbhaar, in: Monte Carlo Methods in Statistical Physics, Ed. K. Binder (Springer, Berlin, 1984) p. 295, and references therein.
[6] W.W. Mullins and R.F. Sekerka, J. Appl. Phys. 35 (1964) 444.
[7] R.F. Sekerka, in: Encyclopedia of Materials Science and Engineering, Ed. R.W. Cahn (Pergamon, New York, 1986) p. 3486.

[70] G.H. Gilmer and K.A. Jackson, in: Current Topics in Materials Science, Vol. 2, Ed. E. Kaldis (North-Holland, Amsterdam, 1977) p. 79.
[71] V.O. Esin and L.P. Tarabaev, Phys. Status Solidi (a) 90 (1985) 425.
[72] M. Elwenspoek and J.P. van der Eerden, J. Phys. A (Math. Gen.) 20 (1987) 669.
[73] C.E. Miller, J. Crystal Growth 42 (1977) 357.
[74] H.J. Human, J.P. van der Eerden, L.A.M.J. Jetten and J.G.M. Odekerken, J. Crystal Growth 51 (1981) 589.
[75] S.D. Peteves and G.J. Abbaschian, J. Crystal Growth 79 (1986) 775.
[76] F. Gallet, S. Balibar and E. Rolley, J. Physique, 48 (1987) 369.
[77] A. Dougherty and J.P. Gollub, Phys. Rev. 38A (1988) 3043.
[78] D.E. Temkin, in: Crystallization Processes, Eds. N.N. Sirota, F.K. Gorskii and V.M. Varikash (Consultants Bureau, New York, 1969) p. 15.
[79] J.W. Cahn, Acta Met. 8 (1960) 554.
[80] P.W. Atkins, Physical Chemistry (Freeman, New York, 1982).
[81] P. von Blanckenhagen, in: Structure and Dynamics of Surfaces II, Phenomena, Models, and Methods, Eds. W. Schommers and P. von Blanckenhagen (Springer, Berlin, 1987) p. 73, and references therein.
[82] J.C. Brice, Crystal Growth Processes (Wiley, London, 1986).
[83] T.G. Petrov, E.B. Treivus and A.P. Kasatkin, Growing Crystals from Solution (Consultants Bureau, New York, 1969).
[84] R. Janssen-Van Rosmalen and P. Bennema, J. Crystal Growth 42 (1977) 224.
[85] G.M. Loiacono, W.N. Osborne and M. Delfino, J. Crystal Growth 41 (1977) 45.
[86] D. Elwell and H.J. Scheel, Crystal Growth from High Temperature Solutions (Academic Press, London, 1975) ch. 6.
[87] Y. Saito and T. Ueta, Phys. Rev. A40 (1989) 3408.

J. Crystal Growth
(in print)

SIMULATION OF SURFACE MORPHOLOGIES IN CRYSTAL GROWTH FROM VAPOR

Rong-Fu XIAO, J. Iwan D. ALEXANDER and Franz ROSENBERGER

Center for Microgravity and Materials Research

University of Alabama in Huntsville

Huntsville, Alabama 35899

ABSTRACT

The morphological evolution of crystals that grow from an incongruent vapor by the surface nucleation and screw dislocation mechanisms is simulated with a Monte Carlo model. The model combines volume transport, based on a modified diffusion-limited aggregation process, with anisotropic surface kinetics without a SOS restriction. It is found that for a given set of simulation parameters and symmetry of the lattice, there is a critical size beyond which a crystal cannot retain its stable, macroscopically faceted shape. This critical size scales linearly with the mean free path in the vapor. While surface diffusion is seen to stabilize the growth morphology on the scale of the surface diffusion length, volume diffusion is always destabilizing. Surface roughness increases with increase in growth temperature and supersaturation, which reduce the anisotropy in kinetics through thermal and kinetic roughening, respectively. For the screw dislocation mechanism, that can dominate at low temperature and supersaturation, we find that the combined effect of bulk and surface diffusion reduces the terrace width of a growth spiral in its center region. At elevated temperature and supersaturation normal growth can dominate in corner and edge regions of a crystal, while the spiral growth mode prevails in the center of a facet.

1. Introduction

Monte Carlo simulation has become a popular method in the study of a crystal growth process since Chernov and Lewis [1]. Typical studies include equilibrium and growth morphologies of crystals [2,3], surface roughening transitions [4,5] and growth rate dependence on supersaturation and temperature [6,7]. For reviews, see [8,9]. These studies were primarily focused on interfacial kinetics and have occasionally included surface diffusion [7]. A solid-on-solid (SOS) restriction [10] (no overhangs) was often assumed. The influence of volume diffusion, i.e., the transport of growth units to the interface, has received less attention until recently [11-15]. In the event that surface diffusion and interfacial kinetics govern the growth morphology, these simplifications are not severe limitation. However, in reality, volume transport often plays a decisive role in limiting morphological stability [16-18].

We have developed a MC model to study the morphological evolution of growing crystals by considering both volume transport and surface kinetics [11-13]. For the volume transport, we modified the diffusion-limited aggregation (DLA) model of Witten and Sander [19]. Our results showed that the diffusion in the volume and the anisotropy in the interface kinetics are morphologically destabilizing and stabilizing, respectively. Through a systematic variation of the simulation parameters (temperature, bond strength and supersaturation), the whole range of growth morphologies from fully faceted to side-branched dendritic growth was recovered. For a given set of simulation parameters and symmetry of the lattice, there is a critical size beyond which a crystal cannot retain its stable, macroscopiclly faceted shape. In this short paper we will pay special attention to the scaling of the critical size as a function of the mean free path in the nutrient. We will investigate the dependence of surface roughness on temperature or bond strength and supersaturation. For crystals with a screw dislocation, we will demonstrate how surface and volume diffusion influence the terrace width of the spiral. In addition, we will study the competition between the two-dimensional nucleation (2DN) and screw dislocation growth mechanisms as a function of temperature and supersaturation.

2. Model

We assume the vapor to be isothermal and composed of an inert gas B in which a growth species A is highly diluted. In addition, A-A interactions, convection and latent heat released during crystallization are ignored. A random walk is used to describe the diffusive motion of growth units from the source [11]. The complex process following the arrival of growth units at the interface is described by impingement, evaporation and surface diffusion rate equations [11-13]. The impingement rate K^+ is assumed to be only dependent on supersaturation (chemical potential difference $\Delta\mu$) between the nearby nutrient and the crystal surface, i.e. $K^+ = K_{eq}\exp(\Delta\mu / kT)$ with K_{eq} being the temperature dependent equilibrium value of K^+. The evaporation rate, on the other hand, is assumed to be sensitive to the local configuration of the site from which a unit is to be dislodged. Hence, following Gilmer and Bennema [7], we cast the evaporation rate K_i^- into the site-dependent form $K_i^- = \nu \exp(-E_i/kT)$, where ν is a lattice vibration factor and, in a nearest neighbor approximation, E_i is simply the product of the pair interaction (bond) energy ϕ of a unit with a nearest neighbor and n_i the number of solid neighbors of site i. For the surface diffusion, we assume that the diffusion rate depends on the occupation condition of both the site i that the particle occupies and the potential jump site j. Hence, we express the jump rate as $K_{i\rightarrow j} = \nu_s \exp(-\Delta E_{ij} /kT)$. Here ν_s is a surface vibration factor, and the activation energy $\Delta E_{ij} = \phi(n_i - n_j) + \delta_i$, where δ_i is the activation energy when $n_j \geq n_i$. With the above rate equations, the corresponding probabilities for attachment, evaporation and surface diffusion can be easily obtained [11,13]. The details of the simulation procedures have been reported elsewhere [11-13].

3. Results

The results in fig.1 were simulated on a two dimensional (2D) square lattice. Initially, a nucleus with a certain size was put at the center of a circular periphery from which random walkers (growth units A) were released. The radius of this source periphery was chosen such that the growth shape was not biased [11]. In this figure, both the temperature and

supersaturation were kept constant ($\phi/kT = 0.69$, $\Delta\mu/kT = 0.69$), and only the mean free path $|a|$ was changed respectively from 1b, 5b, 10b, 25b, 50b to 100b, with b being the lattice constant. Also, a multiple registration scheme [11] was employed to reduce microscopic noise. As can be seen from this figure, a crystal can have very different morphologies when the mean free path is changed. At $|a| = b$ (fig.1a) the crystal shows dendritic patterns with many side-branches from the earlier stages of growth. As $|a|$ increases less side-branches are observed (fig.1b,c), and when the mean free path increases to 25b (fig.1d) the side branches disappear, leaving only depressions at the face center. At a mean free path of 100b, the crystal becomes a square without any depression. Similar changes of the crystal morphology in three dimension (3D) are shown in fig.2. In this case, instead of a circular source, a spherical source was used [13]. Due to computational time limitations, only two different mean free paths were considered, i.e., $|a| = 1b$ (fig.2a,b) and $|a| = 5b$ (fig.2c,d). According to gas kinetic theory, the mean free path is inversely proportional to the total vapor pressure. An increase in the mean free path implies a decrease in the vapor pressure or diffusion barrier. Figs.1 and 2 demonstrate the importance of the total vapor pressure for the morphological stability in vapor crystal growth.

Our results also emphasize a fundamental difference between crystal growth and DLA [19]. As can be seen from the evolution of the growth boundaries in fig.1, the scale invariance exhibited by DLA does not generally hold in crystal growth. The instantaneous fractal dimension decreases as the size of the growing crystal increases. For a given set of growth conditions, a small crystal may be stable, but as it grows bigger and exceeds a certain critical size, the original crystal shape can lose its stability, and develop a different morphology. This observation is compatible with the earlier theories [9,18] of faceted growth shape stability.

To quantitatively characterize the critical size of a growing crystal at the onset of instability, the change of total surface area has been used as a criterion [13]. For a stable morphology the total surface area (or total surface length in 2D) should linearly scale as a 2/3 power (or 1/2 in 2D) with the number of growth particles. When a crystal loses its stability, the

surface area increase significantly [13]. Fig.3 shows the dependence of the critical size on the mean free path at fixed $\Delta\mu/kT$ for both two and three dimensions. As can be seen, the critical size increases with decreasing temperature. At fixed temperature and supersaturation, the critical size scales linearly with the mean free path in the parameter range considered. The corresponding 3D simulations yield larger slopes, which is due to the fact that, on the average, there are more solid neighbors associated with interfacial particles in three dimensions and, thus, the (stabilizing) anisotropy in interface kinetics is more pronounced. Although computational time limitations do not allow for the direct simulation of the critical size at the mean free path used in morphological stability experiments [20], fig.3 encourages us to scale linearly to these conditions. Order-of-magnitude agreement is obtained between experimental and modelling results [12] for the critical size.

Fig.4 shows the effect of surface diffusion on the morphology of a growing crystal. This figure was simulated with a special geometry consisting of two parallel infinite planes, of which one is the growing crystal and the other is the source. Periodic boundary conditions were used laterally in both x and y directions. In this case, instead of using the multiple registration scheme to reduce the noise [11], already attached particles were randomly allowed to evaporate at a rate controlled by a Boltzmann factor [13]. Volume diffusion is not considered in this figure, i.e. we have taken the ballistic impingement approach used, e.g., by [7]. For comparison, a result without surface diffusion is plotted in fig.4a, while fig.4b includes surface diffusion under otherwise the same growth conditions ($\phi/kT=1.6$, $\Delta\mu/kT=0.69$). It can be seen that with surface diffusion the crystal surface is much smoother (fig.4b). This is because surface diffusion can provide an additional way for interfacial particles to relax to some energetically more favorable (low energy) sites and, hence, smooth the surface morphology. As we have discussed before [12], such a smoothing contribution is effective only within a length scale comparable to the surface diffusion length.

Fig.5 illustrates the effect of temperature or bond strength and supersaturation on the morphology of a growing crystal with the inclusion of both volume and surface diffusion. The

geometry and simulation procedures are the same as in fig.4. In fig.5a,b the supersaturation is fixed ($\Delta\mu/kT = 0.69$) and ϕ/kT decreases from 3.9 to 1.6, while in fig.5c,d the temperature and bond strength are fixed ($\phi/kT = 3.9$) and supersaturation increases from 5.0 to 7.0. It can be seen that surface roughness can be influenced by either temperature or supersaturation. In addition to temperature effects (thermal roughening), surface roughening due to increases in supersaturation is evident through the reduction in anisotropy [12]. This leads to growth shapes increasingly influenced by volume diffusion.

Morphological changes under the influence of a single screw dislocation are illustrated by fig.6. Besides the dislocation, the geometry and boundary conditions are the same as for figs.4 and 5. In order to emphasize the effect of the dislocation the attachment of isolated particles (with one solid bond) was suppressed. This approximation is only valid at very low temperatures where the attachment probability for the isolated particle is negligible [13]. For this figure the supersaturation is fixed ($\Delta\mu/kT=0.69$), and the values of ϕ/kT is 3.0, 3.9 and 5.3, respectively in figs.6a-c. One sees that with a decrease in temperature not only do the growth steps become smoother, but also the terrace width increases. Perhaps the feature deviating most from the classical theory [21] and results of earlier MC simulations [22,23], is this variation of terrace width on the crystal. For this simulation where $|a|=b$, narrower widths are found near the center of the spiral. We explain this as a combination effect of volume and surface diffusion. A protrusion is formed at the center of the dislocation during growth. Such a protrusion is better supplied by volume diffusion. In addition, due to small overlaps of surface diffusion fields farther from the dislocation center, the terrace widths will increase as the step velocity increases. Note that in reality, such terrace widening can not be expected to occur in vapor systems where $|a| >> b$.

For fig. 7, a pair of screw dislocations with opposite sign was assumed. As in fig.6, the supersaturation was kept at a constant value ($\Delta\mu/kT=0.69$) and ϕ/kT was taken to be 3.0, 3.9 and 4.6, respectively in fig.7a-c. To reveal the competition between 2DN growth at the corners and the dislocation spiral growth at the center, the attachment of isolated particles is

allowed. Fig.7a shows that at a higher temperature, in spite of a dislocation at the face center, growth occurs essentially from the corners of a crystal through 2DN. As the temperature decreases or bond strength increases, the dislocation growth at the face center becomes increasingly important. At $\phi/kT = 4.6$ (fig.7c) growth occurs only through attachment onto steps that originate at the central dislocation pair. Although a supersaturation difference exists between corner and face center [12], it is still not high enough to overcome the nucleation barrier for 2DN. Instead, the higher supersaturation makes the closed dislocation loop unstable, leading to protrusions at corners. Such star shaped dislocation growth has been observed experimentally; see, for example, fig.60 in [24].

Acknowledgements

The authors are grateful for the support provided by the Microgravity Science and Applications Division of the National Aeronautics and Space Administration under Grant No. NAG1-972. This research has also been supported by the State of Alabama through the Center for Microgravity and Materials Research at the University of Alabama in Huntsville, and the Alabama Supercomputer Network.

References

[1] A. A. Chernov and J. Lewis, J. Phys. Chem. Sol. 28 (1967) 2185.

[2] V. O. Esin, L. P. Tarabaev, V. N. Porozkov and I. A. Vdovina, J. Crystal Growth 66 (1984) 459 and references therein.

[3] G. H. Gilmer and P. Bennema, J. Crystal Growth 13/14 (1972) 148.

[4] H. J. Leamy, G. H. Gilmer and K. A. Jackson, in Surface Physics of Materials I, Ed. J. B. Blakely (Academic Press, New York, 1975), p. 121, and references therein.

[5] R. H. Swendsen, Phys. Rev. B15 (1977) 5421.

[6] V. O. Esin and L. P. Tarabaev, Phys. Stat. Sol. (a) 90 (1985) 425.

[7] G. H. Gilmer and P. Bennema, J. Appl. Phys. 43 (1972) 1347.

[8] H. Müller-Krumbhaar, in Monte Carlo Methods in Statistical Physics, Ed. K. Binder (Springer-Verlag, Berlin, 1979), p.261, and references therein.

[9] P. Bennema and J. P. Van der Eerden, in Morphology of Crystals, part A, Ed. I. Sunagawa (Terra, Tokyo, 1987), p. 1; A. A. Chernov and T. Nishinaga, ibid, p. 207.

[10] D. E. Temkin, in Crystallization Processes (Consultant Bureau, New York, 1966), p.15.

[11] R. F. Xiao, J. I. D. Alexander and F. Rosenberger, Phys. Rev. A 38 (1988) 2447.

[12] R. F. Xiao, J. I. D. Alexander and F. Rosenberger, J. Crystal Growth 100 (1990) 313.

[13] R. F. Xiao, J. I. D. Alexander and F. Rosenberger, to be submitted to J. Crystal Growth.

[14] Y. Saito and T. Ueta, Phys. Rev. A40 (1989) 3408.

[15] S. Krukowski and F. Rosenberger, in preparation.

[16] W. W. Mullins and R. F. Sekerka, J. Appl. Phys. 35 (1964) 444.

[17] J. S. Langer, Rev. Mod. Phys. 52 (1980) 1.

[18] A. A. Chernov, J. Crystal Growth 24/25 (1974) 11.

[19] T. A. Witten and L. M. Sander, Phys. Rev. B27 (1983) 5686.

[20] M. Staynova and C. Nanev, Crystal Res. Technol. 28 (1989) 951, and references therein.

[21] W. K. Burton, N. Cabrera and F. C. Frank, Trans. Roy. Soc. A243 (1951) 299.

[22] G. H. Gilmer, J. Crystal Growth 35 (1976) 15.

[23] R.H. Swendsen, P. J. Kortman, D.P. Landau and Müller-Krumbhaar, J. Crystal Growth 35 (1976) 73.

[24] I. Sunagawa and P. Bennema, in Preparation and Properties of Solid State Materials, Vol.7, Ed. W. R. Wilcox (Marcel Dekker, 1982), p.1, and references therein.

Figure captions

Figure 1 Effect of mean free path on growth morphology for 2D square crystal at $\Delta\mu/kT=0.69$ and $\phi/kT=0.69$: (a) $|a| = 1$; (b) $|a| = 5$; (c) $|a|= 10$; (d) $|a| = 25$; (e) $|a| = 50$; (f) $|a| =100$ lattice units. Contours correspond to addition of 1000 particles each in (a) and 2500 particles in (b)-(f).

Figure 2 Effect of mean free path on growth morphology for 3D cubic crystal at $\Delta\mu/kT = 0.69$ and $\phi/kT=2.3$: (a)-(b) $|a| = 1$; (c)-(d) $|a| = 5$ lattice units.

Figure 3 Dependence of critical size on mean free path at $\Delta\mu/kT = 0.69$ in both 2D and 3D for various ϕ/kT.

Figure 4 Effect of surface diffusion on surface morphologies at $\Delta\mu/kT = 0.69$ and $\phi/kT=1.6$: (a) without surface diffusion; (b) with surface diffusion. No volume diffusion is considered in both cases.

Figure 5 Effect of temperature or bond strength and supersaturation on surface morphologies at $|a| = 1$b: (a) $\Delta\mu/kT = 0.69$ and $\phi/kT=3.9$; (b) $\Delta\mu/kT = 0.69$ and $\phi/kT=1.6$; (c)$\Delta\mu/kT = 5.0$ and $\phi/kT=3.9$; (d) $\Delta\mu/kT = 7.0$ and $\phi/kT=3.9$.

Figure 6 Growth morphologies in the presence of a single screw dislocation with the consideration of both surface and volume diffusions at $\Delta\mu/kT=0.69$: (a) $\phi/kT= 3.0$; (b) $\phi/kT=3.9$; (c) $\phi/kT=5.3$. The growth of isolated particles is suppressed.

Figure 7 Growth morphologies in the presence of a pair of screw dislocations with opposite sign at $\Delta\mu/kT=0.69$. Both surface and volume diffusion are included. (a) $\phi/kT= 3.0$; (b) $\phi/kT=3.9$; (c) $\phi/kT=4.6$.

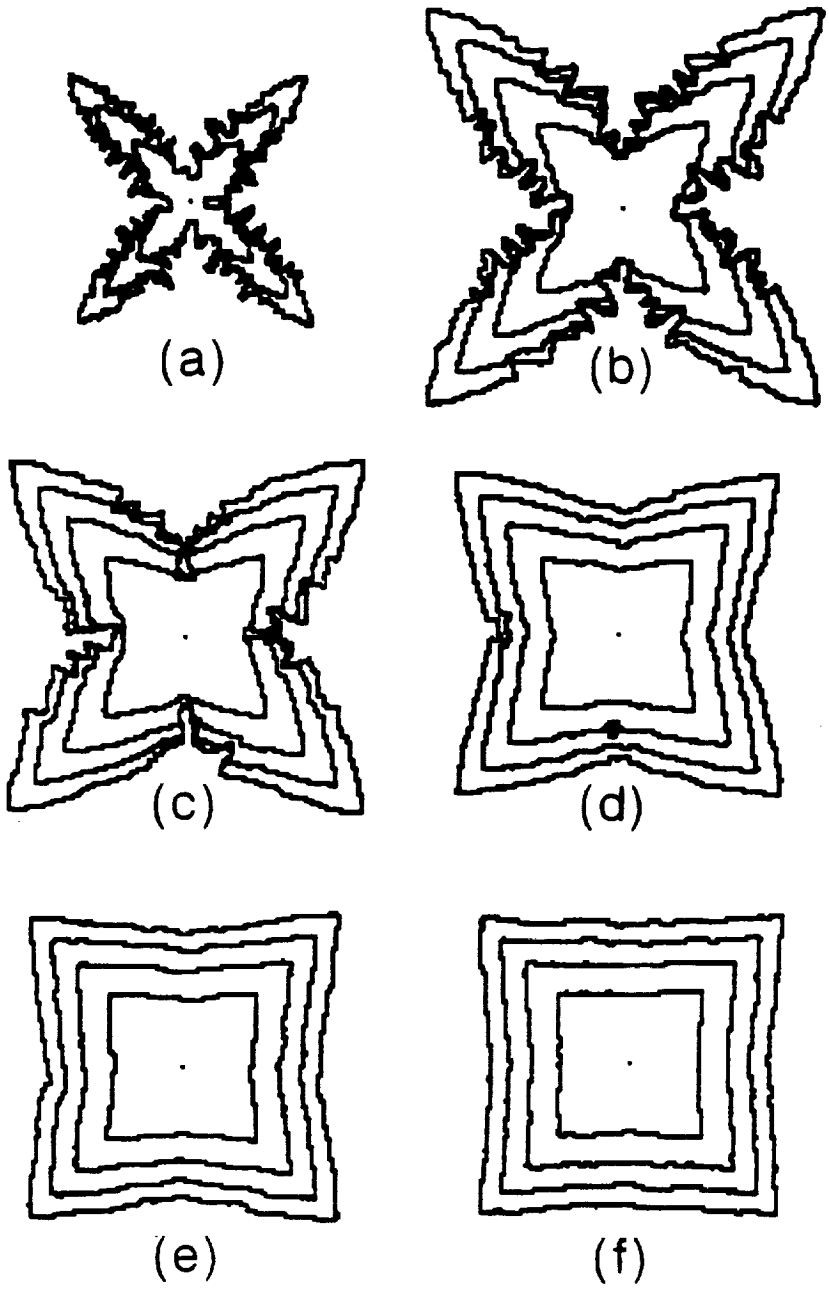

FIG. 1

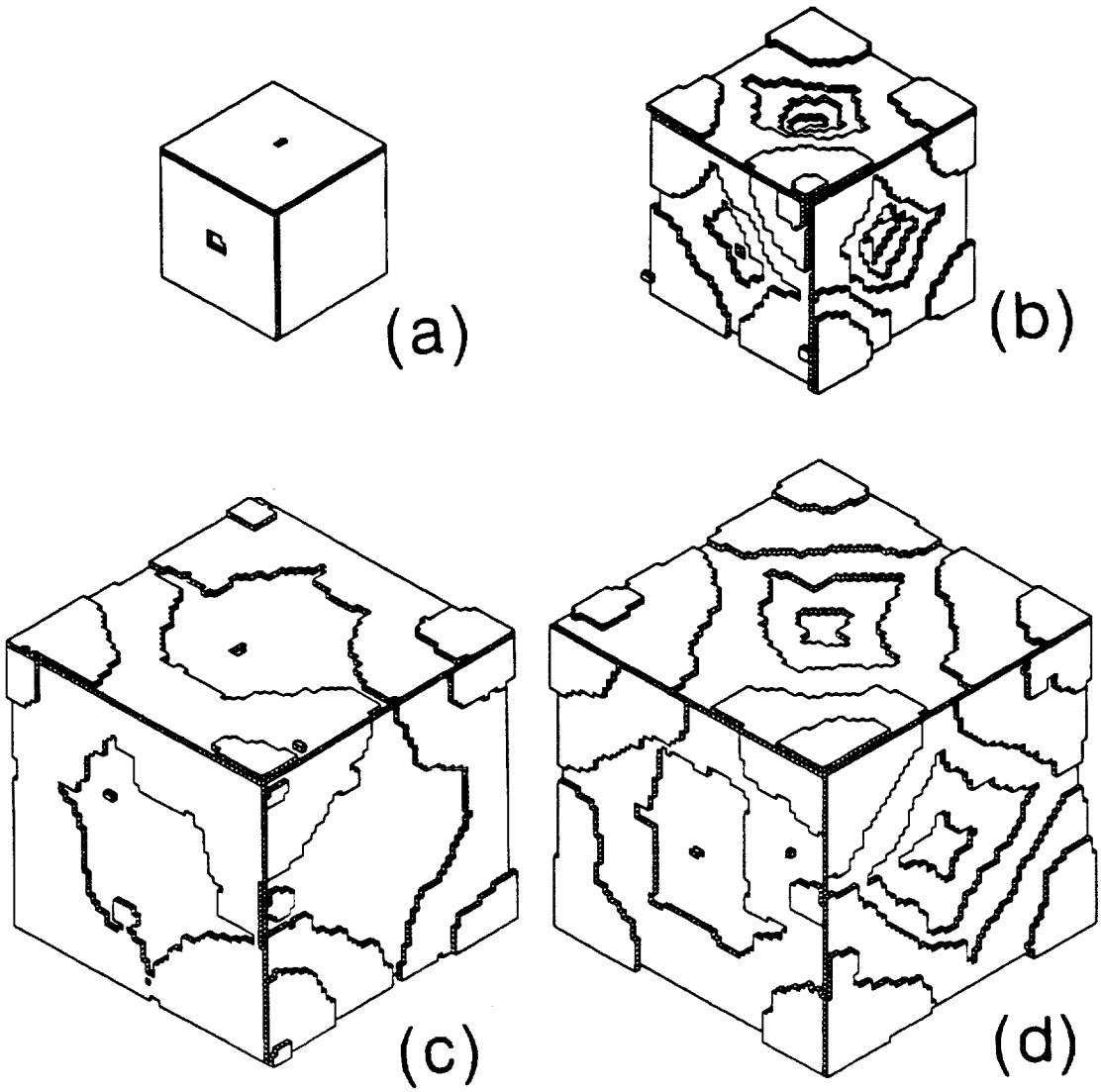

FIG.2

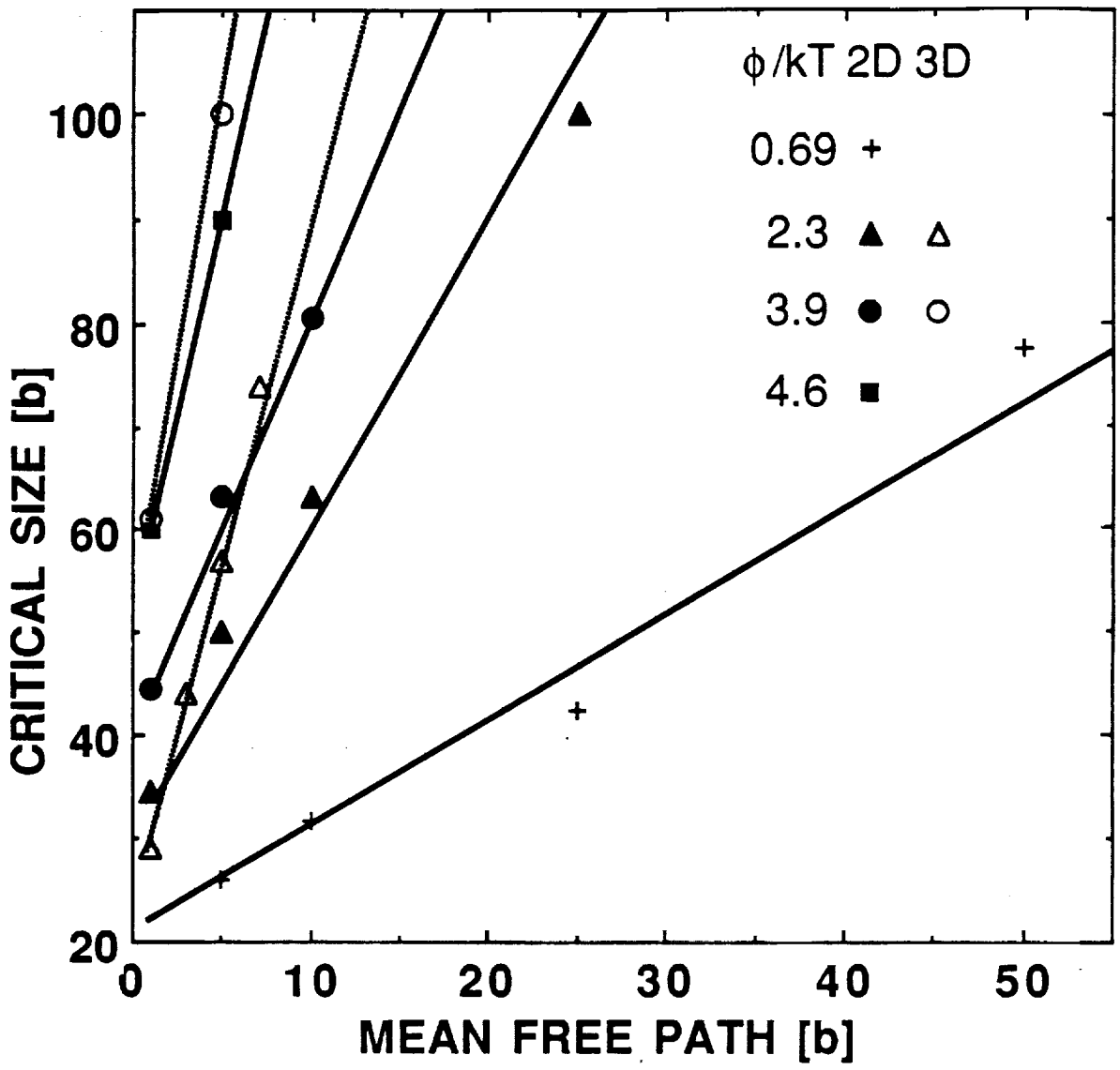
ϕ/kT 2D 3D
0.69 +
2.3 ▲ △
3.9 ● ○
4.6 ■
CRITICAL SIZE [b]
MEAN FREE PATH [b]
20
40
60
80
100
0
10
20
30
40
50

FIG. 3

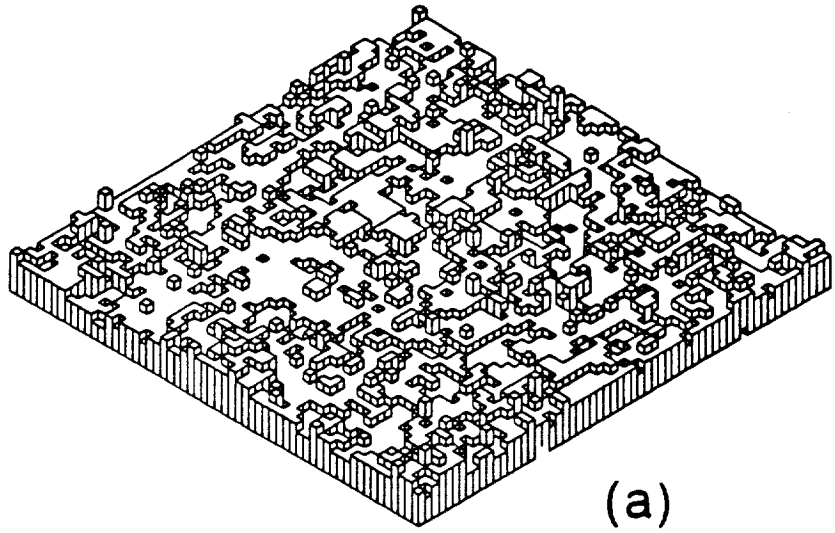

(a)

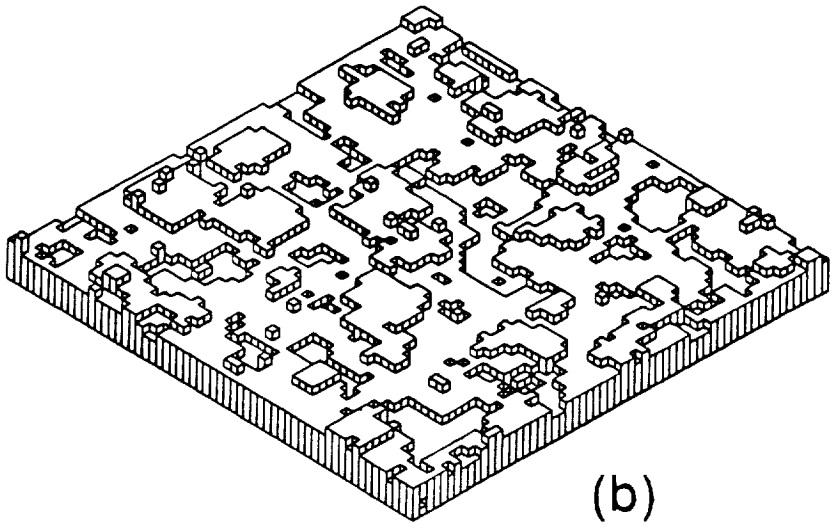

(b)

FIG. 4

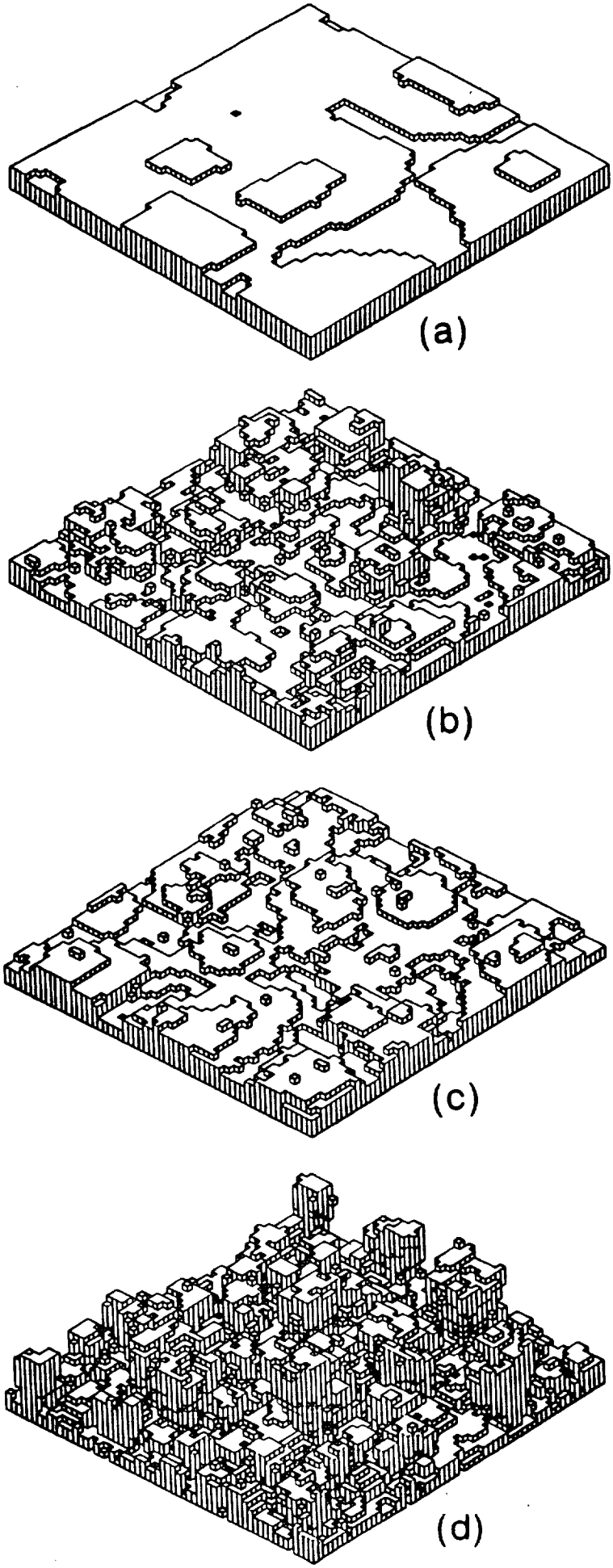

FIG. 5

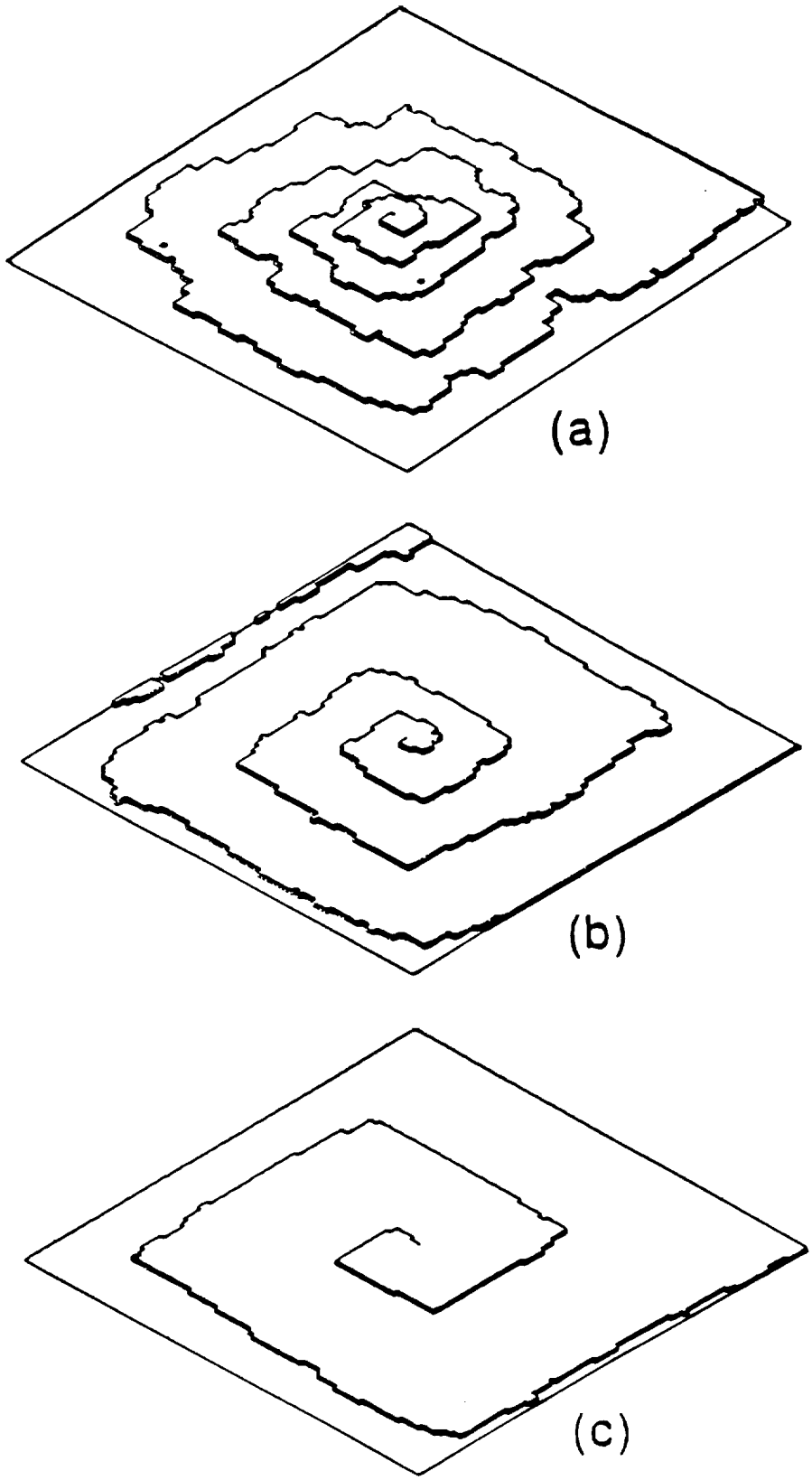

FIG. 6

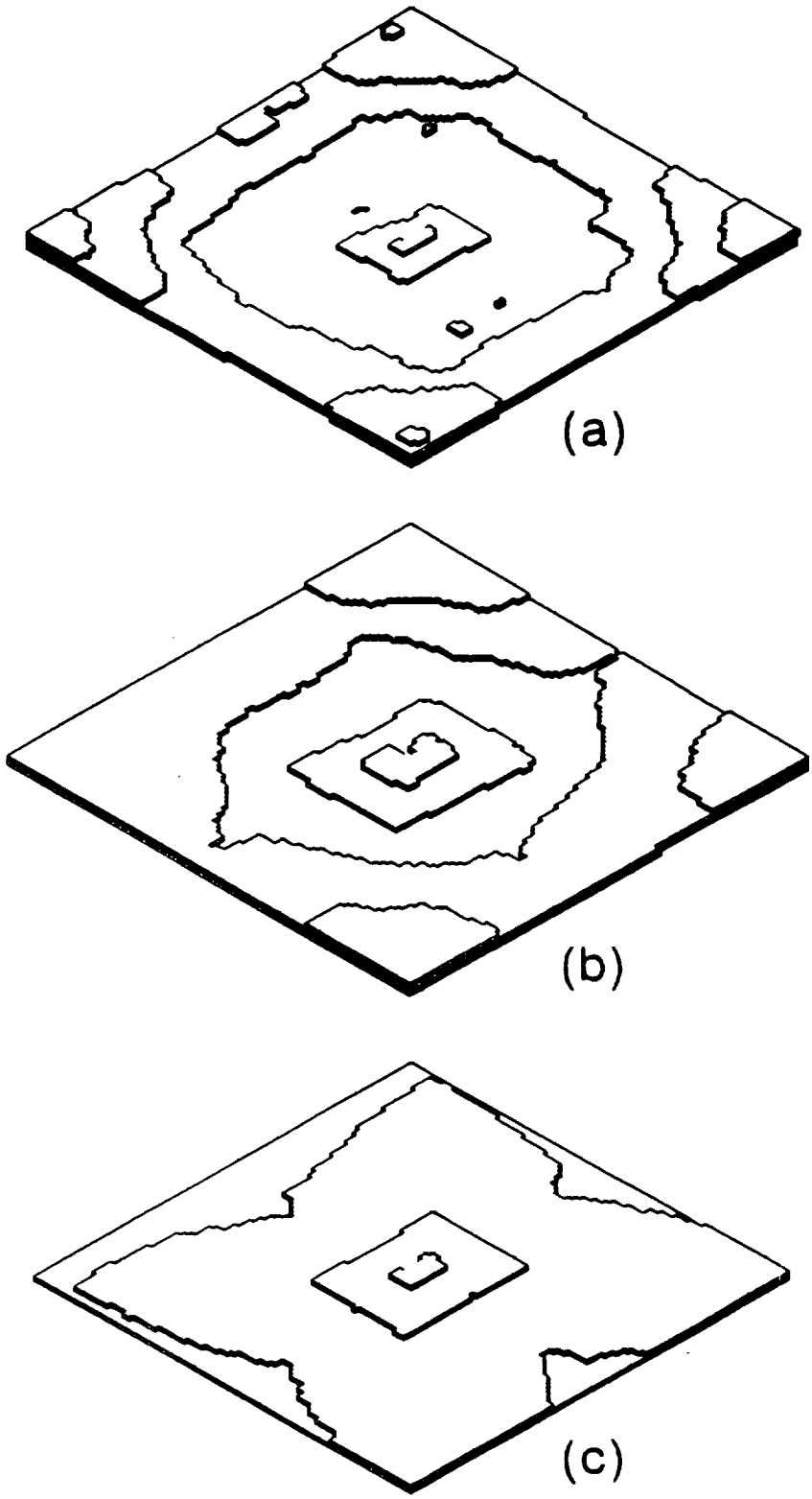

FIG. 7

Physical Review A
(in print)

Growth morphologies of crystal surfaces

Rong-Fu Xiao, J. Iwan D. Alexander and Franz Rosenberger

Center for Microgravity and Materials Research

University of Alabama in Huntsville, Huntsville, Alabama 35899

(Received

We have expanded our earlier Monte Carlo model [Phys. Rev. A38 (1988), 2447; J. Crystal Growth 100 (1990), 313] to three dimensions, included re-evaporation after accommodation, and growth on dislocation-induced steps. We found again that for a given set of growth parameters, the critical size, beyond which a crystal cannot retain its macroscopically facetted shape, scales linearly with the mean free path in the vapor. However, the 3-D systems show increased shape stability compared to corresponding 2-D cases. Extrapolation of the model results to mean free path conditions used in morphological stability experiments leads to order-of-magnitude agreement of the predicted critical size with experimental findings. The stability region for macroscopically smooth (facetted) surfaces in the parameter space of temperature and supersaturation depends on both the surface and bulk diffusion. While surface diffusion is seen to smooth the growth morphology on the scale of the surface diffusion length, bulk diffusion is always destabilizing. The atomic surface roughness increases with increase in growth temperature and supersaturation. That is, the tendency of surface kinetics anisotropies to stabilize the growth shape is reduced through thermal and kinetic roughening. It is also found that the

solid-on-solid assumption, which can be advantageously used at low temperatures and supersaturations, is insufficient to describe the growth dynamics of atomically rough interfaces where bulk diffusion governs the process.

For surfaces with an emerging screw dislocation we find that the spiral growth mechanism dominates at low temperatures and supersaturations. The polygonization of a growth spiral decreases with increasing temperature or supersaturation. When the mean free path in the nutrient is comparable to the lattice constant, the combined effect of bulk and surface diffusion reduces the terrace width of a growth spiral in its center region. At elevated temperatures and supersaturations, 2-D nucleation controlled growth can dominate in corner and edge regions of a facet, while the spiral growth mode prevails in its center. Thus, in addition to confirming the experimental observation that the critical size of a growing crystal depends on the prevailing growth mechanism, we are able to obtain detailed insight into the processes leading to the loss of face and facet stability.

PACS numbers: 05.50.+q, 61.50.Cj, 61.50.Jr, 64.60.Cn, 68.45.-v.

I. INTRODUCTION

Since the first application of the Monte Carlo (MC) method to simulations of crystal growth by Chernov and Lewis [1,2] its use has become widespread. MC studies were concerned with equilibrium and growth morphologies of crystals,[3-5] surface roughening transitions [6-9] and growth rate dependence on supersaturation and temperature.[10,11] For reviews see.[12,13] These studies were primarily focused on interfacial kinetics and have occasionally included surface diffusion.[11] A solid-on-solid (SOS) restriction (no overhangs)[14] was often invoked. The influence of bulk diffusion, i.e., the transport of growth units through the nutrient to the interface, has received less attention until very recently.[15-18] In the event that surface diffusion and interfacial kinetics govern the growth morphology, these simplifications are not severe

limitations. However, in reality, bulk transport often plays a decisive role in limiting morphological stability.[19-26]

Recently, we have studied the morphological evolution of growing crystals in two dimensions by considering both bulk transport and anisotropic interface kinetics.[15,16] For the bulk transport, we employed the diffusion-limited aggregation model of Witten and Sander.[27] In the formulation of the interface kinetics we followed largely Gilmer and Bennema's work.[5,11] Through a systematic variation of the simulation parameters (temperature, bond strength and supersaturation), the whole range of growth morphologies from fully facetted to side-branched dendritic growth was recovered. Our results show that the diffusion in the bulk nutrient and the anisotropy in the interface kinetics act morphologically destabilizing and stabilizing, respectively. For a given set of simulation parameters and symmetry of the lattice, there is a critical size beyond which a crystal cannot retain its stable, macroscopically facetted growth shape. This critical size scales linearly with the mean free path in the vapor.

In our previous studies [15,16] we ignored the fact that after attachment, the particles still have a finite probability to leave the attachment site. This approximation is valid when the system is far from equilibrium, i.e., the flux of particles impinging on the crystal surface largely exceeds that of the evaporating particles. However, close to equilibrium, the rates of impingement and evaporation are comparable. Then a more realistic description of crystal growth must account for the non-negligible chance that interfacial particles either move (diffuse) on the surface or evaporate back into the nutrient *at any time* after the initial accommodation on the surface.

The growth of perfect crystals proceeds typically through two-dimension-nucleation,[28] which is extremely slow at low temperatures and supersaturations. Yet, in reality most crystals posses considerable concentrations of defects. Certain defects facilitate growth at low temperatures and supersaturations. Frank [29] who found that a screw dislocation can provide a inexhaustible source of growth steps. Growth on dislocation-induced steps has since been observed experimentally by many workers [30-34] and various theories for this growth mechanism have been proposed.[28,35-38] However, due to the complexity of the problem, no exact solutions

have been obtained. Typical simplifications include the uniform spacing of growth steps, and the neglect of nutrient bulk diffusion and surface diffusion. Although there have been some Monte Carlo simulations of dislocation-facilitated growth,[39,40] owing to the computational limitations at that time, the transport aspects of the problem were not taken into account.

In this paper we expand our previous studies [15,16] to three dimension and investigate the role of 2-D nucleation growth and dislocation-induced growth in the morphological evolution of growing crystals. Instead of the multiple-registration scheme used in the earlier work to reduce microscopic noise,[15,16] we employ realistic re-evaporation conditions for interfacial particles. The model and simulation procedure are described in Section II. Results on the influence of temperature and supersaturation on the surface morphology of perfect crystals are presented in Section III.A. Based on a criterion originally proposed by Burton-Cabrera and Frank,[28] the thermal and kinetic roughening transitions are quantified. In addition, the scaling between the critical stable size of a facetted crystal and the mean free path of the vapor is studied in three dimensions. In Section III.B we devote our effort to surfaces with dislocations and pay special attention to the shape and spacing of steps of growth spirals. We conclude the paper with results on the competition between normal growth at the corners and dislocation-facilitated growth at the center of a facet.

II. MODEL AND SIMULATION PROCEDURE

A. The model

Two different geometries, planar and spherical, are used to study the effect of bulk transport-induced non-uniformity in nutrient distribution on growth morphology. In the planar cases (Fig.1a), the nutrient is contained between parallel crystal and source planes, which are infinite in lateral extent. In order to save computational time, we only consider a portion of the whole system and apply periodic boundary conditions in the x- and y-directions. In the other cases (Fig.1b) a cubic seed is located at the center of a spherical source. Ideally, the separation between the growing crystal and the source should be infinite. But, again, to save computational

time we choose a finite separation, yet wide enough that the growth shape remains unbiased.[15] As a crystal grows, the distance between crystal surface and source is kept constant.

At molecular length scales, an individual growth unit undergoes generally several basic processes before becoming part of the growing crystal. After detachment from the source, a growth unit is transported by bulk diffusion towards the growing interface. The actual transport kinetics is determined by the interaction of growth units (or their precursors) and other species that form the nutrient. Usually, when a growth unit reaches the interface, it is not immediately incorporated into the growing crystal. It will adsorb and diffuse on the interface in an attempt to find an energetically favorable "final" attachment site, or it will even return to the nutrient before it finds such a site. The latter happens, for instance, when the growth unit is misoriented and cannot form stable bonds with the crystal. Alternatively, the growth unit may impinge onto a site with too few neighbors to prevent it from being dislodged by thermal vibrations before it becomes adsorbed. A growth unit may even become dislodged after having arrived at an energetically favorable site. The probability that any of these processes occur is determined by the local configuration (arrangement of bond-forming neighbors) of the interface sites that the unit happens to visit. Though a complete model of such complex scenarios is not practical at this point, we have formulated a Monte Carlo model which retains the essential physics of both nutrient bulk transport and interface kinetics, including surface diffusion and re-evaporation, without resorting to the SOS approximation.

We assume that the gaseous nutrient phase consists of two components: a growth species A, highly diluted in an inert gas B, such that the B concentration is essentially uniform and A-A interactions can be ignored. Component B randomizes the motion of A. Convection is ignored. The chemical potential is taken to be a linear function of the growth species concentration only. This results in a Fickian transport equation and, thus, a random walk may be used to describe diffusion in the nutrient phase in the form[15,16]

$$U(\vec{r},s\tau) = \frac{1}{c}\sum_{i}^{c} U[\vec{r}+\vec{a}, (s-1)\tau] \quad , \qquad (1)$$

where $U(\vec{r},s\tau)$ is the probability that a walker can be found at location $\vec{r}$ after s steps (with a time interval τ) of jump length (mean free path) $|a|$. The normalization parameter c represents the total number of the possible jump sites.

To approximate the complex processes following the arrival of a growth unit on the interface, we make the following assumptions: The impingement rate K^+ can be obtained, based on ideal gas kinetics, from the chemical potential difference $\Delta\mu$ between interfacial vapor and average surface site in the form [15]

$$K^+ = K_{eq} \exp(\Delta\mu / kT) \quad , \tag{2}$$

where K_{eq} is the temperature dependent equilibrium value of K^+. Note that in reality the overall driving force for the diffusion of A towards the crystal and subsequent interfacial attachment is the difference in chemical potential between the crystal surface and the source. Since we have accounted for bulk diffusion via a random walk process, the chemical potential of the source does not appear explicitly in our model. The $\Delta\mu$ in Eq.2 is therefor governed by the difference between the bulk transport-dependent vapor concentration at the interface and the equilibrium concentration at the same temperature. It should not be confused with the chemical potential difference (bulk supersaturation, undercooling, etc.) used to control experimental crystal growth. This important point is discussed in more detail in [15,16] and also below.

The rates of both the evaporation and surface diffusion processes are sensitive to the local configuration of the site from which a unit is to be dislodged. Hence, following Gilmer and Bennema,[11] we write the evaporation rate K_i^- in the site-dependent form

$$K_i^- = \nu \exp(- E_i/kT) \quad , \tag{3}$$

where ν is a lattice vibration factor and, in a nearest neighbor approximation, E_i is simply the product of the pair interaction (bond) energy ϕ of a unit with a nearest neighbor and n_i, the number of occupied neighbor sites of site i.

For surface diffusion we assume that the diffusion rate depends on the occupation condition of both the site i that the particle occupies and the potential jump site j. Hence, we express the jump rate as

$$K_{i \rightarrow j} = \nu_s \exp(-\Delta E_{ij} / kT) \quad , \tag{4}$$

where ν_s is a surface vibration factor, and the activation energy

$$\Delta E_{ij} = \begin{cases} \delta_i + \phi (n_i - n_j) & \text{for } n_i > n_j \\ \delta_i & \text{for } n_i \leq n_j \end{cases} \quad . \tag{5}$$

In reality the term δ_i depends on the the specific configuration i-j. For simplicity we have assumed that for a given i-j the δ term is independent of jump direction, hence the notation δ_i. As a consequence of this assumed direction independence, the δ_i terms cancel in the following formulations of transition probabilities and, thus do not have to calculated.

In real situations, impingement, surface diffusion and evaporation take place at the same time with different magnitude. But in the MC simulation we consider one event at a time. Therefore, it is necessary to determine the sequence in which the events are to be considered. To this end we define an overall evaporation probability as

$$P^- = \frac{\overline{K^-}}{K^+ + \overline{K^-}} \quad , \tag{6}$$

where $\overline{K^-}$ is the average "evaporation rate"

$$\overline{K^-} = \frac{1}{m} \sum_{i=1}^{m} K_i^- , \qquad (7)$$

and the summation is over all m interfacial particles. By considering a local equilibrium condition for the kink site, on a simple cubic lattice Eq. 6 becomes

$$P^- = \frac{B}{B + \exp(\Delta\mu/kT)\exp(-3\phi/kT)} , \qquad (8)$$

$$\text{with} \quad B = \frac{1}{m} \sum_{i=1}^{m} \exp(-i\phi / kT) \quad .$$

At equilibrium ($\Delta\mu/kT = 0$), Eq. 8 yields $P^- \approx 0.5$, i.e. there are approximately equal amounts of particles evaporating from and impinging onto the crystal surface. At positive supersaturations ($\Delta\mu/kT > 0$), P^- is less than 0.5, i.e. impingement exceeds evaporation. Correspondingly, for negative supersaturations ($\Delta\mu/kT < 0$) the P^- will be larger than 0.5, and more interfacial particles will evaporate and the crystal will shrink. These effects will not only be manifested in the growth and shrinkage rate, respectively, but will also influence the surface morphology.

After having decided the sequence of events, the individual probability for the various events needs to be determined. This depends on the specific site considered. For impingement, the probability, according to Eqs. 2 and 3, is $P_i^s = K^+ / (K^+ + K_i^-)$. For a simple cubic crystal, this can be written as (for a derivation in 2-D see [15])

$$P_i^s = \frac{\exp(\Delta\mu/kT)\exp[-(3-n_i)\,\phi/kT]}{1+\exp(\Delta\mu/kT)\exp[-(3-n_i)\,\phi/kT]} \quad . \qquad (9)$$

The jump probability from site i to a neighboring unoccupied site j (on the surface or in the nutrient), following,[15] is

$$P_{i\to j} = \frac{K_{i\to j}}{\sum_{j=1}^{c'} K_{i\to j}} = \frac{\exp[-(n_i - n_j)\,\phi/kT)]}{\sum_{j=1}^{c'} \exp[-(n_i - n_j)\,\phi/kT)]}\,, \qquad (10)$$

where c' is the number of unoccupied nearest neighbor sites of site i. Clearly, a larger n_j results in a higher probability that a molecule will jump to site j on the interface.

The probability of evaporation for interfacial particles can be expressed as

$$P_i^e = \frac{K_i^-}{\sum_{i=1}^{m} K_i^-} = \frac{\exp(-n_i\,\phi/kT)}{mB} \qquad i = 1, 2,...m. \qquad (11)$$

It can be seen from Eq. 11 that the probability of evaporation decreases exponentially with increasing number of solid bonds and, thus, is highly anisotropic. The most probable sites for evaporation are those with the least solid neighbors, such as admolecules with a single solid bond. As the temperature and, thus, the surface roughness is increased, the anisotropy of the evaporation is decreased.

B. Simulation procedure

A summary of the simulation steps is presented in Fig.2. First the initial conditions are chosen: for growth onto perfect crystals a smooth surface is set at a certain distance (typically 50 lattice units b, for $|a| = b$) from the source. In the planar case the surface is chosen as a square lattice measuring 60b x 60b, with periodic boundary conditions in x and y (lateral) directions. For growth onto dislocated crystals the lateral size is doubled in order to provide space for the evolution of several turns of a spiral. An initial dislocation is introduced by a vertical slip of parts of the lattice similar to.[40] Note also that, as the crystal grows, the source is moved outwards such that the separation remains unchanged, as discussed in.[15]

Following the setting of initial conditions and choice of specific input parameter values, P^- is calculated from ϕ, T, $\Delta\mu$ and the current crystal morphology. Comparison of a random

number R with P^- determines the event to be considered. If $R > P^-$, a growth unit is released from the source and bulk diffusion is simulated through an isotropic sequence of random jumps of equal length (mean free path) |a|. Only when the particle has come within a distance |a| from the crystal surface is a check implemented that determines whether the interface has been reached. The following steps, including the determination of average surface diffusion lengths, are similar to our previous simulations except that we do not impose the multiple registration used in.[15,16] A growth unit is tracked until it has either escaped from the system or is stuck onto the crystal surface.

If $R < P^-$, an evaporation event is selected. Then, all P_i^e (i=1,...m) are calculated from the recorded positions and neighboring configurations. Another random number R' is generated. If by chance R' falls into i^{th} interval, the i^{th} interfacial particle is chosen to move. Then, governed by Eqs. (9), (10) and (11), the particle is kept moving until it has attached to some interfacial site or escaped to the source. If it sticks on site j, the local P_j^e's, around the new site j as well as the earlier site i where the particle originated, are recalculated. By using a new random number, a new evaporation event is selected. The evaporation route is pursued until some particle has escaped to the source. When this happens the P^- is recalculated and a new event is selected.

The simulation is continued until a desired size or layer thickness is reached. In a planar case, the simulation is continued until 14,400 or 10,000 particles, respectively, have been added to a perfect or dislocated surface. In a spherical case, the simulation is stopped after a crystal has become unstable (the criterion for the instability will be discussed later). Typical CPU times were around 3,000-10,000s on a CRAY X-MP/24 and 5 - 50 hours on an ARDENT computer.

Our model has been designed for computational efficiency. As outlined above (see Eqs. 6-8), the event to be considered is decided upon before the execution based on physical criteria rather than random choice only. In this way, any "unnecessary" operation is avoided. For example, evaporation will be executed whenever a random number R is less than P^-, although the selection of the actual execution site is quite random. In the earlier models [11,40] the selection of a particle and calculation of the evaporation probability do not necessarily lead to an actual

execution of an evaporation process. Many interfacial particles may have to be selected, before a real evaporation event takes place. This is particularly time-consuming under conditions of low temperature and supersaturation, in which the interface is rather smooth and the probability of evaporation is very low.

Note that, unless stated otherwise, the simulations were carried out with the magnitude of the mean free path in the vapor equal one lattice constant, $|a| = b$.

III. RESULTS AND DISCUSSION

A. Perfect surfaces

1. Effects of surface and bulk diffusion at various temperatures

As references for the more complex cases to be treated later and for comparison with earlier work,[6-9] we have first examined cases in which both bulk and surface diffusion were neglected. Particles arriving at random locations of the crystal surface either stick or are discarded. Figure 3 shows the effect of growth temperature or bond strength (i.e. ϕ/kT) on the morphology of a planar crystal surfaces at a constant low value of $\Delta\mu/kT = 0.35$. At low temperature, as can be seen from Fig.3a, the growing crystal is atomically smooth with occasional 2-D clusters on the surface, i.e. growth occurs by 2D nucleation only.[28] As the temperature increases (Fig.3b) the surface becomes rougher and more 2D clusters with smaller size are formed on the surface and even on top of large clusters. On further increase in temperature the whole surface becomes atomically rough (Fig.3d), and large size clusters can hardly be discerned. In this situation the crystal grows more readily due to the disappearance of the energy barrier for 2D nucleation. This thermal roughening effect has been extensively studied before under equilibrium conditions.[6-9,12,13] The earlier studies basically employed an algorithm for random pair exchange controlled by a Boltzmann factor $\exp(-\Delta E/kT)$. At equilibrium, the validity of the algorithm is guaranteed by the thermodynamic principle of path independence. For a non-equilibrium situation the random pair exchange algorithm is no longer valid. The final result depends not only on the potential energy between the initial and final sites but also on the

actual path of the particles. In contrast, our model, as discussed in section II, is more general and can be used in both equilibrium and non-equilibrium situations.

To further demonstrate the effect of temperature on the morphology of a growing crystal we have plotted in Fig.4 the surface area, normalized by the area of a perfectly smooth surface, versus number of attached particles (in units of completed layers). The four curves correspond to cases a-d in Fig.3. As can be seen from Fig.4, at the lowest temperature the surface area oscillates periodically with minima on layer completion, alternating with maxima at about half-filled layers. Thus growth proceeds essentially layer by layer. When, following the formation of a 2-D nucleus, a layer spreads, the surface area increases until a half-filled layer state is reached and then it decreases until a layer is completed. However, when the temperature is increased and, thus, the surface becomes rougher, the distinction between a half-filled layer and completed layers is blurred, i.e. new layers form before completion of the earlier layers. With increasing roughness, the periodicity disappears and the surface becomes delocalized.

Figure 5 illustrates the consequences of surface diffusion. Bulk diffusion is not considered in these examples with $\phi/kT=1.6$, $\Delta\mu/kT=0.69$. It can be seen that with surface diffusion (Fig. 5b) the crystal surface is much smoother than without (Fig.5a). The reason is that surface diffusion can provide an additional way for interfacial particles to relax to some energetically more favorable (low energy) sites and, hence, reduces the amplitude of the surface roughness. Of course, as we have shown before,[16] such a stabilizing contribution is effective only at a length scale comparable to the surface diffusion length, which, in turn, is sensitive to the surface roughness.[16] Generally speaking, the smoother a surface is, the farther an interfacial particle can diffuse during its lifetime on the surface. Hence, as shown by the simulation results of Fig.6, the surface diffusion length decreases with increasing temperature. In addition to the temperature effect, Fig.6 also reveals a strong dependence of surface diffusion length on supersaturation. This was not taken into account in earlier simulations,[11] in which the surface diffusion length was considered as an externally adjustable parameter, independent of

temperature and supersaturation. By contrast, in our model surface diffusion is an integral part of the attachment and evaporation processes.

Unlike surface diffusion, bulk diffusion acts destabilizing on the interface morphology.[15-17] This is shown in Fig.7 for a case with surface diffusion, $\Delta\mu/kT = 3.0$ and $\phi/kT = 2.3$. For the three subfigures the mean free path in the nutrient was decreased from "infinite" (Fig.7a), to ten (Fig.7b) and one crystal lattice constant (Fig.7c), respectively. The infinite mean free path corresponds to direct jumps of growth units from the source onto the crystal surface, as in the simulations leading to Figs.3 and 5. A mean free path of one lattice unit implies an extremely dense nutrient similar to a liquid. It is evident from this figure that bulk diffusion, particularly in the case of a short mean free path (Fig.7c), destabilizes the surface morphology. With increasing surface roughness not only is the stabilizing effect of surface diffusion weak, but simultaneously the stabilizing anisotropy in surface kinetics is decreased. Once a protrusion forms by chance, it will be amplified by the bulk diffusion. At intermediate values of temperature and supersaturation, there exists a competition between surface kinetics and bulk diffusion. Only if the surface kinetics prevails, can crystal surfaces remain stable, i.e. facetted.[16] More pronounced destabilization from bulk diffusion at higher temperatures will be shown later.

2. Supersaturation effects

Increases in supersaturation can also affect the crystal morphology through kinetic roughening.[41-44] This is also born out by our 2-D simulations.[15,16] The influence of supersaturation on a 3D growth morphology is shown in Fig.8, in which the temperature and bond strength are kept constant ($\phi/kT = 3.9$). Both surface and bulk diffusion are included. One sees that with increasing supersaturation the size of the 2-D clusters decreases, the surface roughens, eventually leading to many depressions and protrusions on the surface, and even vacancies in the crystal. As formulated in section II.A, an increase in supersaturation causes an increase in impingement rate (Eq.2) and, hence, a relative decrease in evaporation probability (Eq.6). When the supersaturation reaches some critical value, the surface kinetics become relatively less important and the growth process is controlled by bulk diffusion. The ensuing loss

of facet stability is further illustrated in Fig.9 by profiles of the interfacial layer occupation numbers. The four profiles correspond to the cases depicted in Fig. 8. One clearly sees that the interfacial width grows with increasing supersaturation.

The above results reveal significant concentrations of overhangs and vacancies in the crystal at higher supersaturations and temperatures. Hence, under these conditions, the SOS (no overhang) assumption is unrealistic for the description of crystal growth morphologies. Thus, the SOS assumption is only a good approximation at low temperatures and supersaturations where the surface morphology is controlled by surface kinetics rather than bulk diffusion. Note, however, that the supersaturation value required for significant kinetic roughening depends on both bond strength and temperature. A crystal surface can have the same roughness at different combinations of supersaturation and temperature.

In order to illustrate the dependence of the anisotropy in interface kinetics parameters on growth conditions, we have plotted in Fig.10 the sticking probabilities at sites with various numbers of nearest neighbors as a function of temperature/bond strength and supersaturation (Eq. 9). For clarity only surfaces for P_1^s , P_3^s (kink site) and P_5^s are plotted in this figure. Note the temperature independence of P_3^s that results from the assumption of local equilibrium at the kink site underlying Eq.9. Figure 10 well illustrates the strong dependence of the anisotropy in sticking probability (separation between P_1^s and $P_5^{s)}$ on temperature and supersaturation. At low values of these parameters, P_1^s and P_5^s are nearly constant and close to 0 and 1 respectively. This reflects the difficulty of the attachment of isolated particles and the ease with which holes (i.e. sites with more than 3 solid nearest neighbors) are filled. One can also see from this figure that the anisotropy in sticking probability can be more effectively reduced by increasing the temperature than by increasing the supersaturation. There is a rapid decrease in the anisotropy of the sticking probability around ϕ/kT = 1.0 - 2.0 at low supersaturation. The value of the anisotropy in sticking probability is a fundamental quantity for controlling the morphology of a crystal surface. Only when the anisotropy is significant can a crystal retain a stable, facetted form.

3. Surface roughness

To further quantify the surface morphology features we use a criterion originally introduced by Burton-Cabrera and Frank (BCF) [28] that defines the surface roughness R_S in terms of the surface energy E (i.e. the number of broken bonds times ϕ) at temperature T and the surface energy E_0 for a perfectly smooth surface at zero temperature, in the form

$$R_s = \frac{E - E_o}{E_o} \quad . \qquad (12)$$

This R_S is a merely geometrical measure that depends only on the number of broken lateral bonds per unit area. The variation of R_S with temperature obtained from a simulation of an equilibrium situation ($\Delta\mu/kT = 0$) is plotted in Fig.11. One can see that the surface roughness monotonically increases with temperature, with a slope that is highly temperature dependent. There is also a unique inflection point (location of maximum slope), which, as better indicated by the plot of the derivative $dR_S/dT(T)$ in the same figure, lies at $kT/\phi \approx 0.62$. Since R_S is proportional to the surface energy, dR_S/dT should be proportional to the heat capacity or specific heat of the surface. A singularity in heat capacity is characteristic for a phase transition. But in MC simulation, the singularity has been degraded owing to the effect of finite system size.[45,46] Swendsen [9] first used a maximum in heat capacity in a MC simulation to define the roughening transition temperature. He obtained for a simple cubic lattice $T_R \approx 0.575\ \phi/k$. Leamy and Gilmer [7] found, by using a different criterion and employing the SOS restriction, a roughening transition temperature $T_R \approx 0.64\ \phi/k$, which is surprisingly close to our value. This indicates again that the SOS approximation is appropriate for the description of surface morphology under equilibrium conditions. However, as has been shown above, the SOS assumption is no longer valid when the growth becomes bulk diffusion controlled, i.e. the surface has become rough.

In Fig.12 we have delineated the temperature-supersaturation combinations for surface roughening transitions, as obtained from our MC results and Eq.12 with the inflection point

criterion, for systems with various combinations of surface and bulk diffusion conditions. As reflected by the extent of the respective stability regions (smooth vs. rough), surfaces on which surface diffusion is significant can retain atomic smoothness up to higher temperatures and/or supersaturations than without surface diffusion. Bulk diffusion, on the other hand, reduces the smooth (stable) region in the ϕ/kT vs. $\Delta\mu/kT$ plane, as we have seen more qualitatively before.

4. Re-evaporation effects

All of the above results were obtained with the new algorithm that accounts for the possibility of re-evaporation of interfacial particles. To gauge the effect of re-evaporation with respect to the earlier noise reduction algorithm,[15,16] Fig.13 presents some results obtained without re-evaporation and either without or with the multiple-registration scheme used in our earlier work. Otherwise the growth conditions in Fig.13 a-b are the same as in Fig. 8a ($\Delta\mu/kT$ = 0.69) while the conditions in Fig.13c-d are the same as in Fig.8c ($\Delta\mu/kT = 5.0$), with $\phi/kT = 3.9$ for all. The multiple-registration noise reduction scheme[15,16] used for Figs.13b and 13d requires 10 registrations of incoming particles at a site i before that site is considered occupied. Comparison of the corresponding cases in Figs. 8 and 13 shows that at low supersaturations the noise reduction scheme is somewhat more effective in smoothing the surface than re-evaporation At high supersaturation, however, both schemes give nearly the same smoothness (compare Figs.8c and 13d). Similar conclusions can be drawn for the smoothing effect of the two schemes upon variations of ϕ/kT. Hence we conclude that at situations far from equilibrium or at high temperatures, the noise reduction scheme can give qualitatively similar results as the new evaporation scheme, for which, however, the physical implications are much clearer.

5. Spherical source

The above results were based on the uniform nutrient flux conditions of the planar geometry of Fig.1a . But in reality nutrient flux conditions are most often non-uniform. To further explore the effect of nonuniform supply beyond the 2-D results obtained in [15,16] with a circular source, we have performed MC runs with growth onto a cubic surface inside a spherical source; see fig 1b. Figure 14 presents surface morphologies obtained in this geometry with ϕ/kT

= 2.3 and $\Delta\mu/kT = 0.69$. The mean free path or jump length is one lattice constant, i.e. $|a| = b$ in Fig.14a-b, and five lattice constants ($|a| = 5b$) in Fig.14c-d. Similar to the 2-D findings in,[15,16] one sees that loss of stability of a facet is associated with the formation of a depression in its center and, correspondingly, preferred growth at corners and edges. As discussed before [15,16] this occurs because the anisotropy in surface kinetics can compensate for the nonuniformity in nutrient supply only up to a certain critical size of the crystal. This nonuniformity decreases with increasing mean free path of the diffusing nutrient particles. Hence, as is shown by Fig. 14, the critical crystal size increases with increasing mean free path. To quantify the critical size we have plotted in Fig.15 the normalized total surface area of the growing cubic crystal versus the size of the crystal . The surface area is normalized by the total surface area (six faces) $6M^{2/3}$ of a perfectly smooth cubic crystal consisting of M growth units. As long as the surface area follows the $6M^{2/3}$behavior, a crystal is considered morphologically stable. When a crystal begins to lose its stable facetted form its normalized total surface area increases. Somewhat arbitrarily, we define the critical size as the one at which the surface area exceeds that of a smooth surface by 15%. Thus we find that the crystals depicted in Fig.14 have critical sizes of about 27b and 52b, respectively , for $|a| = b$ and $|a| = 5b$.

In Fig.16. we have summarized our 3-D results for the dependence of the critical size on mean free path at fixed $\Delta\mu/kT$ and various ϕ/kT 's, together with the earlier 2-D results.[16] One can see that the critical size increases with decreasing temperature. At fixed temperature and supersaturation, the critical size scales linearly with the mean free path in the parameter range considered. The 3-D simulations yield larger slopes than the corresponding 2-D cases, i.e. the 3-D cases are morphologically more stable. This results from the fact that, on average, there are more solid neighbors associated with interfacial particles in three dimensions and, thus, the (stabilizing) anisotropy in interface kinetics is more pronounced. Although computational time limitations do not allow for the direct simulation of the critical size at the mean free path used in morphological stability experiments,[22-26] Fig.16 encourages us to scale linearly to these conditions. This leads to an order-of-magnitude agreement between experimental and modelling

results for the critical size, with the 3-D results approaching the experimental findings closer than the 2-D results.[16]

B. Surfaces with dislocations

1. Temperature effects

The development of a growth spiral from an initially straight step that results from a screw dislocation with Burgers vector of one lattice constant normal to the (001) face is illustrated in Fig.17. The bond strength/temperature (i.e. ϕ/kT) dependence of the surface morphology with a single screw dislocation is shown in Fig.18. In this simulation, both surface and bulk diffusion were ignored.The supersaturation was kept constant ($\Delta\mu/kT=0.69$) while the ϕ/kT was decreased successively from 5.3, 4.6, 3.0 to 2.0. One sees that at low temperature or high bond strength (Fig.18.a) the steps of the resulting growth spiral are quite smooth and the shape is highly polygonized, leaving essentially only low-index steps exposed. As the temperature is increased (Fig.18b-d) not only do the steps roughen but also the shape of the spiral becomes rounder and eventually indiscernible as 2-D nucleation becomes pronounced. These morphological changes are a result of the increase in surface roughness with growth temperature. At low temperatures (Fig.18a), growth occurs only via attachment to the spiral steps, since the roughness of the remainder of the facet is too low to result in significant sticking probabilities. Furthermore, due to the low roughness of the steps, the step attachment kinetics is highly anisotropic, leading to rather straight step shapes. As temperature is increased, the steps and remainder of the face roughen. This results in a reduction of the anisotropy in step attachment kinects and, thus, rounding of the steps. Simultaneously, with increasing face roughness, the energy barrier for 2-D nucleation is reduced. On further temperature increase 2-D nucleation-assisted growth becomes increasingly important, until it dominates at $\phi/kT = 2.0$.

These results confirm that it is reasonable to neglect 2-D nucleation in simulations of dislocation-assisted growth morphologies at low temperature and supersaturation, where the sticking probability P_1^s (see Fig.10) is very small. This allows for a drastic reduction in

computational times required.[39] Hence, throughout the following simulations of dislocation-assisted growth, the attachment of isolated particles, i.e. with one bond to the surface, is suppressed.

Figure 19 was obtained by considering a pair of screw dislocation with opposite sign, i.e. a Frank-Reed step source.[47] In order to save computer time and memory, the separation between the centers of the dislocations was chosen to be only 7b. In reality, this separation may be much larger. When the two growth spirals turn in opposite direction and meet, closed loops are formed periodically. During this sequence of simulations the supersaturation was kept constant while ϕ/kT was decreased from 5.3 to 4.6 and 3.9, respectively, and surface and bulk diffusion were ignored. Again, as the temperature increases the steps become rougher and the closed loops become rounder and spaced more closely, analogous to the temperature dependent behavior displayed in Fig.18.

2. Supersaturation effects

The effect of supersaturation on the growth morphology of a face with a single screw dislocation is shown in Fig.20, in which the ϕ/kT is kept at 5.3 while the $\Delta\mu/kT$ is increased successively from 0.69 to 2.0 and 3.0, again ignoring surface and bulk diffusion. As can be seen, increases in supersaturation also make steps rougher and less polygonized, similar to the effect of ϕ/kT in Figs. 18 and 19. This morphological change is, of course, due to kinetic roughening of the steps, in contrast to the thermal roughening occurring as the temperature is increased. In addition, the terrace widths between adjacent spiral arms decrease with increasing supersaturation, consistent with the prediction of classical theories.[28,35-38]

3. Effects of surface and bulk diffusion

As has been discussed in section III.A, surface diffusion can greatly smooth the morphology of perfect surfaces. The effect of surface diffusion in the presence of a single dislocation is demonstrated in Fig.21. For this sequence, nutrient bulk diffusion was ignored and the growth conditions (i.e. ϕ/kT and $\Delta\mu/kT$) were the same as those for Fig.20. We find, in comparison to Fig.20, not only smoother steps, but also more pronounced polygonization. This

is because with surface diffusion, more growth units can reach rounded corners, where, due to the higher kink density, the attachment probability is higher. The spirals also become more polygonized due to the resulting increase in anisotropy of step attachment kinetics This is at variance with the conclusion of Sunagawa and Bennema,[34] who expected that surface diffusion will suppress the formation of close-packed or periodic-bond-chain oriented steps.

Growth morphologies of a dislocated surface in the presence of both surface and bulk diffusion are depicted in Fig.22. The growth conditions are the same as in Figs. 20 and 21, i.e. ϕ/kT is kept at 5.3 and the supersaturation is increased. It is evident from this figure that bulk diffusion is also destabilizing for steps, as revealed, for instance, by the lateral depressions at high supersaturation (Fig.22c). But probably the most interesting new feature revealed by this simulation is the variation of the terrace width, with narrower terraces found near the center of the spiral, particularly at higher supersaturation (Fig.22c). This is at variance with earlier MC simulations without bulk diffusion [39-41] and classical theories.[8,35-38] Realizing that the above simulation is based on a mean free path length (in the bulk) equal to a lattice constant, the decrease in terrace width toward the center of the spiral can be understood as a combined effect of bulk and surface diffusion. Since the growth hillock protrudes into the nutrient, steps and terraces close to its center of the spiral are somewhat better supplied with growth units by bulk diffusion. This leads to tighter winding of the spiral.[28] On the other hand, the surface diffusion fields of terraces at the periphery of the spiral overlap less than those near the center. Overall, this leads to higher spreading velocities of the outer turns of the spiral and, thus, an increase in terrace width with distance from the spiral's center. In real vapor systems,where $|a| >> b$, such behavior should not be expected. It is more likely to occur in growth from condensed phases.

4. Spherical source

All of the above results for dislocation-assisted growth were obtained for the planar geometry of Fig.1a. To demonstrate the competing effect of 2-D nucleation growth and dislocation growth in a non-uniform concentration field, we have carried out a simulation for the 3-D geometry of Fig.1b with the same growth conditions as for Fig.14b. Among the six faces of

the cubic crystal, five are assumed to be perfect and only one has a pair of dislocations with opposite sign. Surface diffusion is taken into account. Figure 23 shows the crystal at a stage after exceeding its critical stable size (see discussion in section III.A). The subfigures show different faces of the same crystal, with (a) displaying three of the five faces without dislocation and (b) the dislocated face on top. The dislocation pair is seen to enhance the face stability. All five originally perfect faces have developed central depressions similar to that found in Fig.23a. This finding can be understood in terms of the different supersaturation dependence of the growth rate in 2-D nucleation and dislocation-assisted growth. Bulk diffusion results in a lower supersaturation in the face center than at the edges and corners. Yet, the face center region, due to the presence of dislocation-induced surface steps, offers a higher probability for the attachment of growth units than the edge regions in which steps are generated only by 2-D nucleation. This increased attachment probability in the center of the face can compensate for the leaner supply of growth units into this region, see also.[15,16] This competition of growth steps originating at dislocations in center regions of facets, with growth steps from 2-D nucleation near corners, has been experimentally observed by several workers; for references see.[48] Also, the better utilization of growth units (through the anisotropy of kinetics coefficients) in regions that are less readily supplied by the bulk diffusion field is the key point of Chernov's anisotropic stability theory for facet growth. [21]

To further illustrate the competition between 2-D nucleation growth and dislocation growth in a non-uniform nutrient field, we have carried out a simulation at a much lower temperature ($\phi/kT = 5.3$) than that used for Fig.23. At the lower temperature the surface roughness and, thus, the sticking probability is considerably reduced. Hence, in order to not exceed prudent computational times, we have modelled only the 3-D evolution on one face, with special periodic conditions on the lateral boundaries of the pyramid outlined in Fig.1b. Note that the outer boundary condition in this configuration still corresponds to a spherical source as in Fig.23. In this simulation, ϕ/kT is kept at 5.3, and the supersaturation is increased from 0.6 to 2.0 and 3.0, respectively. The simulations include surface diffusion and unsuppressed

attachment of single particles. Figure 24 shows the results after attachment of 20,000 particles in all three cases. One sees that at low supersaturation (Fig.24a) growth occurs only through attachment onto steps that originate at the central dislocation pair. Under these growth condition, the supersaturation increase at the corners[16] is not high enough to overcome the nucleation barrier for 2-D nucleation, which, due to the low surface roughness, is high. The higher supersaturation at the corner, though, destabilizes the dislocation-induced growth step loops, leading to lateral protrusions towards the corners, similar to the growth patterns obtained in the 2-D situation.[15,16] Such star shaped dislocation growth has been observed experimentally; see, for example, Fig.60 in.[34] As the supersaturation is increased, the controlling effect of the central dislocations decreases and 2-D nucleation becomes significant at the corners (Fig.24b). At an even higher supersaturation (Fig.24c), growth is essentially dominated by 2-D nucleation at the corners, in spite of the dislocations at the face center.

IV. CLOSING REMARKS

The above simulations, as well as most earlier efforts to model surface morphologies, are based on the supersaturation/temperature and bond strength/temperature parameters $\Delta\mu/kT$ and ϕ/kT, respectively. These are highly idealized scaling parameters, which require utmost caution in attempts to *quantitatively* compare the model predictions with actual experiments.

Specifically, it must be reemphasized that, as discussed in section II.A in connection with Eq.2, the chemical potential difference or supersaturation used in these models is *not equal* to the bulk nutrient supersaturation typically determined by the experimentalist. This chemical potential difference is solely that part of the overall difference that drives the attachment of growth units once they have been transported to the interfacial region, say to within a mean free path of the growing surface. Though possible in principle, no unambiguous measurements of this interfacial supersaturation have become available as yet. However, all crystal growth theories, as well as measurements of interfacial undercoolings in facetted and non-facetted regions of an interface that grows from a melt [49,50] indicate that this interfacial chemical potential difference necessary to

drive a certain attachment (growth) rate depends on the local interface morphology (kink and step density, etc.) and, thus, on the locally governing growth mechanism. This fact is ignored by all modelling at this point by fixing the interfacial $\Delta\mu$ irrespective of the "underlying" surface morphology.

With respect to correlations of the bond or pair interaction energies, used in these models, with values of actual systems, similar caution is required. In addition to the fact that the simple, highly symmetric bond picture is hardly an accurate representation for actual atomic (quantum mechanical) interactions, one must realize that the magnitudes for bond strengths are traditionally derived from averaged bulk properties, rather than the (relaxed) surface states that govern the attachment kinetics. Some, small improvement of this coarse description, based on a "variable bond model", has been made by our group earlier.[51]

The above material shows that current kinetic crystal growth modelling can provide considerable physical insight into the effect of various growth parameters. Yet, it is also clear that much more experimental and theoretical work is required before quantitative fidelity can be expected.

Acknowledgements

The authors are grateful for the support provided by the Microgravity Science and Applications Division of the National Aeronautics and Space Administration under Grant No. NAG1-972. This research has also been supported by the State of Alabama through the Center for Microgravity and Materials Research at the University of Alabama in Huntsville, and the Alabama Supercomputer Network.

References

1 A. A. Chernov, in *Crystal Growth*, edited by H. S. Peiser (Pergamon, Oxford 1967), p.25.

2 A. A. Chernov and J. Lewis, J. Phys. Chem. Sol. **28**, 2185 (1967).

3 V. O. Esin, V. I. Danilyuk and V. N. Porozkov, Phys. Stat. Sol. (a) **81**, 163 (1984).

4 V. O. Esin, L. P. Tarabaev, V. N. Porozkov and I. A. Vdovina, J. Crystal Growth **66**, 459 (1984).

5 G. H. Gilmer and P. Bennema, J. Crystal Growth **13/14**, 148 (1972).

6 H. J. Leamy and K. A. Jackson, J. Appl. Phys. **42**, 2121 (1971) .

7 H. J. Leamy and G. H. Gilmer, J. Crystal Growth **24/25**, 499 (1974).

8 H. J. Leamy, G. H. Gilmer and K. A. Jackson, in *Surface Physics of Materials I*, edited by J. B. Blakely (Academic Press, New York, 1975), p. 121, and references therein.

9 R. H. Swendsen, Phys. Rev. B**15**, 5421 (1977).

10 V. O. Esin and L. P. Tarabaev, Phys. Stat. Sol. (a) **90**, 425 (1985) .

11 G. H. Gilmer and P. Bennema, J. Appl. Phys. **43**, 1347 (1972).

12 H. Müller-Krumbhaar, in *Monte Carlo Methods in Statistical Physics*, edited by K. Binder (Springer, Berlin, 1979), p.261, and references therein.

13 P. Bennema and J. P. Van der Eerden, in *Morphology of Crystals,* Part A, edited by I. Sunagawa (Terra, Tokyo, 1987), p.1; A. A. Chernov and T. Nishinaga, ibid, p.207 .

14 D. E. Temkin, in *Crystallization Processes* (Consultant Bureau, New York, 1966), p.15.

15 R. F. Xiao, J. I. D. Alexander and F. Rosenberger, Phys. Rev. A **38**, 2447 (1988).

16 R. F. Xiao, J. I. D. Alexander and F. Rosenberger, J. Crystal Growth **100**, 313 (1990).

17 Y. Saito and T. Ueta, Phys. Rev. A **40**, 3408 (1989).

18 S. Krukowski and F. Rosenberger, J. Chem. Phys.(submitted).

19 W. W. Mullins and R. F. Sekerka, J. Appl. Phys. **35**, 444 (1964).

20 J. S. Langer, Rev. Mod. Phys. **52**, 1 (1980).

21 A. A. Chernov, J. Crystal Growth **24/25**, 11 (1974).

22 C. Nanev and D. Iwanov, J. Crystal Growth **3/4**, 530 (1968).

23 D. Nenow and V. Stoyanova, J. Crystal Growth **41**, 73 (1977).

24 C. Nanev and D. Iwanov, Crystal Res. Technol. **17**, 575 (1982).

25 D. Nenow and V. Stoyanova and N. Genadiev, J. Crystal Growth **66**, 489 (1984).

26 M. Staynova and C. Nanev, Crystal Res. Technol. **24**, 951 (1989).

27 T. A. Witten and L. M. Sander, Phys. Rev. B **27**, 5686 (1983).

28 W. K. Burton, N. Cabrera and F. C. Frank, Trans. Roy. Soc. A **243**, 299 (1951) .

29 F. C. Frank, Disc. Faraday Soc. **48,** 67 (1949).

30 L. J. Griffin, Phil. Mag. **41**, 196 (1950) .

31 H. Bethge, Phys. Stat. Sol. **2**, 3 (1962).

32 K. W. Keller, in *Crystal Growth and Characterization,* Proceedings of the ISSCG2 Springschool, Japan, 1974, edited by R. Ueda and J. B. Mullin (North-Holland, Amsterdam, 1975), p. 361.

33 K. Tsukamoto, J. Crystal Growth **61**, 199 (1983).

34 I. Sunagawa and P. Bennema, in *Preparation and Properties of Solid State Materials,* Vol. 7, edited by W. R. Wilcox (Marcel Dekker, New York, 1982), p. 1, and references therein.

35 N. Cabrera and M. M. Levine, Phil. Mag. **1**, 450 (1956).

36 R. Kaishev, Crystal Growth **3,** 29 (1962).

37 T. Surek, J. P. Hirth and G. M. Pound, J. Crystal Growth **18,** 20 (1973).

38 H. Müller-Krumbhaar, T. W. Burkhardt and D. M. Kroll, J. Crystal Growth **38,** 13 (1977).

39 R. H. Swendsen, P. J. Kortman, D. P. Landau and H. Müller-Krumbhaar, J. Crystal Growth **35**, 73 (1976).

40 G. H. Gilmer, J. Crystal Growth **35**, 15 (1976).

41 A. A. Chernov, Ann. Rev. Materials Science **3**, 397 (1973) .

42 C. E. Miller, J. Crystal Growth **42**, 357 (1977) .

43 G. H. Gilmer and K. A. Jackson, in *Current Topics in Materials Sciences*, Vol.2, edited by E. Kaldis and H. J. Scheel (North-Holland, Amsterdam, 1977), p.79.

44 J. D. Weeks, in *Ordering in Strongly Fluctuating Condensed Matter Systems*, edited by T. Riste (Plenum, New York, 1980), p.293.

45 K. K. Mon, S. Wansleben, D. P. Landau and K. Binder, Phys. Rev. Lett. **60**, 708 (1988).

46 P. Peczak and D. P. Landau, Phys. Rev. B **39,** 11932 (1989), and references therein.

47 F. C. Frank and W, T. Reed, Phys. Rev. **79**, 722 (1950).

48 W. R. Wilcox, J. Crystal Growth **38,** 73 (1977).

49 J. C. Brice, J. Crystal Growth **6**, 205 (1970).

50 T. Abe, J. Crystal Growth **24,** 463 (1974).

51 J.-S. Chen, N.-B. Ming and F. Rosenberger, J. Chem Phys. **84**, 2365 (1986).

Figure captions

Fig. 1. Schematics of simulation geometries. (a) Planar case: lateral dimensions 60 x 60 lattice constants, with periodic boundary condition in the x- and y-directions. Space between crystal surface and source contains nutrient through which growth units diffuse to the crystal surface. (b) Spherical case: growing crystal in center of spherical source. Pyramidal section is used with periodic boundary conditions in azimuthal direction for simulation of 3-D growth morphology at low temperatures; see text.

Fig. 2. Flowchart of simulation steps.

Fig. 3. Effect of temperature and bond strength on crystal surface morphologies at fixed supersaturation, $\Delta\mu / kT = 0.35$. Both surface and bulk diffusion are excluded. (a) $\phi/kT=3.9$, (b) $\phi/kT=2.0$, (c) $\phi/kT=1.6$, (d) $\phi/kT=1.4$.

Fig. 4. Normalized surface area as function of number of attached particles (in units of full layer, i.e., 3600 particles). The normalization is based on the area of a perfectly smooth surface. The growth conditions are the same as in Fig.3.

Fig. 5. Effect of surface diffusion on surface morphologies at $\phi / kT = 1.6$ and $\Delta\mu / kT = 0.69$ without consideration of bulk diffusion. (a) without surface diffusion, (b) with surface diffusion.

Fig. 6. Dependence of average surface diffusion length on bond strength/temperature at two different supersaturations, $\Delta\mu / kT = 0.69$ and 3.0.

Fig. 7. Effect of the mean free path length in bulk diffusion on surface morphologies at $\phi / kT = 2.3$ and $\Delta\mu / kT = 3.0$. Surface diffusion is included. (a) $|a|=\infty$ (b) $|a| = 10b$, (c) $|a|=1b$.

Fig. 8. Effect of supersaturation on surface morphologies at $\phi / kT = 3.9$ and a mean free path of one lattice unit. (a) $\Delta\mu/kT=0.69$, (b) $\Delta\mu/kT=3.0$, (c) $\Delta\mu/kT=5.0$, (d) $\Delta\mu/kT=7.0$.

Fig. 9. Coverage of interfacial layers in the surface morphologies of Fig.8.

Fig. 10. Sticking probability P_i^s (Eq. 9) as a function of ϕ/kT and $\Delta\mu/kT$. For clarity, only P_1^s, P_3^s and P_5^s are shown.

Fig.11. Surface roughness and its derivative with respect to temperature as function of ϕ/kT at equilibrium ($\Delta\mu/kT=0$). The numbered arrows on the abscissa indicate roughening temperatures obtained earlier by .[7,9]

Fig. 12. Stability diagram for smooth (stable) and rough (unstable) growth morphologies as a function of ϕ/kT and $\Delta\mu/kT$. SD: with surface diffusion; BD: with bulk diffusion.

Fig. 13. Effect of noise reduction (multiple registration)[15] on surface morphologies at $\phi/kT = 3.9$. (a) $\Delta\mu/kT = 0.69$, without noise reduction; (b) $\Delta\mu/kT = 0.69$ with noise reduction; (c) $\Delta\mu/kT = 5.0$, without noise reduction; (d) $\Delta\mu/kT = 5.0$, with noise reduction.

Fig.14. Growth morphology of three dimensional cubic crystal in a spherical source at $\phi/kT = 2.3$ and $\Delta\mu/kT = 0.69$. Noise reduction through multiple-registration. (a,b) $|a| =1b$, (c, d) $|a| =5b$.(a) On addition of 6340 particles to nucleus with 21x21x21; (b) Further addition of 31056 particles to (a); (c) On addition of 28828 particles to nucleus with 47x47x47; (d) Further addition of 52542 particles to (c)

Fig.15. Normalized total surface area as function of crystal size for a growing cubic crystal The growth conditions are the same as in Fig.13a and b.

Fig. 16. Dependence of critical size on mean free path at $\Delta\mu/kT = 0.69$ and various ϕ/kT for both 2D[16] and 3D results.

Fig. 17. Time evolution of growth step originating at single screw dislocation .$\phi/kT = 5.0$ and $\Delta\mu/kT=0.69$. (a) initial straight step, (b) after attachment of 1000 particles, (c) after attachment of 5000 particles.

Fig.18. Bond strength/temperature dependence of surface morphology of face with a single dislocation. $\Delta\mu/kT=0.69$. Both surface and bulk diffusion are ignored.
(a) $\phi/kT = 5.3$, (b) $\phi/kT = 4.6$, (c) $\phi/kT = 3.0$, (d) $\phi/kT = 2.0$.

Fig. 19. Bond strength/temperature dependence of surface morphology of face with a pair of dislocations with opposite sign. $\Delta\mu/kT=0.69$. Attachment of isolated particles suppressed, both surface and bulk diffusion are ignored. (a) $\phi/kT = 5.3$, (b) $\phi/kT = 4.6$, (c) $\phi/kT = 3.9$.

Fig. 20. Supersaturation dependence of surface morphology with a single screw dislocation. $\phi/kT = 5.3$. Both surface and bulk diffusion are ignored. (a) $\Delta\mu/kT=0.69$, (b) $\Delta\mu/kT=2.0$, (c) $\Delta\mu/kT=3.0$.

Fig. 21. Effect of surface diffusion on surface morphology with a single screw dislocation. Same growth conditions as in Fig.20. Bulk diffusion is neglected.

Fig. 22. Effect of surface and bulk diffusion on surface morphology with a single screw dislocation with same growth conditions as in Fig.20.

Fig. 23. Growth morphology of a cubic crystal in a spherical source. The growth conditions are the same as in Fig.14b. Different faces on the same crystal, (a) all faces without defects, (b) top face with pair of dislocations of opposite sign.

Fig. 24. Growth morphology of a dislocated face in a spherical source at $\phi/kT = 5.3$ with bulk and surface diffusion, and unsuppressed formation of 2D nuclei. (a) $\Delta\mu/kT=0.69$, (b) $\Delta\mu/kT=2.0$, (c) $\Delta\mu/kT=3.0$.

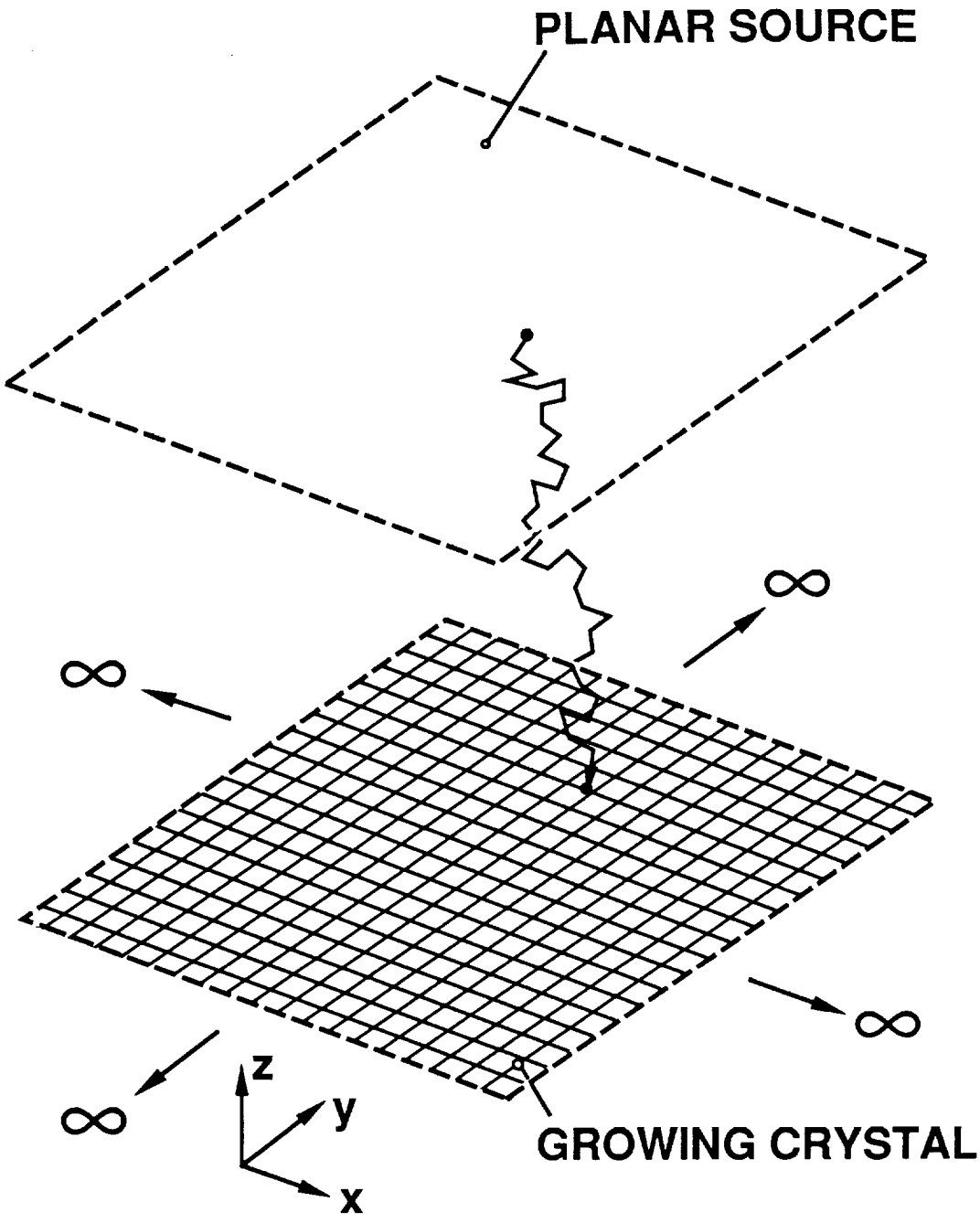

FIG. 1a

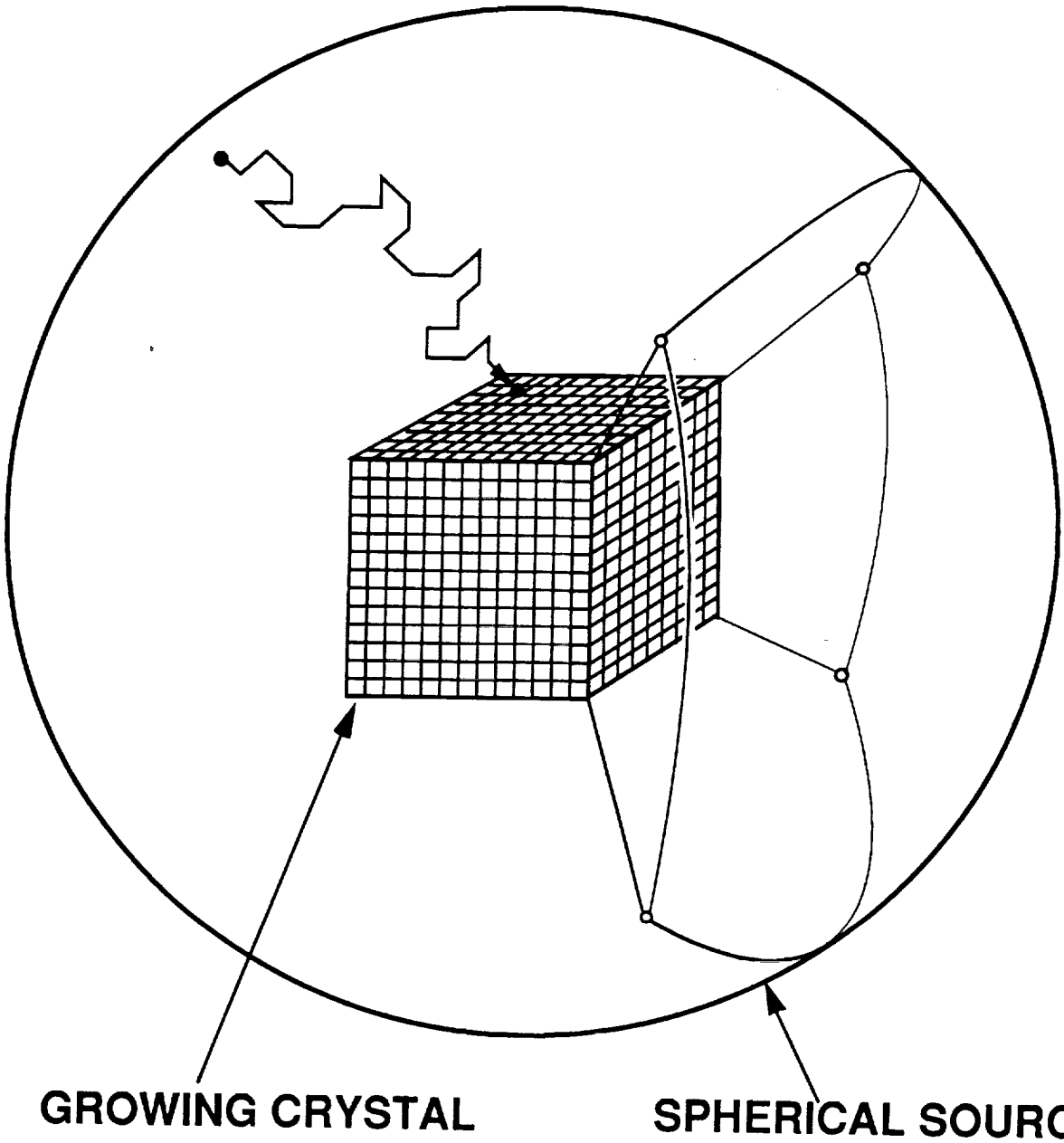

FIG.1b

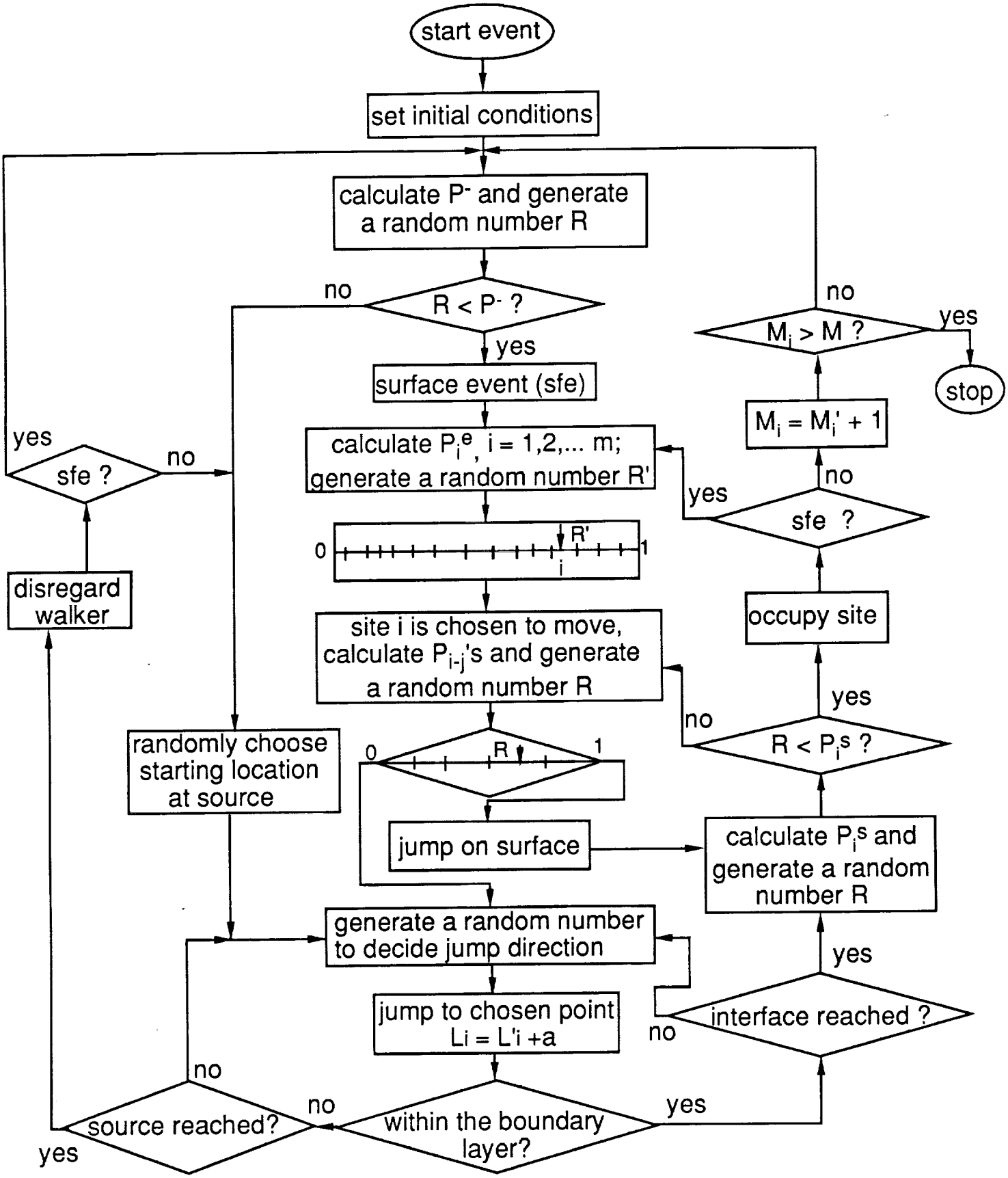
start event
set initial conditions
calculate P- and generate a random number R
R < P- ?
no
yes
surface event (sfe)
calculate Pi e, i = 1,2,... m; generate a random number R'
0
R'
i
1
site i is chosen to move, calculate Pi-j's and generate a random number R
0
R
1
jump on surface
generate a random number to decide jump direction
jump to chosen point Li = L'i +a
within the boundary layer?
no
yes
source reached?
no
yes
randomly choose starting location at source
sfe ?
yes
no
disregard walker
calculate Pi s and generate a random number R
R < Pi s ?
no
yes
occupy site
sfe ?
yes
no
Mi = Mi' + 1
Mi > M ?
no
yes
stop
interface reached ?
no
yes

FIG.2

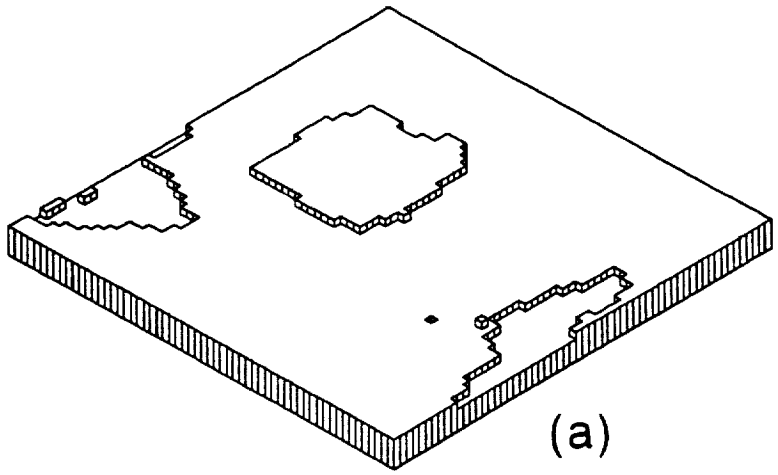

(a)

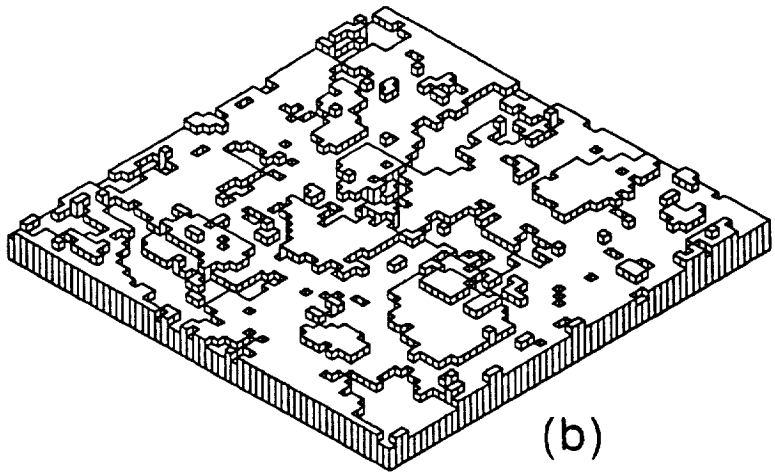

(b)

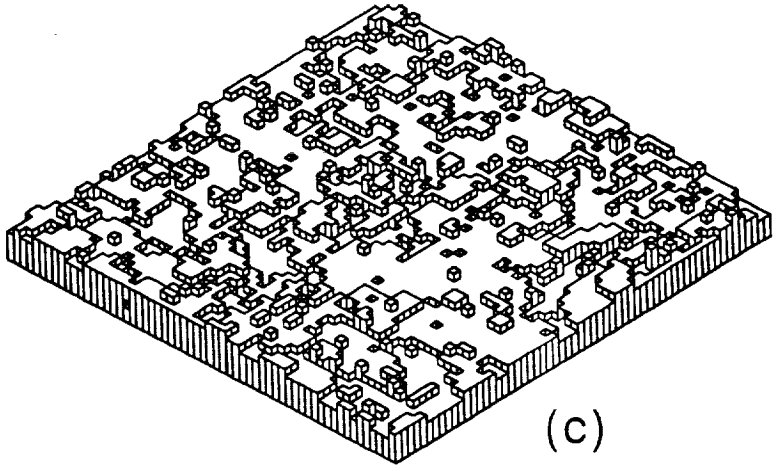

(c)

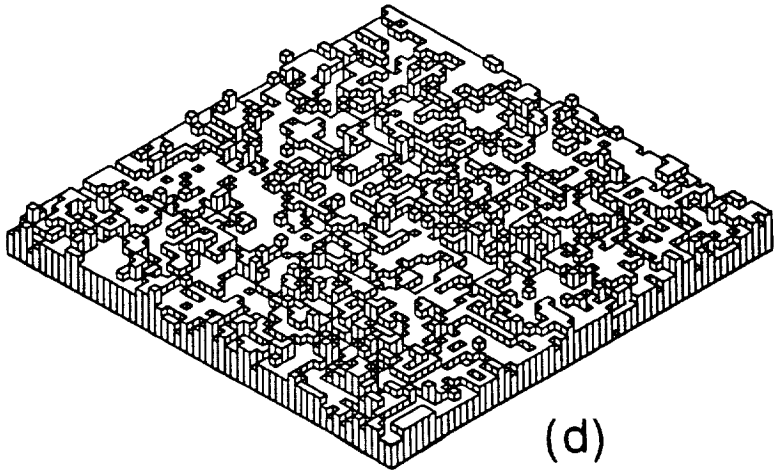

(d)

FIG. 3

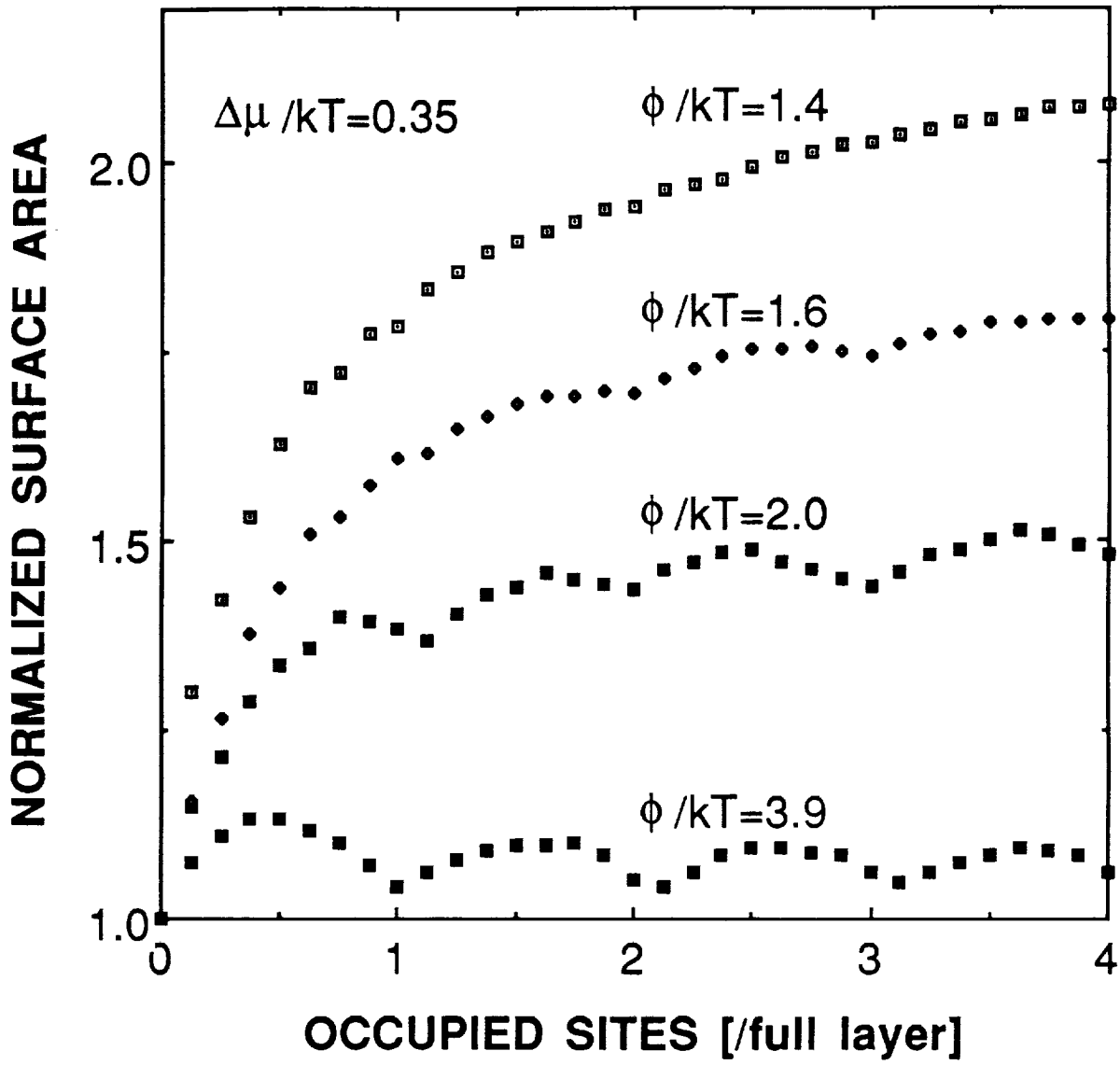
Δμ /kT=0.35
ϕ /kT=1.4
ϕ /kT=1.6
ϕ /kT=2.0
ϕ /kT=3.9
NORMALIZED SURFACE AREA
2.0
1.5
1.0
0
1
2
3
4
OCCUPIED SITES [/full layer]

FIG.4

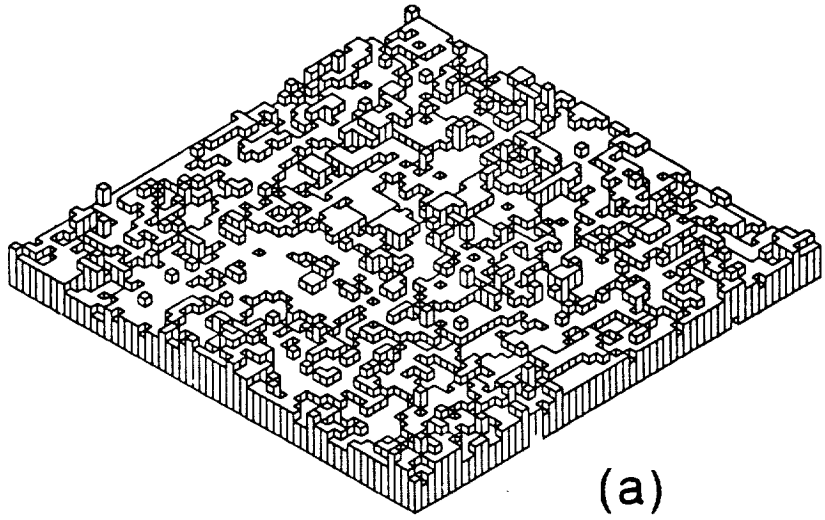

(a)

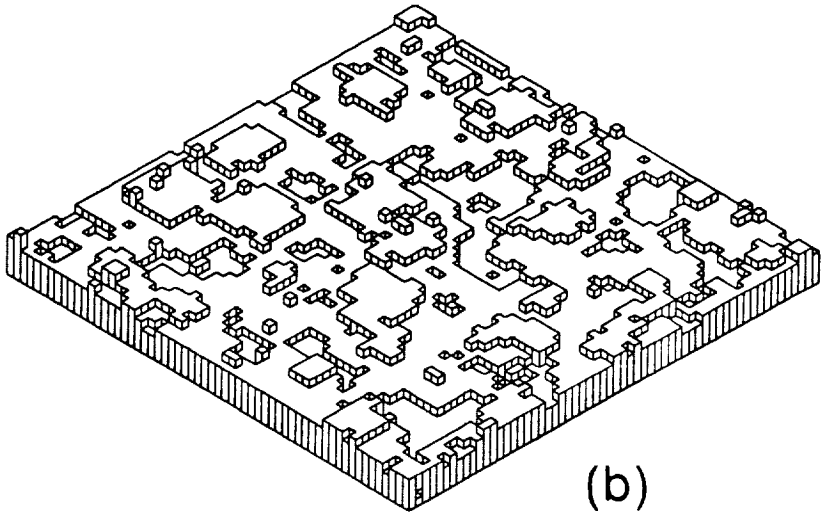

(b)

FIG.5

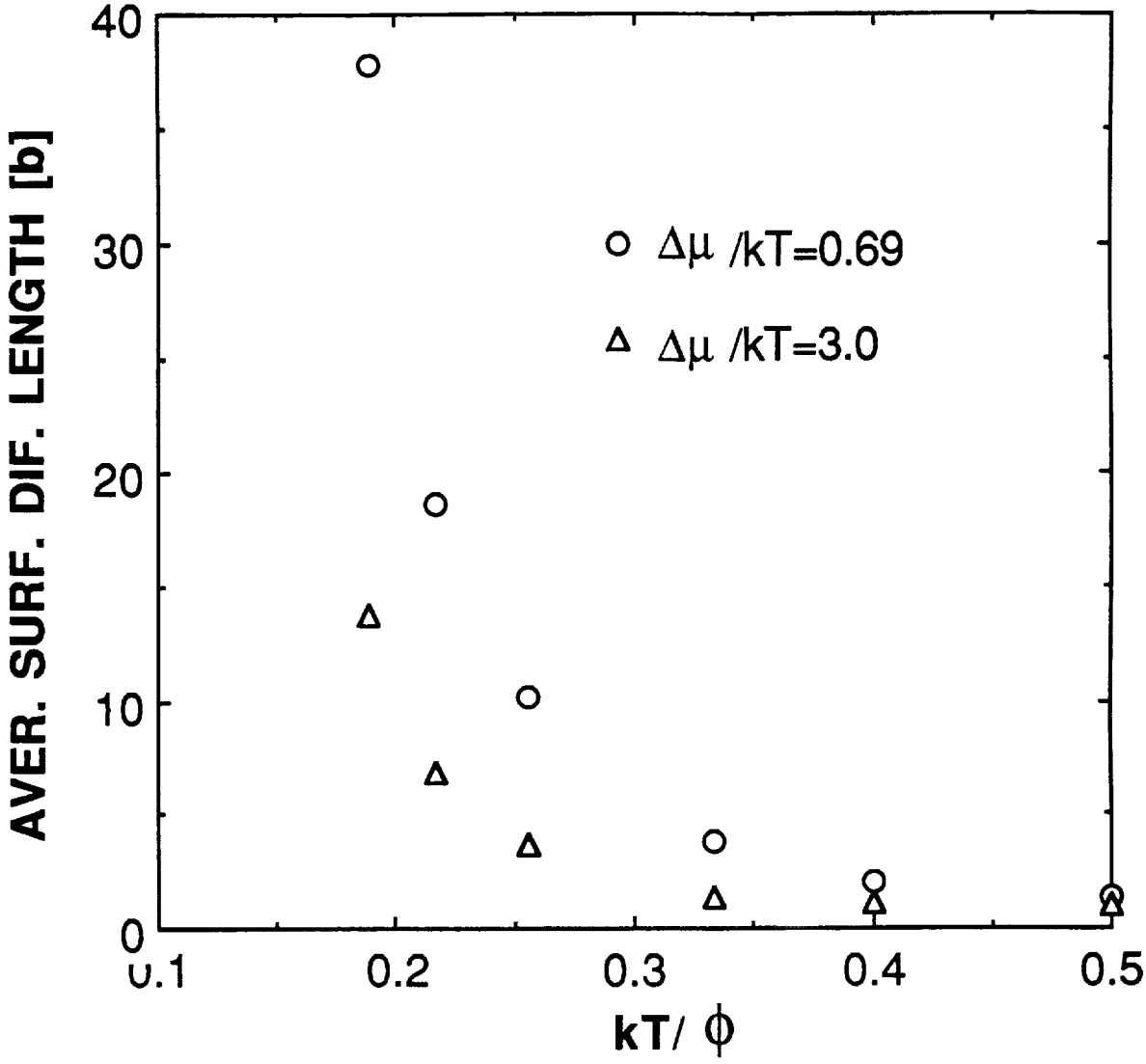
40
30
20
10
0
υ.1
0.2
0.3
0.4
0.5
AVER. SURF. DIF. LENGTH [b]
kT/ ϕ
Δμ /kT=0.69
Δμ /kT=3.0

FIG.6

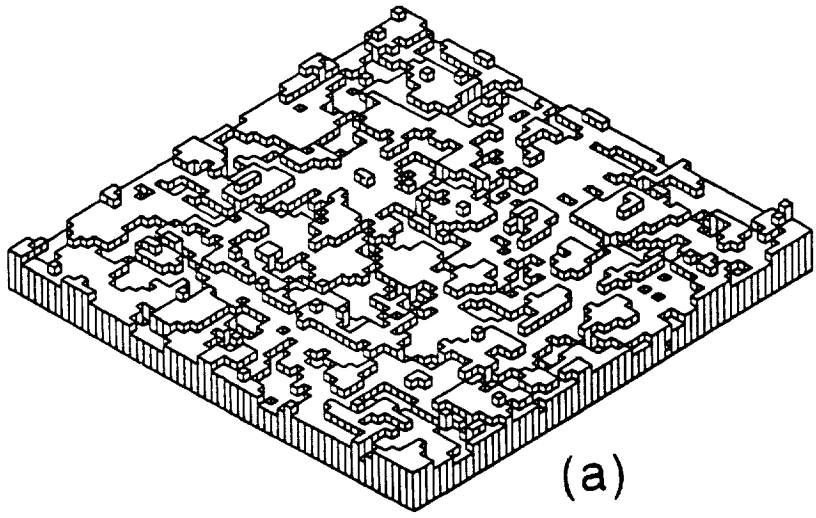

(a)

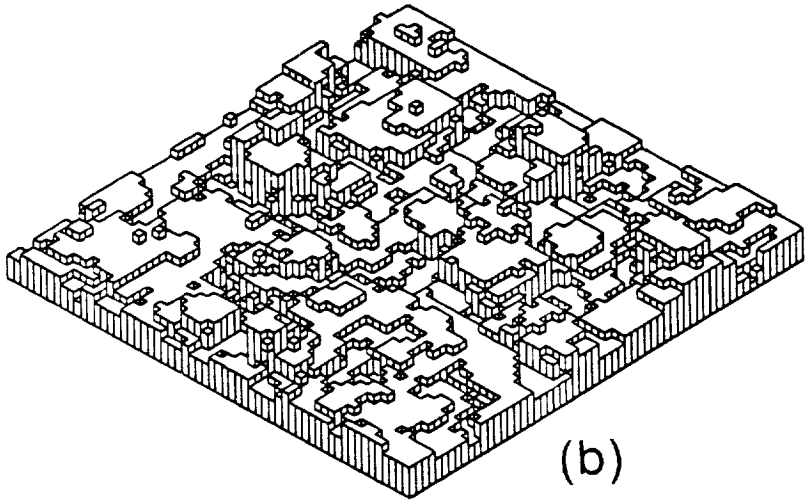

(b)

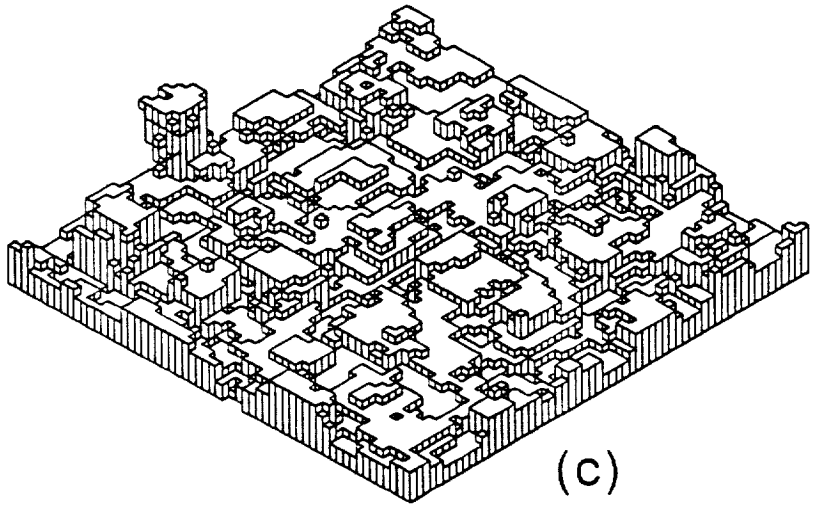

(c)

FIG.7

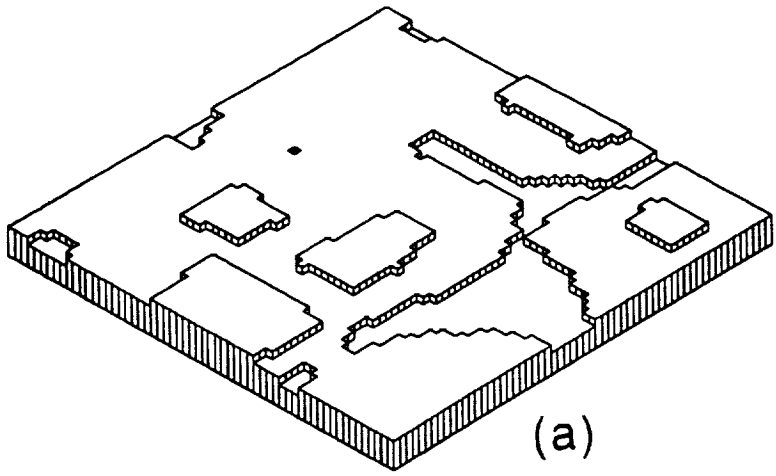

(a)

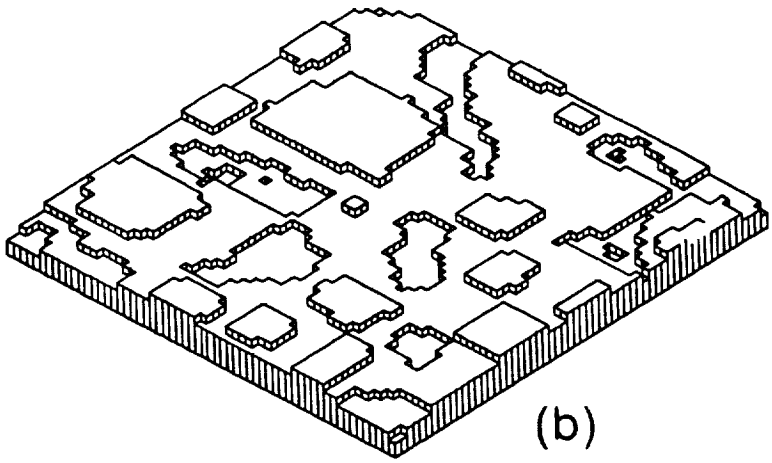

(b)

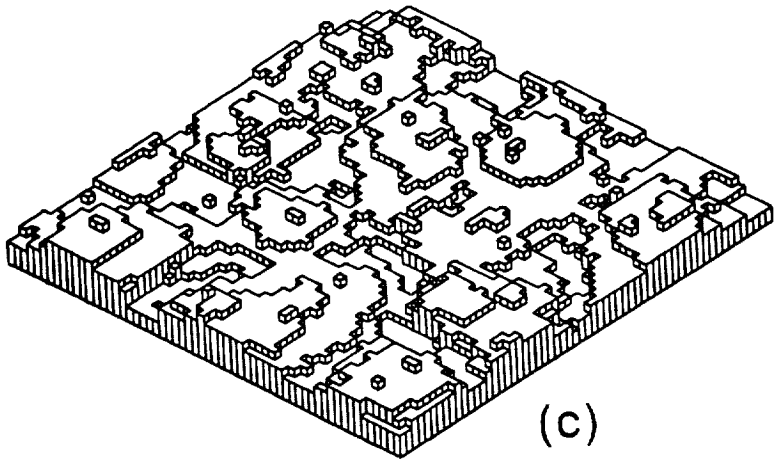

(c)

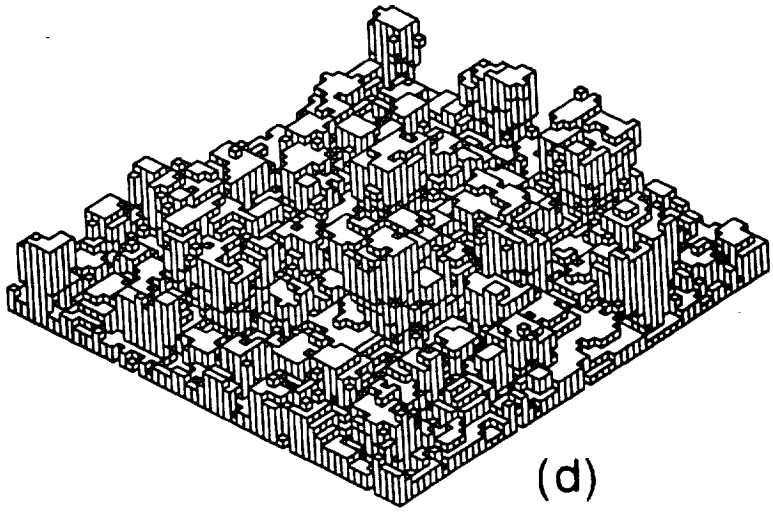

(d)

FIG. 8

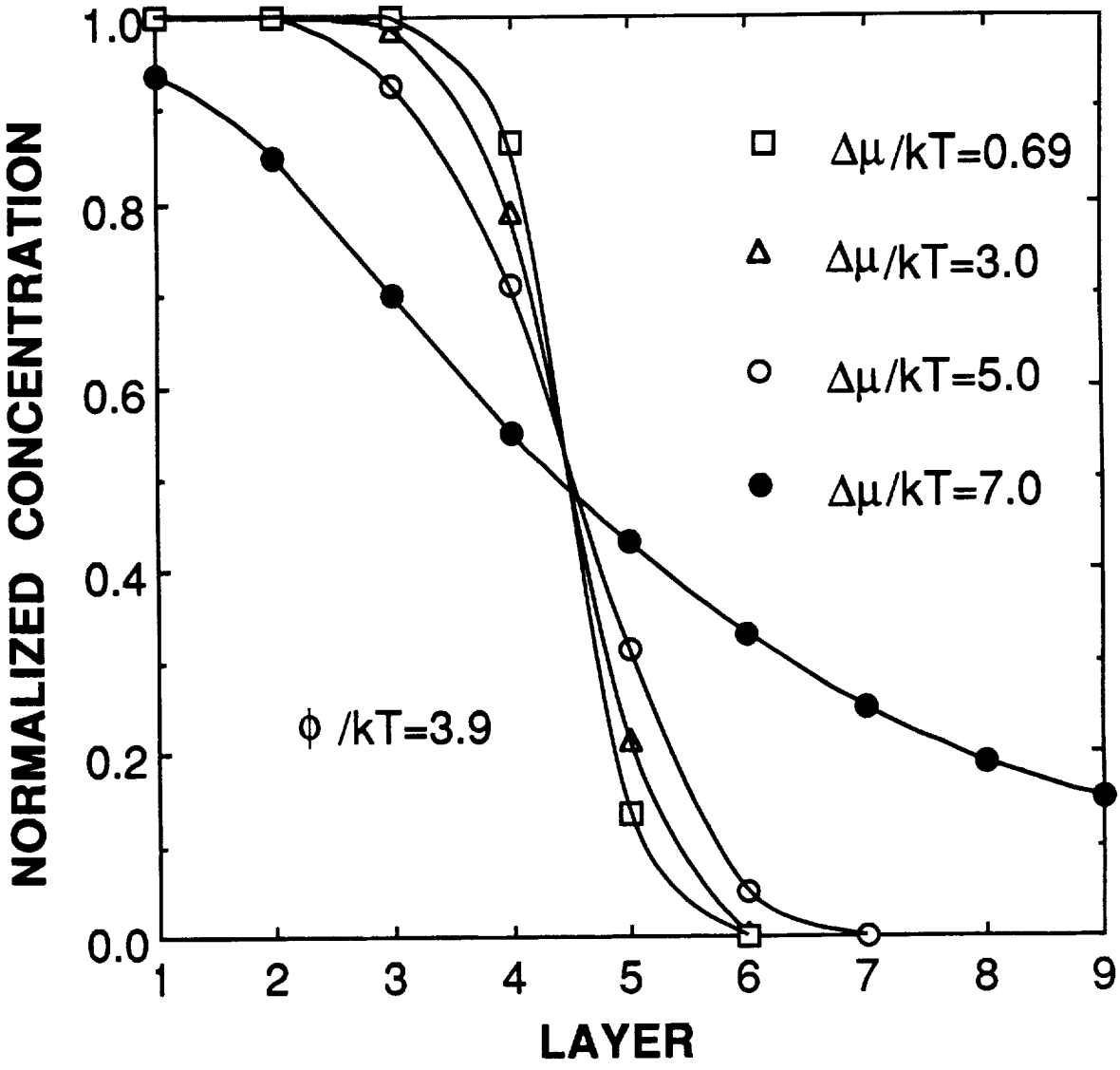
NORMALIZED CONCENTRATION
1.0
0.8
0.6
0.4
0.2
0.0
1
2
3
4
5
6
7
8
9
LAYER
Δμ/kT=0.69
Δμ/kT=3.0
Δμ/kT=5.0
Δμ/kT=7.0
φ /kT=3.9

FIG.9

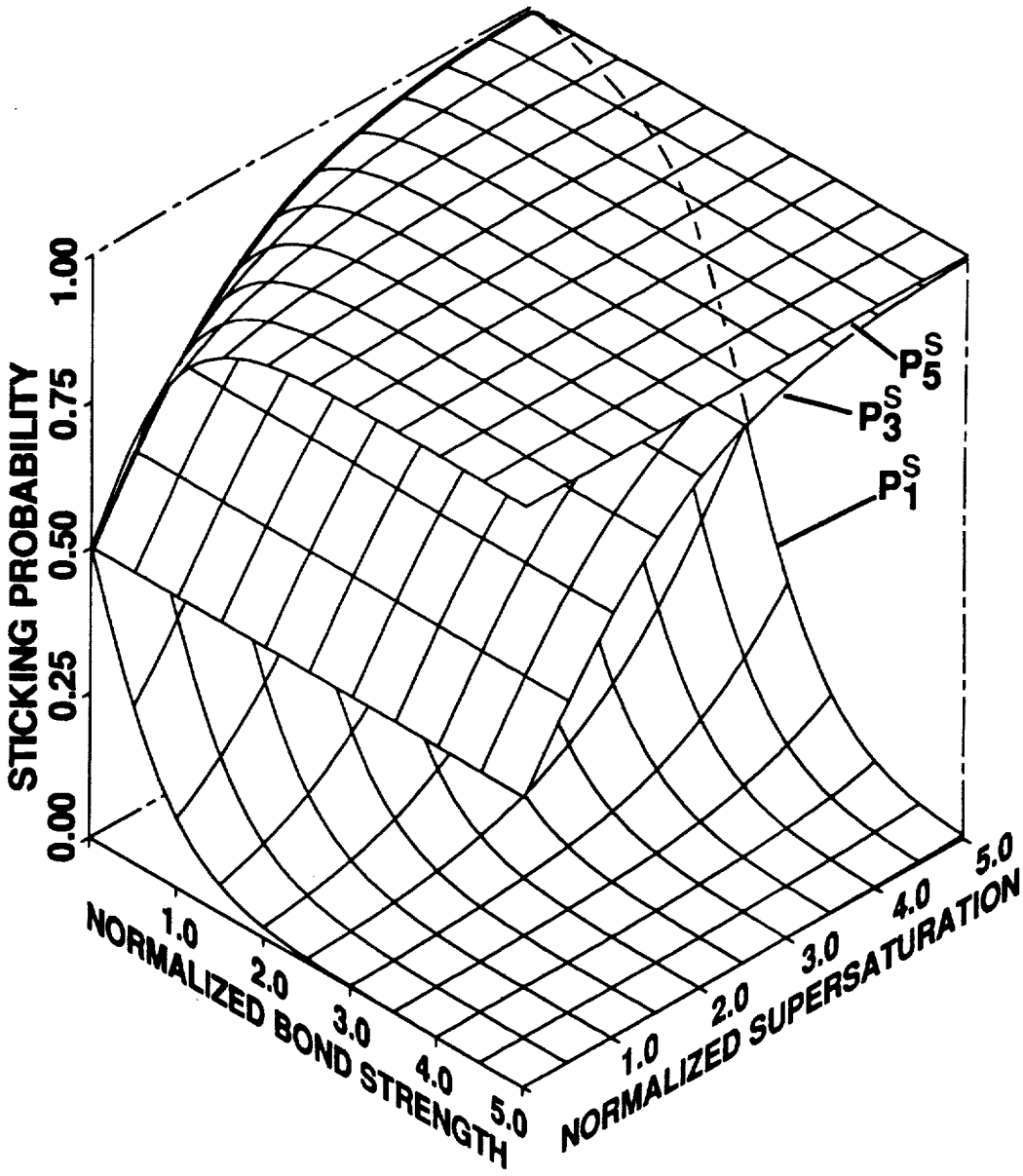
STICKING PROBABILITY
0.00
0.25
0.50
0.75
1.00
NORMALIZED BOND STRENGTH
1.0
2.0
3.0
4.0
5.0
NORMALIZED SUPERSATURATION
1.0
2.0
3.0
4.0
5.0
P_5^S
P_3^S
P_1^S

FIG. 10

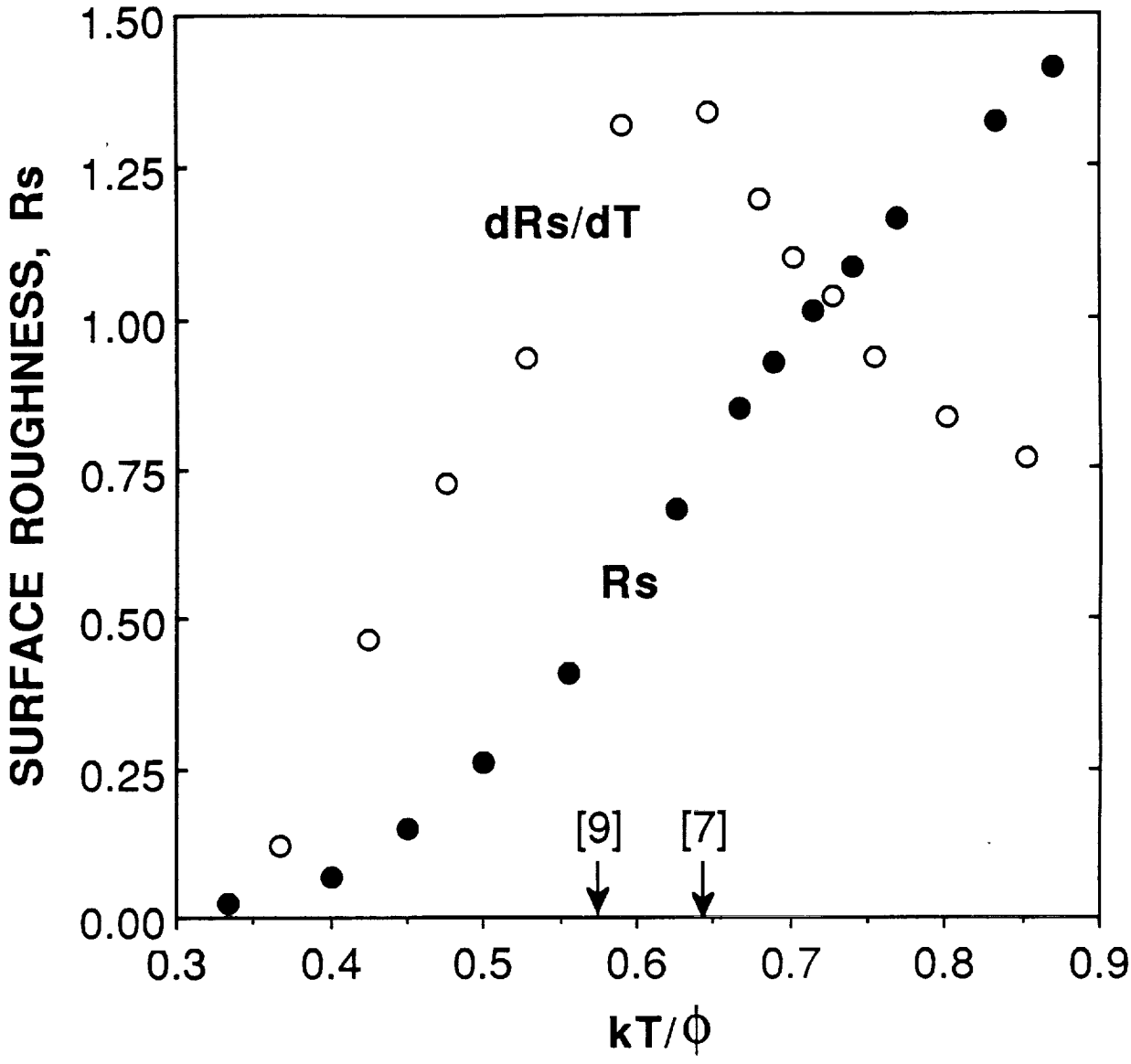
SURFACE ROUGHNESS, Rs
1.50
1.25
1.00
0.75
0.50
0.25
0.00
0.3
0.4
0.5
0.6
0.7
0.8
0.9
kT/ϕ
dRs/dT
Rs
[9]
[7]

FIG. 11

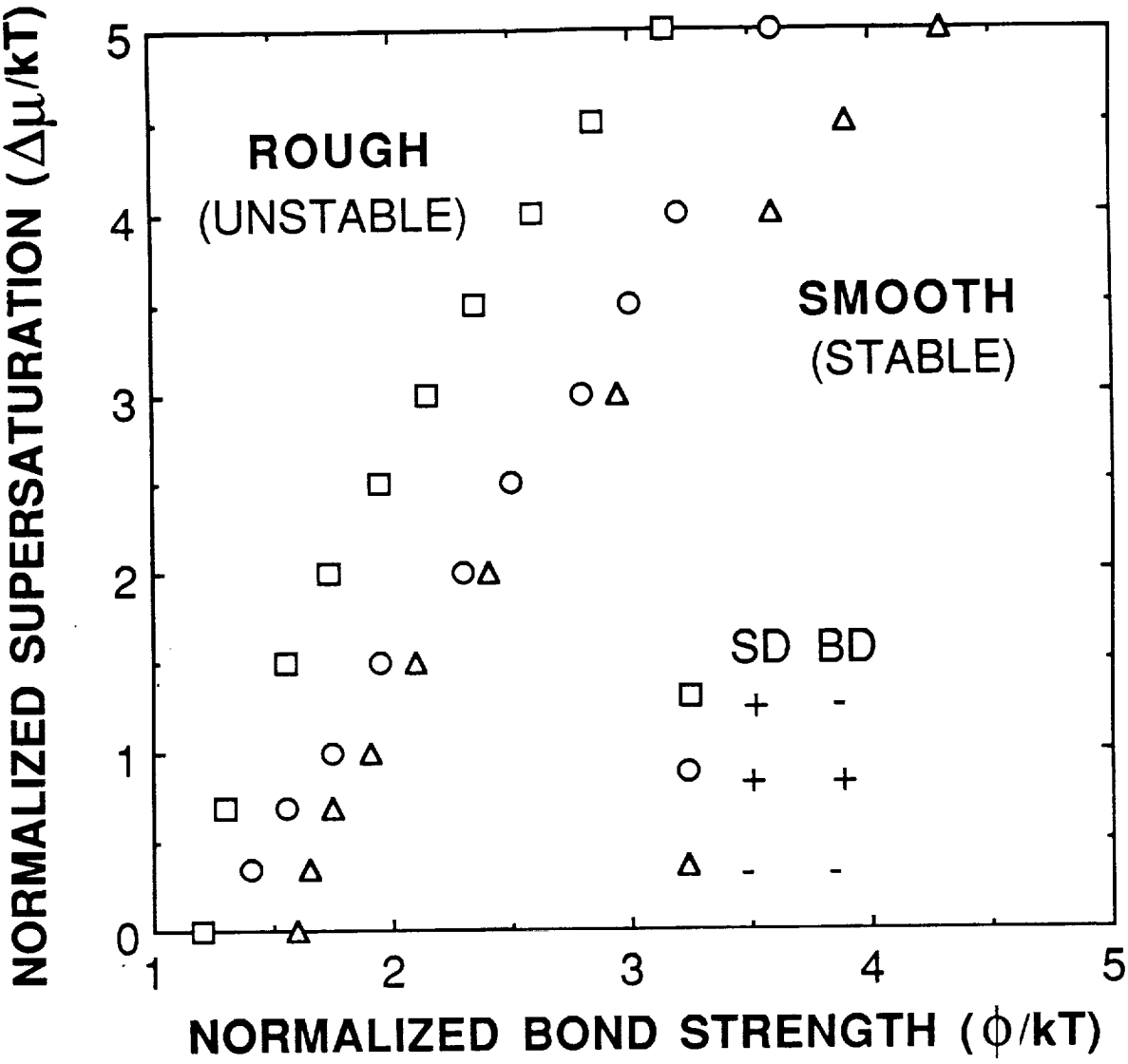
NORMALIZED SUPERSATURATION (Δμ/kT)
NORMALIZED BOND STRENGTH (ϕ/kT)
ROUGH
(UNSTABLE)
SMOOTH
(STABLE)
SD BD
+ -
+ +
- -
0
1
2
3
4
5

FIG. 12

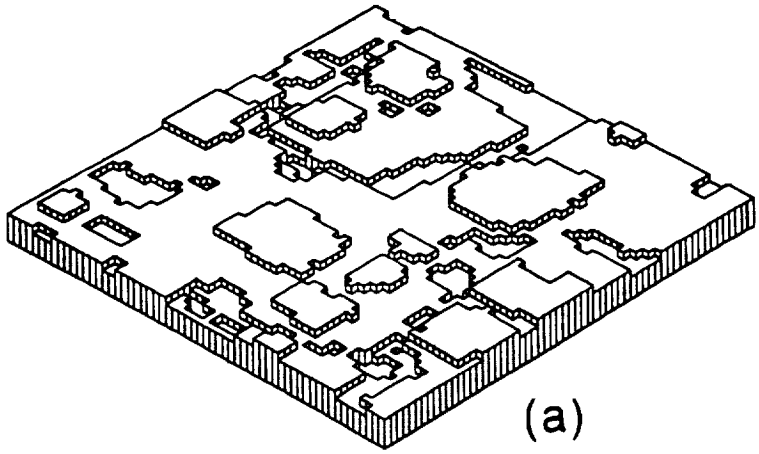

(a)

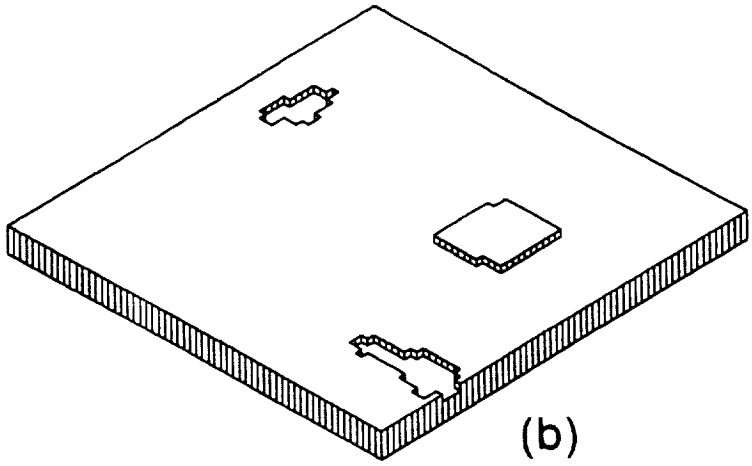

(b)

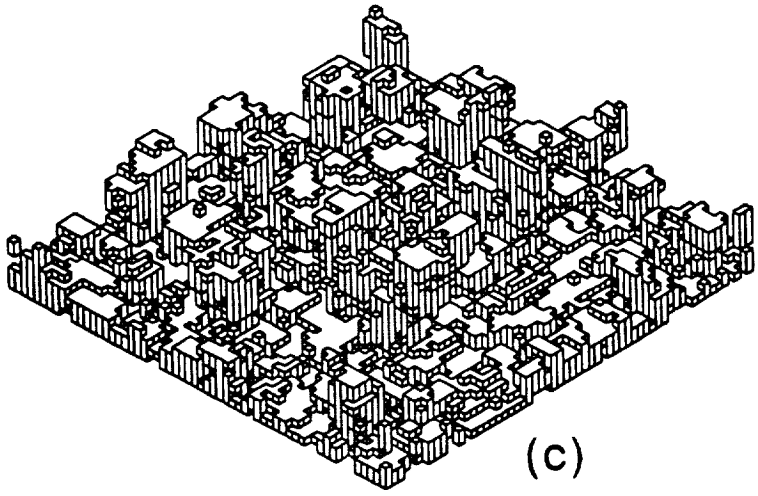

(c)

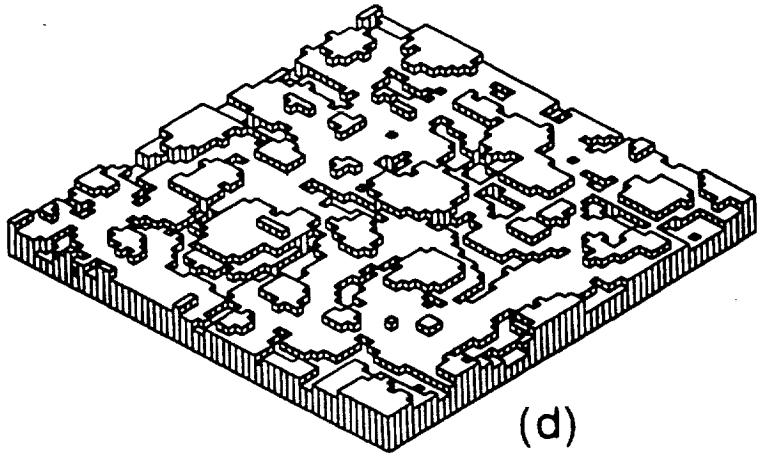

(d)

FIG. 13

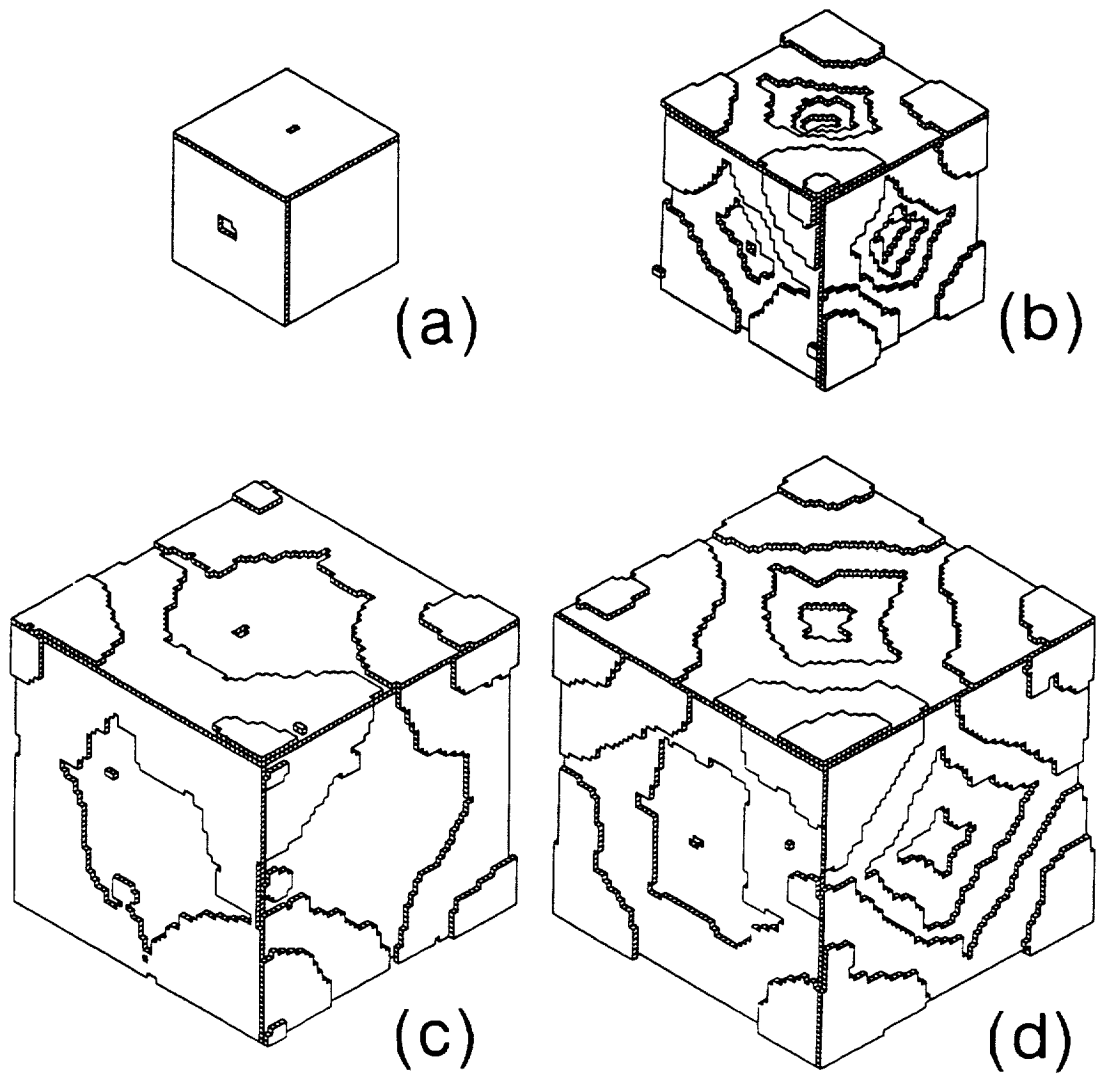

FIG.14

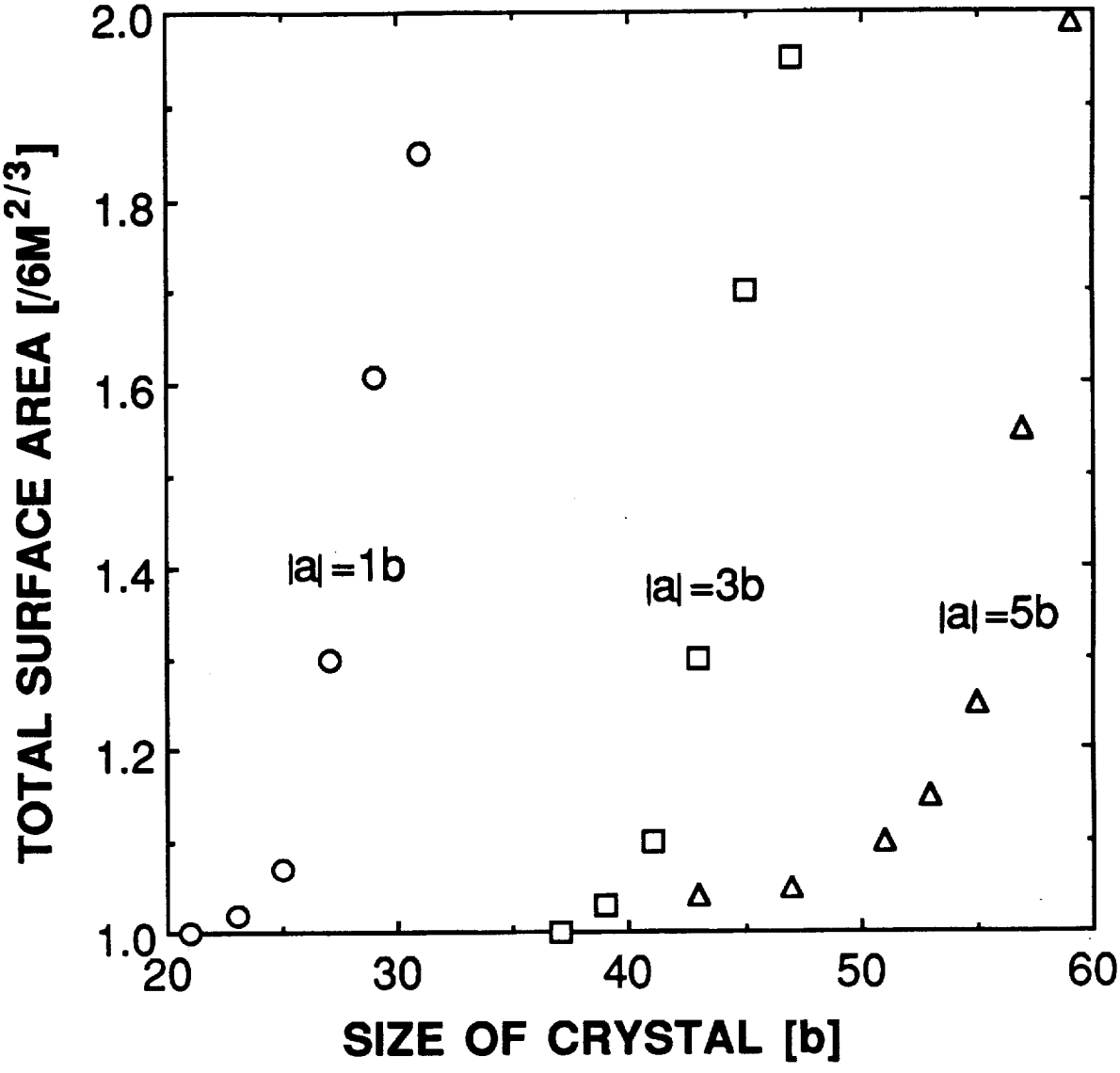
2.0
1.8
1.6
1.4
1.2
1.0
20
30
40
50
60
TOTAL SURFACE AREA [/6M^2/3]
SIZE OF CRYSTAL [b]
|a|=1b
|a|=3b
|a|=5b

FIG.15

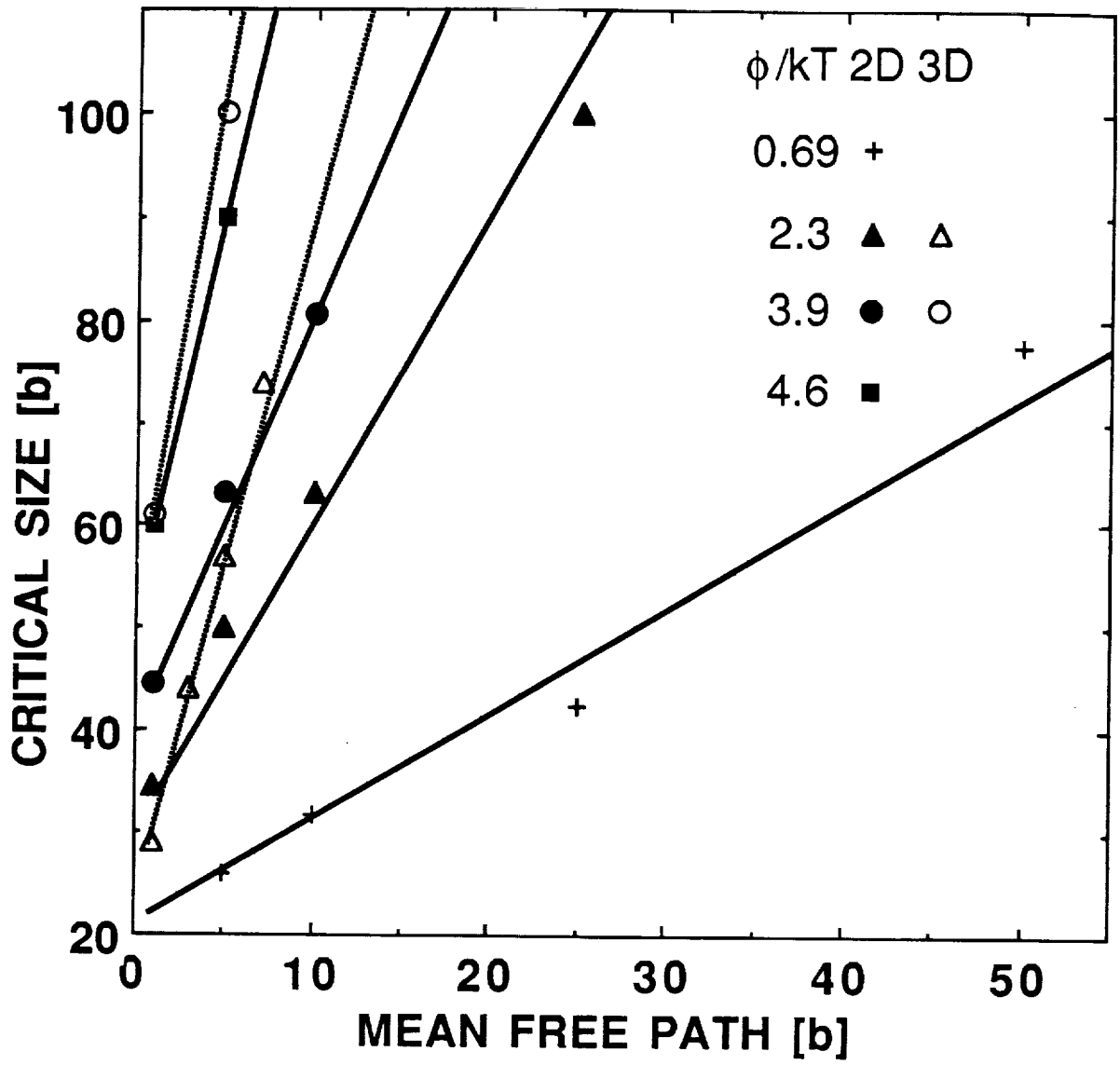
φ/kT 2D 3D
0.69 +
2.3 ▲ △
3.9 ● ○
4.6 ■
CRITICAL SIZE [b]
MEAN FREE PATH [b]
100
80
60
40
20
0
10
20
30
40
50

FIG. 16

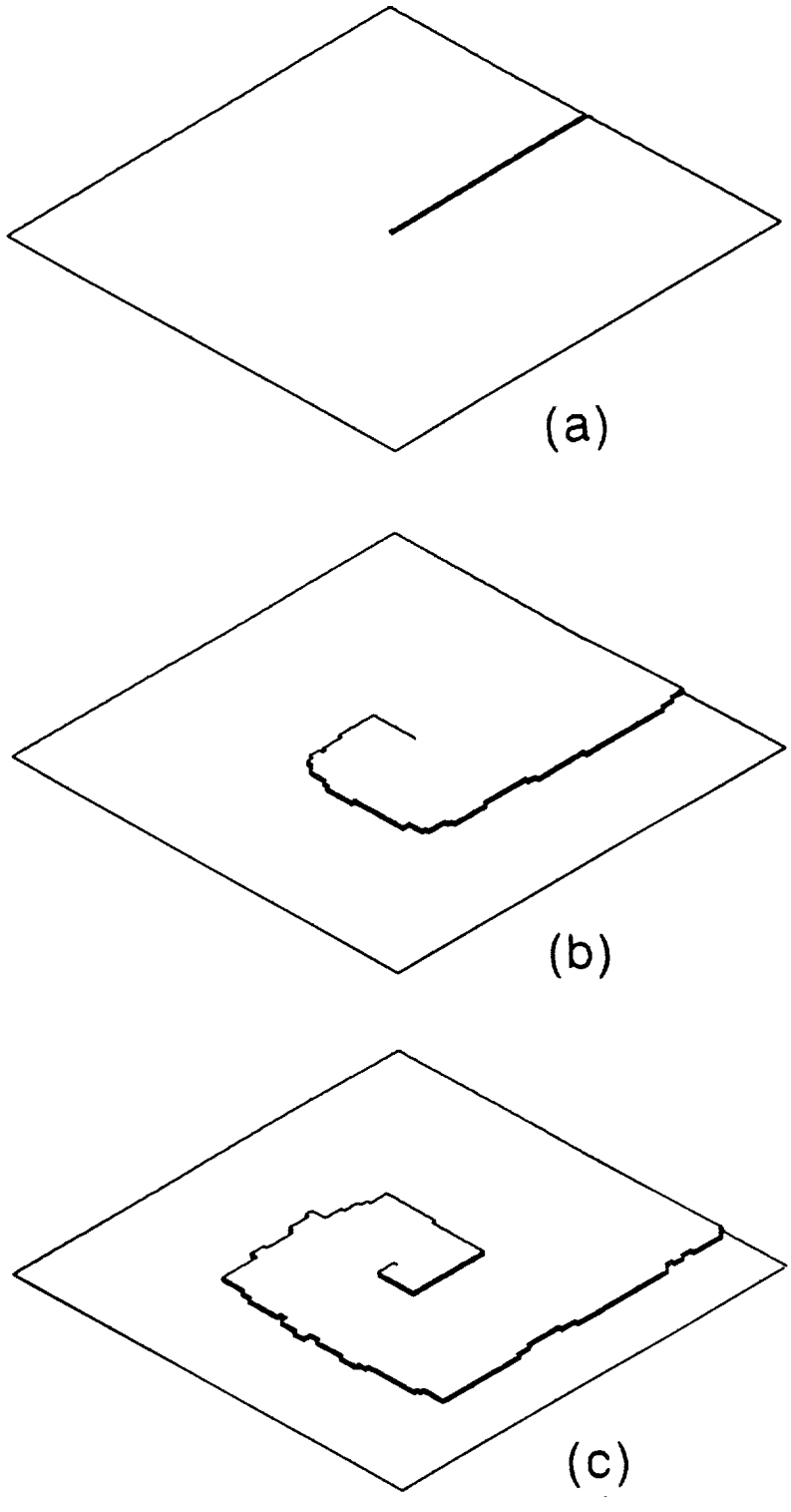

FIG.17

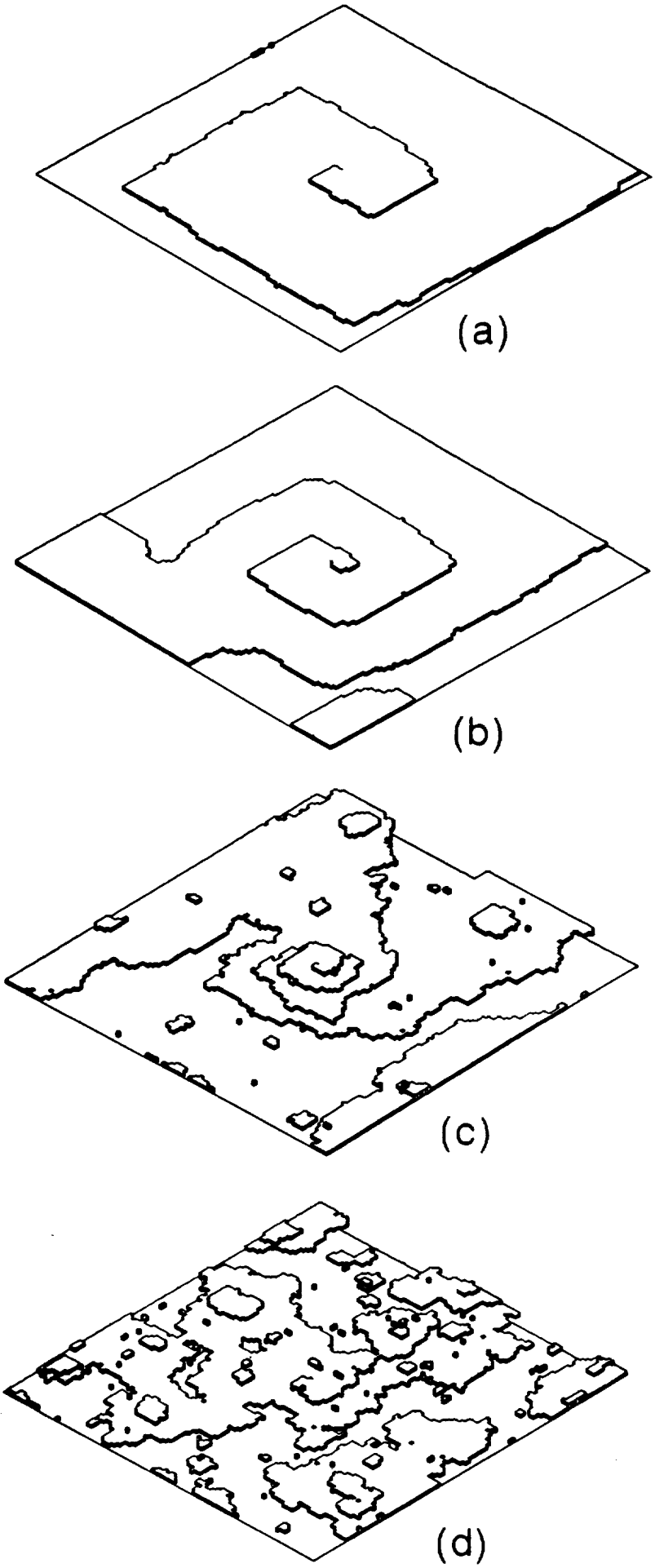

FIG. 18

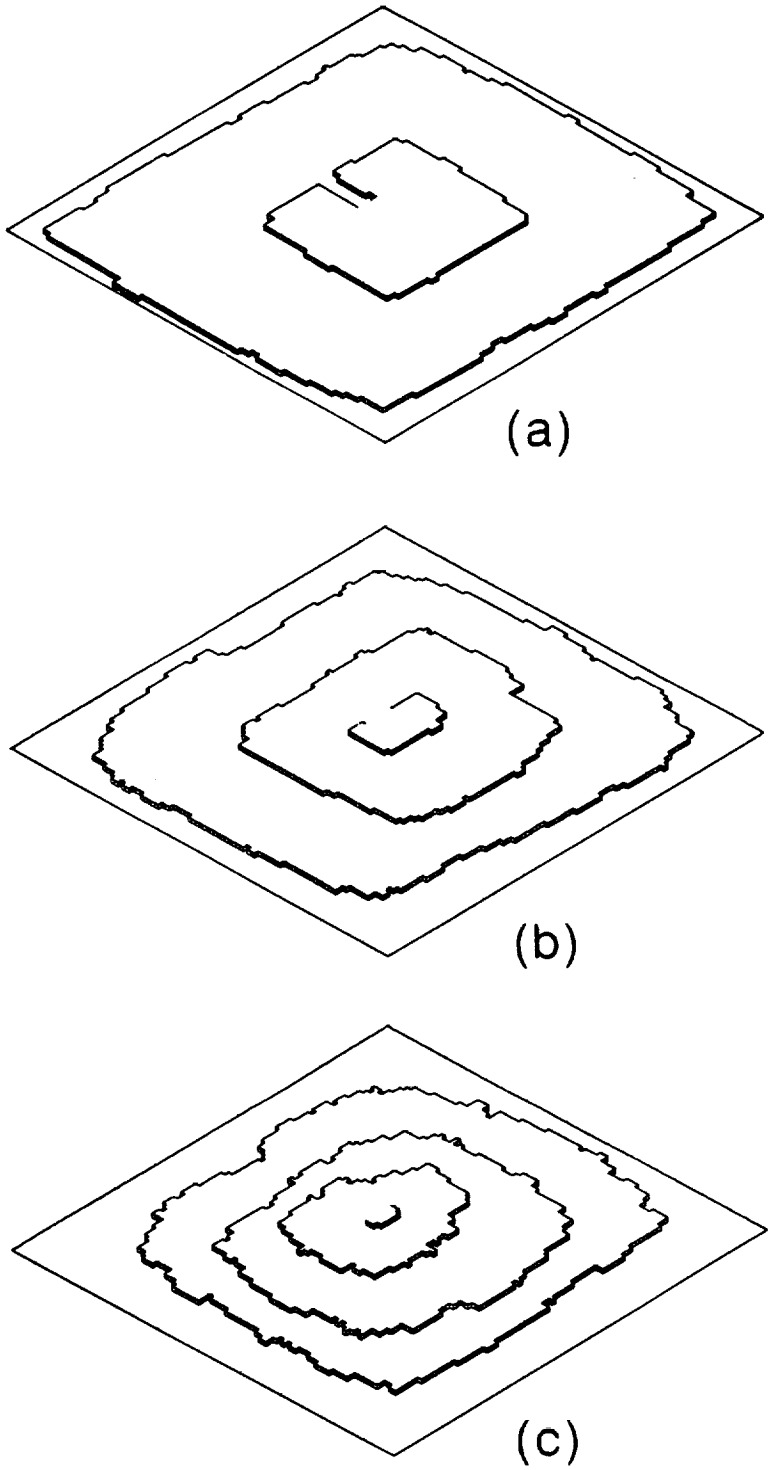

FIG.19

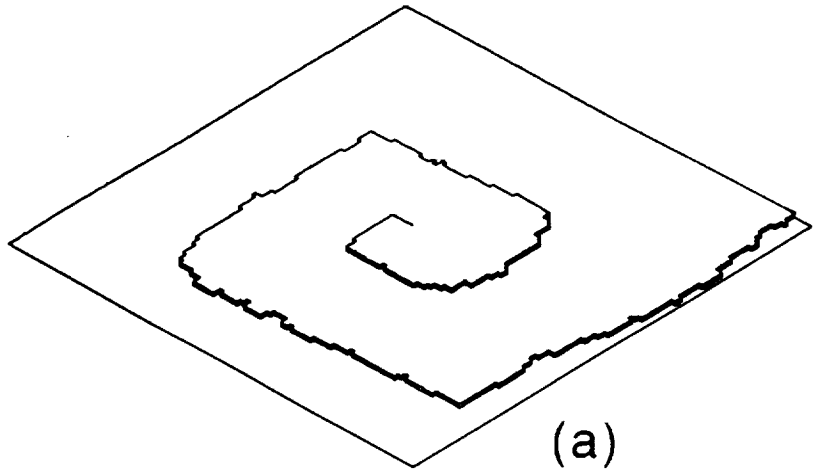

(a)

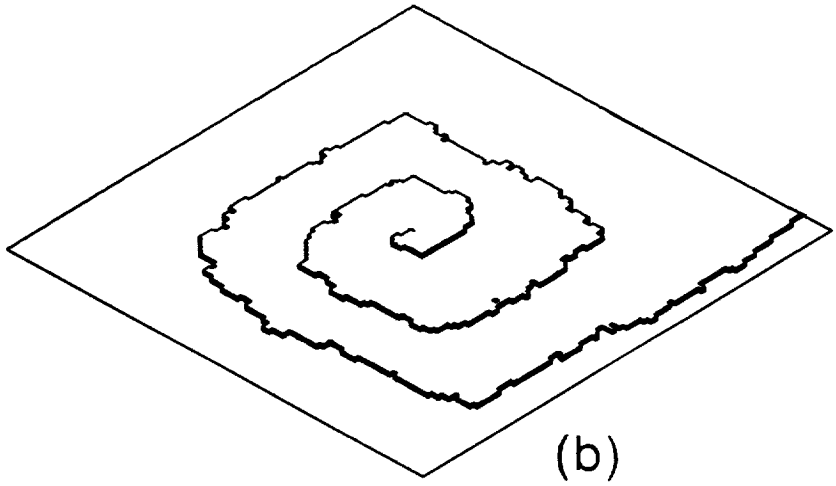

(b)

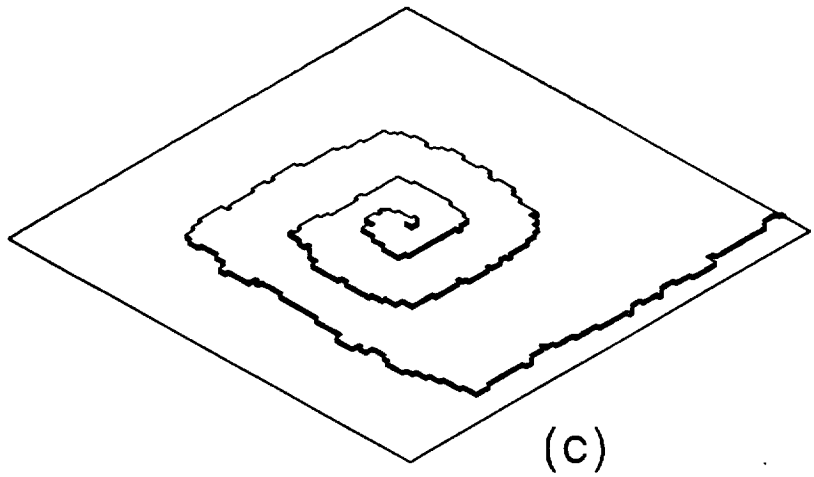

(c)

FIG.20

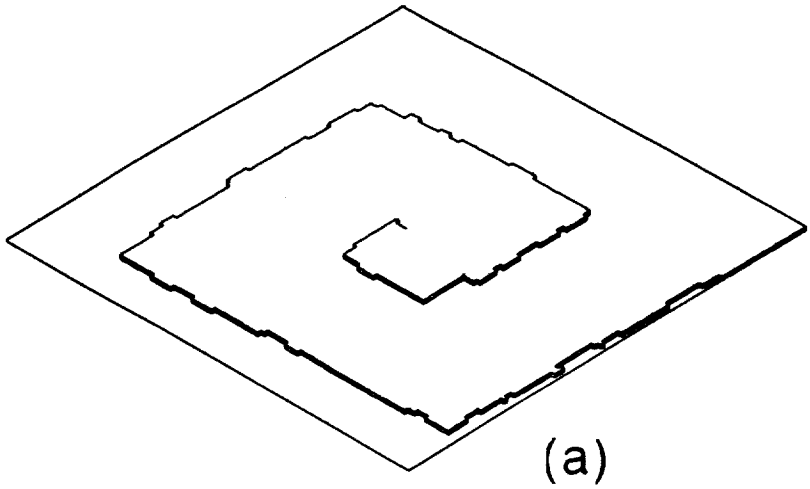

(a)

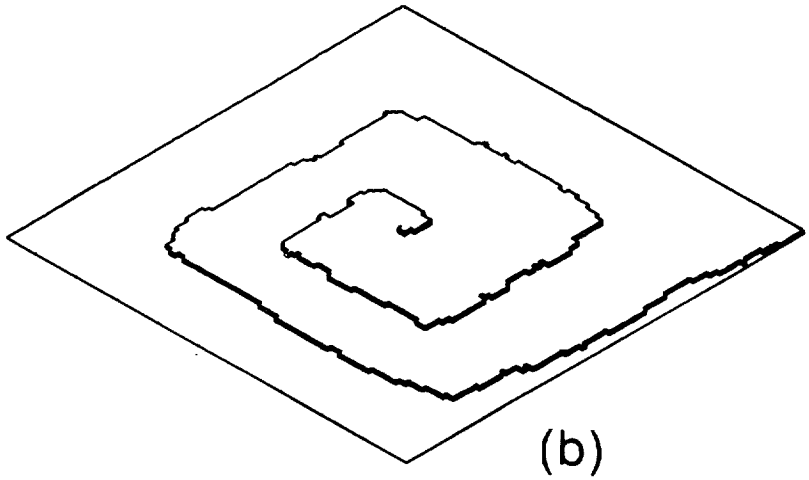

(b)

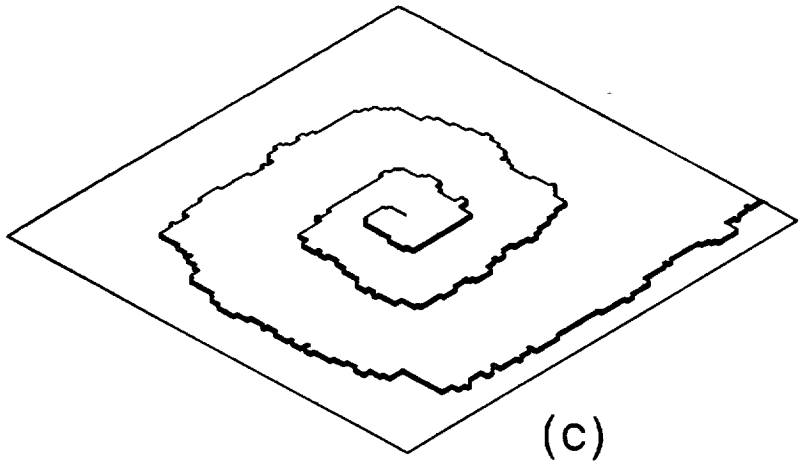

(c)

C-2

FIG.21

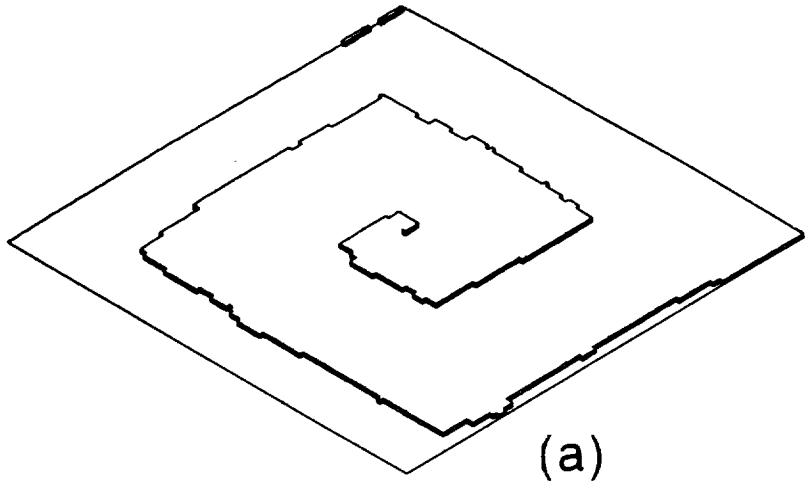

(a)

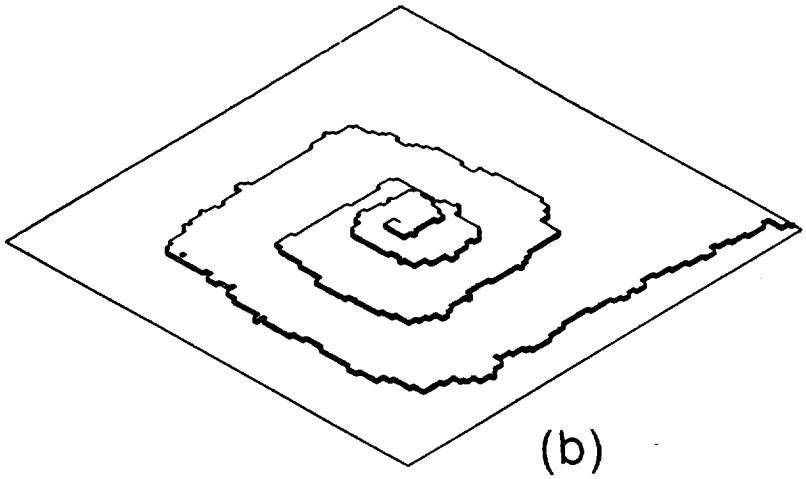

(b)

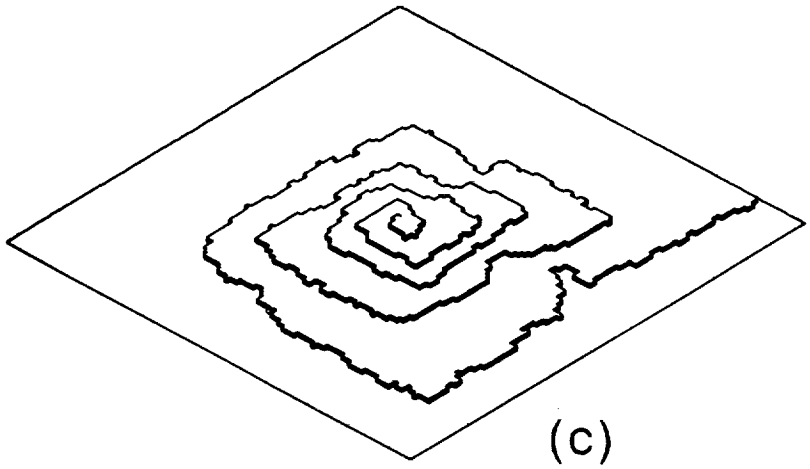

(c)

FIG.22

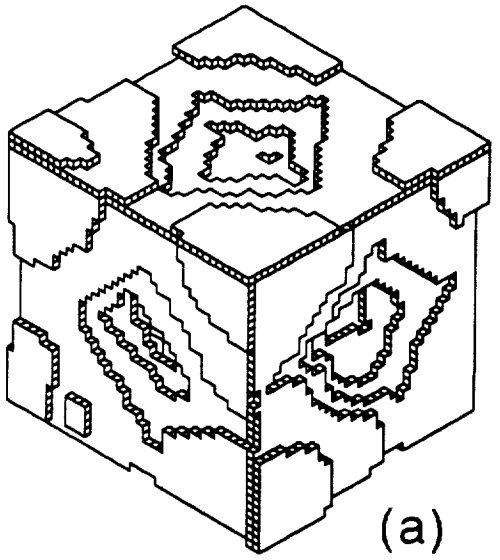

(a)

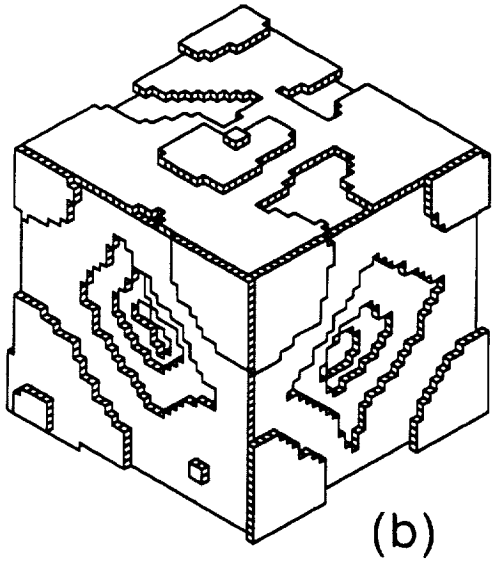

(b)

FIG.23

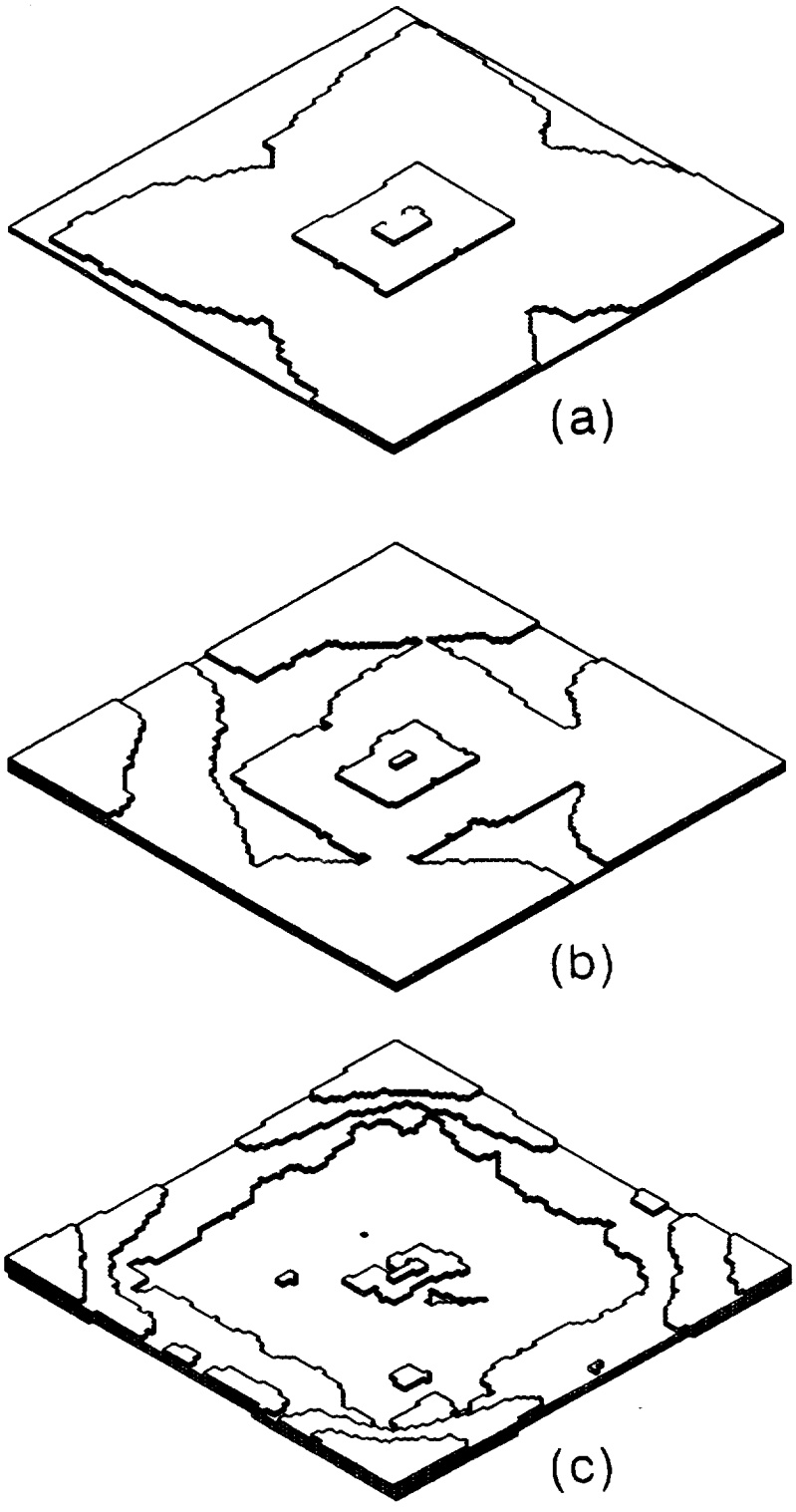

FIG.24

To be published in:
Lectures on Crystal Growth
Edited by H. Komatsu

MORPHOLOGICAL STABILITY OF INTERFACES WITH STRONG ANISOTROPY IN GROWTH KINETICS

Franz ROSENBERGER, Rong-Fu XIAO and
J. Iwan D. ALEXANDER

Center for Microgravity and Materials Research
University of Alabama in Huntsville
Huntsville, Alabama 35899, U. S. A

ABSTRACT

A Monte Carlo model is used to simulate the morphological evolution of crystals growing from an incongruent vapor phase. The model combines nutrient transport, based on a modified diffusion-limited aggregation process, with anisotropic surface kinetics and surface diffusion. Through a systematic variation of the simulation parameters (temperature, bond strength and supersaturation), the whole range of growth morphologies from fully facetted to side-branched dendritic growth is recovered.

The diffusion in the bulk nutrient and the anisotropy in the interface kinetics are seen to be morphologically destabilizing and stabilizing, respectively. It is found that for given bond strength and symmetry of the lattice, there is a critical size for stable, macroscopically facetted growth. This critical size scales linearly with the mean free path in the vapor. Since both thermal and kinetic roughening reduce the kinetic anisotropy, the critical size decreases as either temperature or supersaturation are increased. Surface diffusion is seen to stabilize facetted growth on the shorter scale of the mean surface diffusion length.

In simulations with a uniform drift superimposed on the random walk nutrient transport, crystal faces oriented towards the drift exhibit enhanced morphological stability in comparison to the purely diffusive situation. Rotational drifts with periodic reversal of direction are found to be morphologically stabilizing for all faces of the crystal.

INTRODUCTION

The characterization of the conditions under which a growing crystal is capable of preserving its shape, i.e. is morphologically stable, is both scientifically challenging and technologically important. Morphological stability is necessary for the growth of homogeneous single crystals that are needed for numerous device applications. The growth morphology and morphological stability of

a crystal, however, is an extremely complex problem, involving, in general, an interaction between nutrient transport and interface kinetics [1-3].

Two basic approaches to the morphological description of crystal growth have been adopted. The first is the macroscopic approach which involves the solution of a continuum transport equation coupled with moving boundary conditions [4]. The second is the simulation of microscopic processes by tracking the individual growth units [5].

The continuum approach has lead to significant insight into the morphological evolution of essentially isotropically responding, i. e. nonfacetted interfaces, such as prevail in many melt growth systems. The theory of morphological stability of non-facetted growth is well established. Stability conditions are known for a variety of simple geometries [4,6-9], including systems with weakly nonlinear [9-11] and highly nonlinear isotropic response [12-14]. In addition, the coupling between morphological and hydrodynamic instabilities has been examined [15-20]. Continuum models have also been developed for the morphological stability of nonfacetted interfaces with anisotropies in surface tension and growth kinetics [e.g. 21-24]. One of the most important results of these treatments is the insight that anisotropies can stabilize otherwise unstable closed growth forms up to a critical size. For facetted interfaces, that typically prevail in vapor and solution growth systems, and on which strongly anisotropic growth occurs via atomic layer spreading, the necessary conditions for morphological stability are only partly understood. Several workers have proposed an isotropic continuum formulation for morphological stability in vapor growth. These models are based on the assumption that stability is controlled either by the temperature gradient [25, 26] or by capillarity and the dependence of equilibrium concentration on curvature [27]. However, the morphologies of vapor-solid [28-32] and solution-solid interfaces [2, 33] are found to be more stable than predicted by isotropic models. This suggests that interface kinetics play a key role in morphological stability during facetted growth. It has been argued that polycrystalline vapor-solid interfaces should exhibit isotropic morphological stability [27]. In general, however, this argument is incorrect, for as long as the grain or facet size exceeds the adatom surface diffusion distance of, typically, 100 Å, anisotropic layer growth will prevail [3, 28]. The stabilizing effect of atomistic interfacial kinetics has been incorporated in several anisotropic morphological stability models [34-41]. Again, probably the most important result obtained from these models is the loss of stability beyond a critical crystal size [34, 41]. Such behavior has been observed in experiments [29-33]. Yet, a complete solution which includes coupling between nutrient transport, the moving boundary and anisotropic surface kinetics is still lacking.

An alternative to continuum descriptions of the growth process is the tracking of individual growth units using a Monte Carlo (MC) simulation method [5,42]. MC simulations have been used in a number of studies of the dependence of surface roughening and growth rate on supersaturation, and temperature [5,43,44]. These studies are primarily focused on microscopic interfacial kinetics, and occasionally include surface diffusion [45]. The influence of transport of growth units in the bulk nutrient to the interface has received less attention. In the event that interface kinetics govern the growth morphology, this simplification is not a severe limitation. However, in reality, nutrient bulk transport also appears to play a decisive role and often limits the stability of growing faces [29-33, 46].

The recently developed diffusion-limited aggregation (DLA) model of Witten and Sander [47] seems particularly appropriate to describe nutrient diffusion in crystal growth. The DLA model simulates the growth of an aggregate by considering the random walk of a succession of particles on

a discretized grid. The DLA model has been adopted by many workers to simulate various types of non-equilibrium pattern formation [48, 49]. Typical modifications include the introduction of "capillarity" [50, 51], anisotropic sticking probability [52, 53] and noise reduction [54-57]. Recently, we have modified the DLA model to include anisotropic interfacial attachment kinetics and surface diffusion to study the morphological evolution of crystals growing from a stagnant vapor or from a vapor with externally imposed uniform and rotational drift [58-61]. A variety of conditions, ranging from kinetics- to transport-controlled growth were examined, and successive transitions from compact to open dendritic morphologies were obtained. Diffusion in the nutrient, and increases in growth temperature and bulk supersaturation were found to be morphologically destabilizing; whereas surface diffusion and anisotropy in attachment kinetics act stabilizing. Specifically, we found that a given set of growth parameters defines a critical crystal size beyond which the crystal's faces cannot retain their macroscopic flatness, i. e. become morphologically unstable. Surface diffusion, on the other hand, continues to play a stabilizing role for micro-facets long after the loss of macroscopic stability. In the following section we will summarize our efforts and results. Most recently, Saito and Ueta have obtained similar growth shape evolutions from a Monte Carlo model with anisotropic attachment and evaporation kinetics features, using a DLA technique which launches many walkers at once [62].

MODEL

Crystal growth consists, in general, in the transport of growth units towards an interface, followed by a typically rather complex series of interfacial kinetics processes, before "final" incorporation into the lattice occurs [63]. The rates of the interface kinetics processes of individual growth units will be determined by the local configuration of the interface sites that the units happen to visit. Hence, at molecular length scales, the crystal symmetry will inevitably be reflected in the anisotropy of the attachment kinetics. This underlying symmetry will also be manifested at macroscopic length scales unless the atomic roughness of the interface is high enough to allow diffusion in the nutrient to control the evolution of the growing shape. Though a complete model of such complex scenarios is not practical at this point, we have formulated a Monte Carlo model which retains the essential physics of both nutrient transport and interface kinetics, including surface diffusion.

The gaseous nutrient is assumed to consist of highly dilute growth species A in an inert gas B that randomizes the motion of A. The random walk (diffusion) of A in the nutrient is restricted to a discrete lattice of spacing b, with equal jump length (representative of a mean free path) , a, in all directions, unless a drift is superimposed on the random walk. The grid spacing b represents a lattice unit of the crystalline nucleus, which is initially prescribed in the central region of the nutrient, and which grows through the addition of random walkers. While we may choose the jump length and grid spacing to be the same to minimize computation time, in a real vapor-crystal system a >>b.

To approximate the complex processes following the arrival of a growth unit (random walker) at the interface we made the following assumptions. The impingement rate can be obtained, based on ideal gas kinetics, from the chemical potential difference between supersaturated bulk vapor and average surface site, $\Delta\mu$, in the form [58, 61]

$$K^+ = K_{eq} \exp(\Delta\mu/kT) , \qquad (1)$$

where K_{eq} is the temperature dependent equilibrium value of K^+. Since the evaporation rate is sensitive to the local configuration of the site from which a unit is to be dislodged, we cast it, following Gilmer and Bennema [45], into the site-dependent form

$$K_i^- = \nu \exp(-E_i/kT) \ , \qquad (2)$$

where ν is a lattice vibration factor and E_i is the product of the pair interaction (bond) energy ϕ of a unit with a nearest neighbor and the number of occupied neighbor sites of site i, n_i.

The probability that a growth unit sticks onto a crystal surface is then $P_i = K^+/(K^+ + K_i^-)$. In order to relate K_{eq} and ν we assume local equilibrium and thus equate impingement and evaporation rates at equilibrium and obtain [58]

$$P_i = \frac{\gamma \beta^{(n_0 - n_i)}}{1 + \gamma \beta^{(n_0 - n_i)}} \ , \qquad (3)$$

where n_0, the number of nearest neighbors in a kink site, is 2 for a square lattice and 3 for a triangular lattice, and $\nu = \exp(\Delta\mu/kT)$ and $\beta = \exp(-\phi/kT)$.

If the growth unit does not stick onto the site i, it will jump to one of its unoccupied neighbor sites on the surface or in the nutrient. The jump probability from site i to a neighboring unoccupied site j is assumed to be [58, 61]

$$P_{i \to j} = \frac{\beta^{n_i - n_j}}{\sum_{j}^{c'} \beta^{n_i - n_j}} \ , \qquad (4)$$

where c' is the number of unoccupied nearest neighbor sites of site i. Clearly, a larger n_j results in a higher probability that a molecule will jump to site j on the interface.

The combination of equations 3 and 4 contains the essential physics of the surface kinetics for a crystal growing from a vapor. It should be realized that the crystal anisotropy has already been taken into account implicitly in equations 3 and 4, since both n_i and n_j are anisotropic factors.

The strength of surface diffusion (described by equation 4) is characterized by the diffusion time or diffusion length on the surface. An exact calculation of surface diffusion length is difficult. In our model we estimate the average surface diffusion length $\bar{\lambda}_s$ according to

$$\bar{\lambda}_s \sim \sqrt{\bar{n}_t}\, b \ , \qquad (5)$$

where $\bar{n}_t$ is the average (residence) "time" (actually the number of MC steps) for a random walker to diffuse on the interface.

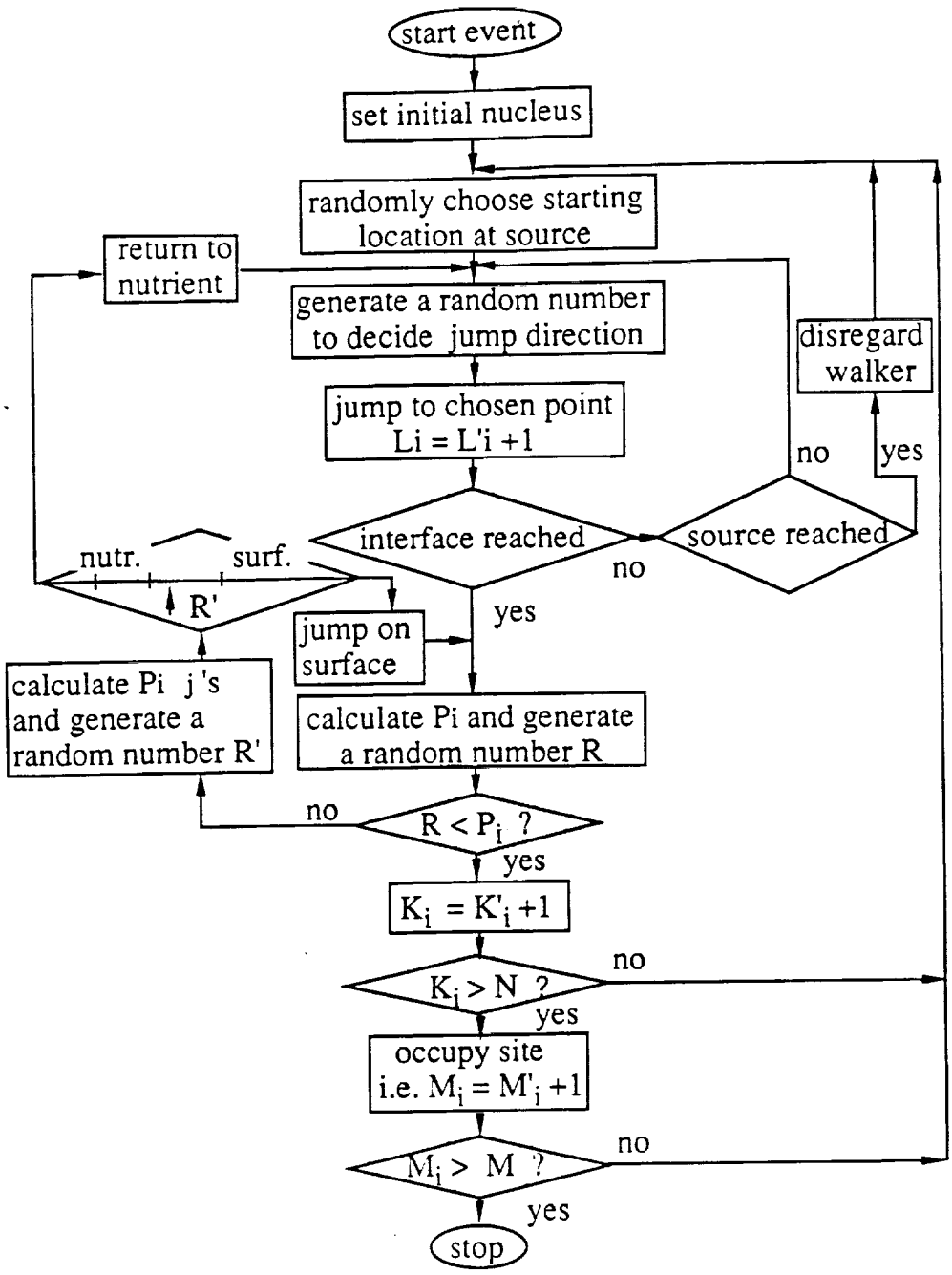

Figure 1. Flowchart of simulation steps.

SIMULATION PROCEDURE

A summary of the steps involved in the MC simulation is presented in the flowchart of figure 1. A growth unit is released from a circular source that surrounds the prescribed crystal nucleus. (The choice of source diameter is discussed in [58, 61]). The random walk is continued until the walker encounters the interface. The number of neighbors of the impingement site is then determined and the sticking probability P_i calculated according to equation 3. A random number R, $0 < R \leq 1$, is generated. If $R < P_i$, a registration to site i is made, and then that walker is retired. When an interfacial site has been registered N times it is considered to be occupied. A larger number of registrations N has the effect of reducing the noise inherent in a simulation of this kind [54-58]. If

$R \geq Pi$, the walker will leave site i without registration and jump to one of its unoccupied neighboring sites. The jump probability which determines the new location on the interface or in the nutrient is calculated according to equation 4 and compared to a random number R'. As the walker jumps to a new unoccupied site i', the above procedure is repeated. For typical values of the interaction parameters the probability that the particle returns to the nutrient is much less than that for continued residence on the surface. Successive walkers are released from the outer source and they proceed to undergo random motion until they either escape across the source boundary or make a registration at an interfacial site. The simulation is continued until the crystal reaches a specified size M. Note that, in contrast to real systems, once a site is considered occupied, its particle cannot leave the site, i.e. evaporation is only permitted in transit.

The simulation was implemented on a CRAY X-MP/24. Typical CPU times used for each simulation were between 2,000-7,000 sec. To show the sequence of growth patterns, we divided the total growth particles into consecutive groups and outlined the morphology resulting after completion of each group.

RESULTS AND DISCUSSION

Growth morphology and nutrient concentration distribution at mean free path of one lattice unit

First we present selected results obtained with a = b. In this case the simulation was terminated when the growth pattern had gained $3x10^3$ particles, which were consecutively divided into three groups of 1,000 each. Figure 2 shows the effect of growth temperature and/or bond strength on

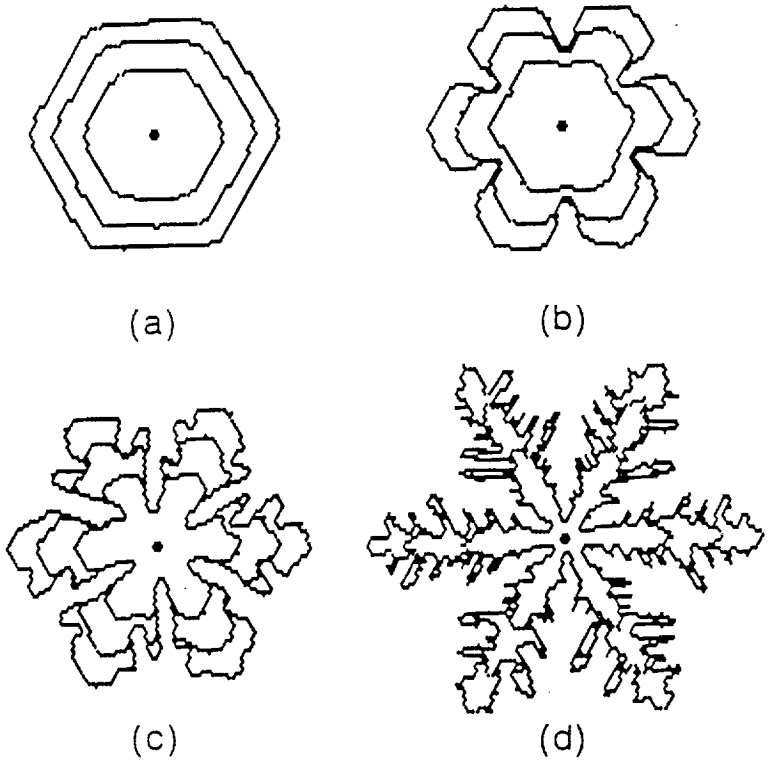

Figure 2. Effect of bond strength and temperature on growth patterns of a crystal (triangular lattice) at a fixed normalized supersaturation ($\Delta\mu/kT = 0.69$). (a) $\phi/kT = 3.91$; (b) $\phi/kT = 2.30$; (c) $\phi/kT = 0.69$; (d) $\phi/kT = 0.36$.

growth morphology at a fixed normalized supersaturation ($\Delta\mu/kT = 0.69$ or $\gamma = 2.0$). At low temperatures the growing "crystals" retain a compact, facetted form up to their terminal size (figure 2a) despite the appreciable supersaturation. With increasing temperature or decreasing ϕ/kT, the even smaller growth forms, i.e. after 1000-2000 growth units, show "microscopic" depressions (of a few lattice constants) in the center of the facets. Later growth under these or even lower ϕ/kT conditions, leads to the evolution of "macroscopic" depressions (figure 2b). On further increase of the temperature, this transition occurs at even smaller sizes and dendritic growth evolves (figure 2c) which subsequently exhibits extensive side-branching (figure 2d).

Figure 2 provides considerable insight into the morphologically stabilizing effect of anisotropic surface kinetics. One sees that the formation of depressions always sets in at facet (face) centers. This, as has been shown in detail in [60], is associated with a local decrease in both the nutrient concentration and its gradient. However, at the corners, which are more readily reached by building blocks, both the concentration and its gradient remain high. Furthermore, as can be seen from the sequence of contours of the lower temperature parts of figure 2, the formation of a microscopic depression is associated with the exposure of a higher step density in that region. Hence, both local sticking probability (equation 3) and jumping probability from neighboring sites (equation 4) increase. Consequently, not only is the leaner supply of growth units in the central region better utilized, but the surface diffusion flux is also increased. Both aid the crystal in retaining its (macroscopically) facetted morphology. This stabilizing effect reaches a limit as, with increasing depression, the growth step density becomes sufficient to accommodate the attachment of most growth units that arrive at the depleted face centers. Further increase in the crystal size is then accompanied by the loss of morphological stability.

This interplay between destabilizing bulk diffusion and stabilizing interface kinetics has been invoked before in Chernov's theory of growth-shape preservation for facetted crystals [34] and its adaption by Kuroda et al. [35].

The above simulation also shows, for the first time, the destabilizing effect of an increase in the growth temperature, that can be deduced from the transition from facetted to non-facetted shapes in figure 2. This transition is loosely speaking analogous to thermal roughening; for a detailed discussion see [64-66].

We have also investigated the effect of supersaturation on growth morphology [58], which enters in our model through the dependence of the sticking probability P_i (equation 3) on the impingement rate K^+ (equation 1). We found that an increase in supersaturation also decreases the critical crystal size beyond which the macroscopic face stability is lost. This is analogous to kinetic roughening observed in earlier MC modelling [67-69] and in experimental studies [69-73]. The dependence of the crystal morphology on normalized supersaturation and bond strength/temperature is tightly coupled. All our results for a triangular lattice are summarized in figure 3 [58]. Depending on the value of ϕ/kT and $\Delta\mu/kT$, the growing crystal can acquire one of the following morphologies: compact facetted (region I), compact branched (region II), and open branched and sidebranched (region III). In general, the supersaturation above which the compact facetted form is no longer stable decreases with decreasing bond strength or increasing temperature.

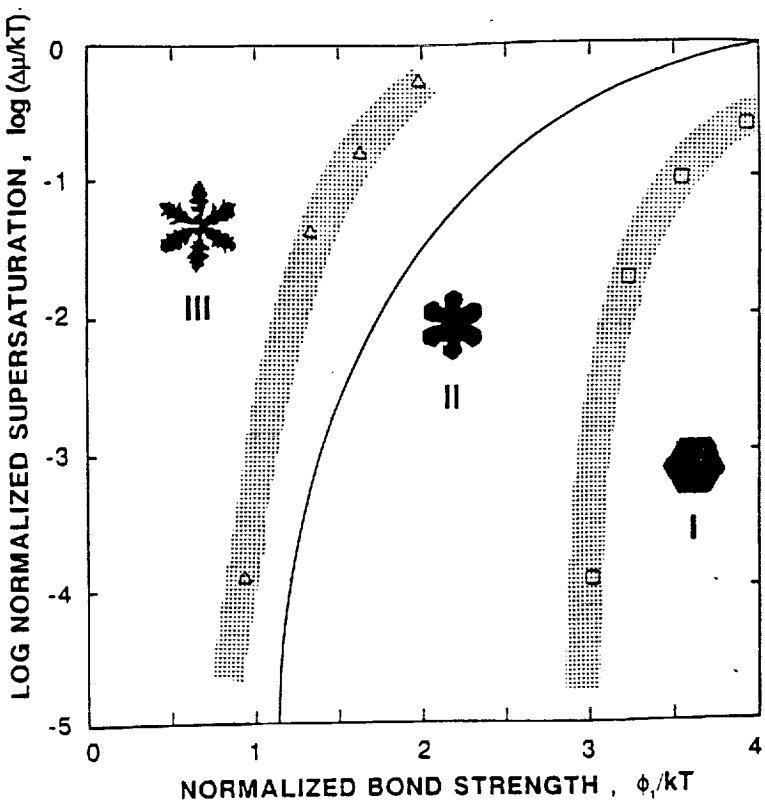

Figure 3. Crystal-growth morphology as a collective effect of supersaturation and bond strength (or temperature) for triangular lattice at mean free path of one lattice unit. In region I crystals acquire compact-facetted forms; in region II compact branched with six-fold symmetry; in region III dendritic with multiple sidebranches. Symbols: Monte Carlo results judged as "boundary cases". Solid line: Temkin's boundary between facetted and nonfacetted growth for a simple cubic lattice [74]. For further details see [58].

Changes in growth morphology with increase in mean free path

In this section we increase the mean free path and present growth patterns arising on a square lattice after addition of four groups of 2,500 particles each. Figure 4 shows the effect on morphology of bond strength or temperature at a constant normalized supersaturation, and a mean free path of a = 10b. As compared to results obtained on a square lattice for a=b [60] the critical size of a facet has increased about tenfold. The stabilizing effect of an increase in the mean free path is further illustrated in figure 5, which is for the same fixed values of growth temperature and supersaturation as figure 4d. One sees that the growth morphology becomes increasingly compact and facetted as a is increased in steps from 5 to 100b. Such morphological changes have been observed experimentally [29-33]: growing facetted crystals became centrally depressed as the mean free path was decreased by increasing the partial pressure of the inert gas. We have found that the critical crystal size scales linearly with the mean free path in the parameter range considered [60]. Extrapolation of the critical size to more realistic conditions [60] gave reasonable agreement with critical sizes found experimentally [31].

Critical inspection of figures 4 and 5 shows that even under conditions in which macroscopic facet stability is lost, the contours possess microscopic facets, i.e. flat regions of a much shorter length scale which, as shown in [60, 61], corresponds to the average surface diffusion length.

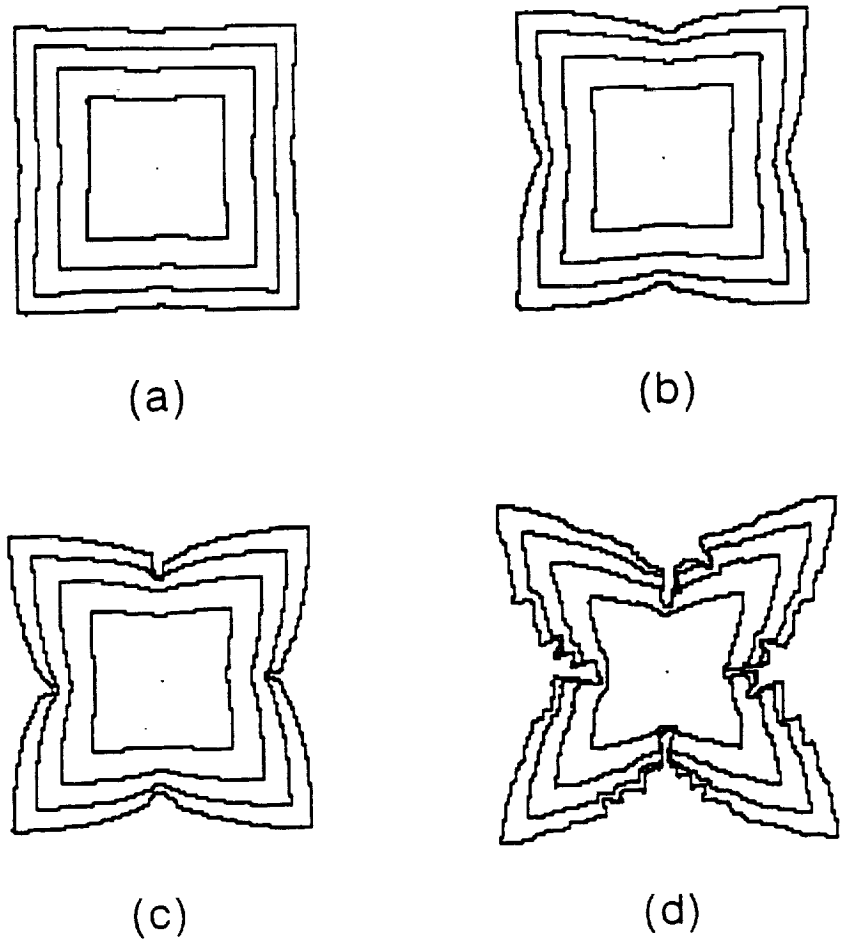

Figure 4. Effect of bond strength and temperature on growth patterns at a large mean free path (a = 10 lattice units) at a fixed supersaturation ($\Delta\mu/kT = 0.69$). (a) $\phi/kT = 4.60$; (b) $\phi/kT = 3.91$; (c) $\phi/kT = 2.30$; (d) $\phi/kT = 0.69$. Contours corresponds to addition of 2,500 particles each.

Changes in crystal morphology in the presence of a drift

With an externally imposed drift, the individual jumps of a random walker will be biased, see [59, 60]. Figure 6 shows the effect of a uniform drift (i.e. with an additional unidirectional displacement of d = 2b at each random jump) on growth morphology for the same conditions as figure 4. One sees that the drift causes asymmetric growth. Sites facing the drift acquire building blocks more readily than those on the lee side. Although the drift affects all cases, the response of the growth morphology increases with decreasing bond strength or increasing temperature (figure 6a-d). In addition to modifying the growth rate, the drift is also seen to stabilize the front face in comparison to the corresponding "no-drift cases of figure 4.

In addition to unidirectional drifts, we have also investigated the consequences of rotational drifts [60]. In particular, rotational drifts with periodic reversal of direction were found to stabilize facetted morphologies. This is in agreement with observed growth morphologies of crystals subject to frequent rotation reversals [60].

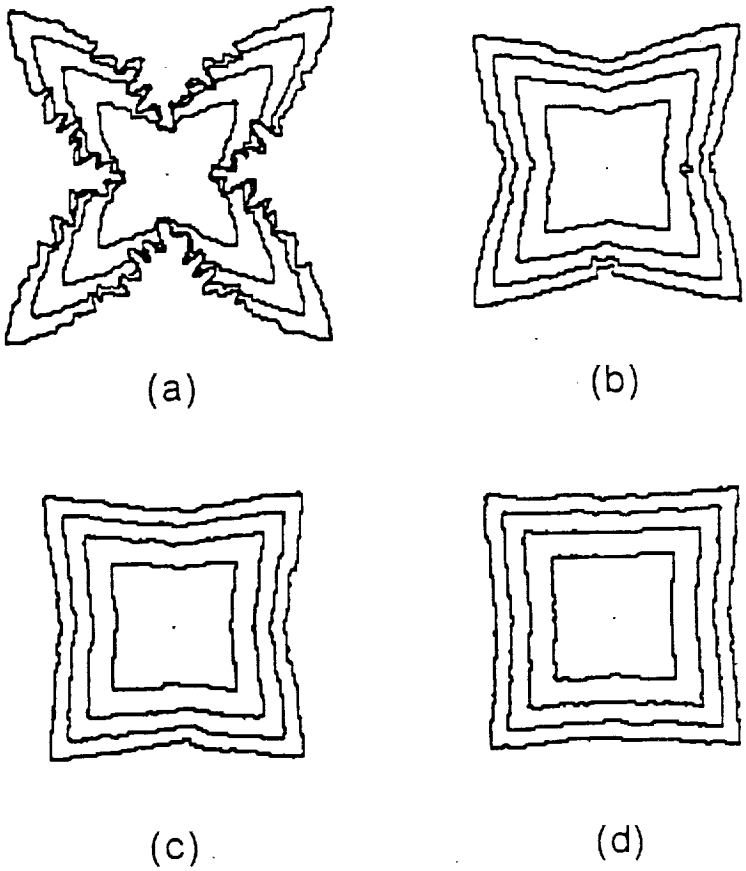

Figure 5. Effect of mean free path on growth patterns at $\Delta\mu/kT = 0.69$ and $\phi/kT = 0.69$. (a) a = 5b; (b) a = 25b; (c) a = 50b; (d) a= 100b. Contours correspond to addition of 2,500 particles each.

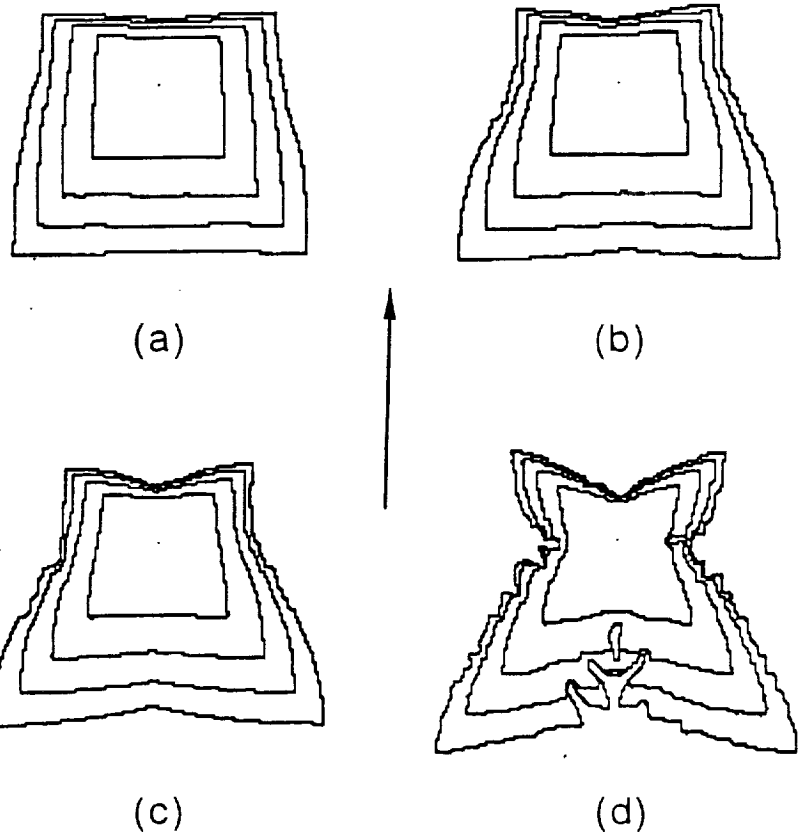

Figure 6. Effect of drift with d = 2b on growth morphology. Growth conditions otherwise the same as in figure 4, i.e., $\Delta\mu/kT = 0.69$. (a) $\phi/kT = 4.60$; (b) $\phi/kT = 3.91$; (c) $\phi/kT = 2.30$; (d) $\phi/kT = 0.69$. The arrow indicates the direction of the drift.

ACKNOWLEDGEMENTS

The authors are grateful for the support provided by the Microgravity Science and Applications Division of the National Aeronautics and Space Administration under Grant NAG1-972. This research as also been supported by the State of Alabama through the Center for Microgravity and Materials Research at the University of Alabama in Huntsville, and the Alabama Supercomputer Network.

REFERENCES

[1] Parker, R. L.: Solid State Physics, Vol. 25, Eds. Ehrenreich, H.,Seitz, F. and Turnbull, D. (Academic Press, New York, 1970) 151, and references therein

[2] Chernov, A. A.: Modern Crystallography III: Crystal Growth, *Springer Series in Solid State Sciences*, Vol. 36, Eds. Cardona, M., Fulde, P. and Queisser, P. (Springer, Berlin, 1984), and references therein

[3] Rosenberger, F., in: Interfacial Aspects of Phase Transformations, Ed. Mutaftschiev, B. (Reidel, Dordrecht, 1982) 315, and references therein

[4] Langer, J. S.: Rev. Mod. Phys , 1980, 52, 1

[5] Müller-Krumbhaar, H., in: Monte Carlo Methods in Statistical Physics, Ed. Binder, K. (Springer-Verlag, Berlin, 1984) 295, and references therein

[6] Mullins, W. W. and Sekerka, R. F.: J. Appl. Phys., 1964, 35, 444

[7] Sekerka, R. F., in: Encyclopedia of Materials Science and Engineering, Ed. Cahn, R. W. (Pergamon, New York, 1986) 3486

[8] Delves, R. T.: Crystal Growth, Ed. Pamplin, B. R. (Pergamon, Oxford, 1975) 40

[9] Wollkind, B. R., in: Preparation and Properties of Solid State Materials, Ed. Wilcox, W. R. (Dekker, New York, 1979) 4, 111

[10] Alexander, J. I. D., Wollkind J. D. and Sekerka, R. F.: J. Crystal Growth, 1986, 79 , 849

[11] Caroli, B. and Roulet, B.: J. Physique, 1982, 43, 1767

[12] Ungar L. H. and Brown, R. A.: Phys. Rev., 1984, B30, 3993

[13] Ungar, L. H., Bennett M. J. and Brown, R. A.: Phys. Rev., 1985, B31, 5923

[14] Ramprasad, N., Bennett, M. J. and Brown, R. A.: Phys. Rev., 1988, B38 , 583

[15] Coriell, S. R., Cordes, M. R., Boettinger, W. J. and Sekerka, R. F.: J. Crystal Growth, 1980, 49, 13

[16] Coriell, S. R. and Sekerka, R. F.: PhysicoChem. Hydrodyn, 1982, 2, 281

[17] Hurle, D. T. J., Jakeman, E. and Wheeler, A. A.:, J. Crystal Growth, 1982, 58,163

[18] Coriell, S. R., McFadden, G. B., Boisvert, R. F. and Sekerka, R. F.: J. Crystal Growth, 1984, 69, 15

[19] McFadden, G. B., Coriell, S. R. and Alexander, J. I. D., Comm. Pure and Appl. Math., 1988, 41, 683

[20] Brattkus K. and Davis, S. H.: J. Crystal Growth, 1988, 87, 385

[21] Cahn, J. W., in: Crystal Growth, Ed. Peiser, H. S. (Pergamon, Oxford, 1967) 681

[22] Young, G. W., Davis, S. H. and Brattkus, K.: J. Crystal Growth, 1987, 83, 560

[23] Yokoyama, E. and Kuroda, T., in: Dynamics of Ordering Processes in Condensed Matter, Eds. Komura, S. and Furukawa, H. (Plenum 1988) 95

[24] Brush, L. N. and Sekerka, R. F.: J. Crystal Growth, 1989, 96, 419, and references therein

[25] Reed, T. B., LaFleur, W. J. and Strauss, A. J.: J. Crystal Growth, 1968, 3/4, 115

[26] Reed, T. B. and LaFleur, W. J.: Appl. Phys. Lett., 1964, 5, 191

[27] Van den Brekel, C. H. J. and Jansen, A. K.: J. Crystal Growth, 1978, 43, 364 and 371

[28] Rosenberger, F., Delong, M. C., Greenwell, D. W., Olson, J. M. and Westphal, J. M.: J. Crystal Growth, 1975, 29, 49
[29] Nenow, D. and Stoyanova, V.: J. Crystal Growth, 1977, 41, 73
[30] Nenow, D., Stoyanova, V. and Genadiev, N.: J. Crystal Growth, 1984, 66, 489, and references therein
[31] Nanev, C. and Iwanov D.: J. Crystal Growth, 1968, 3/4, 530
[32] Nanev, C. and Iwanov, D.: Crystal Res. & Technol., 1982, 17, 575, and references therein
[33] Staynova, M. and Nanev, C.: Cryst. Res. Technol., 1988, 23, 1061
[34] Chernov, A. A.: J. Crystal Growth, 1974, 24/25, 11
[35] Kuroda, T., Irisawa, T. and Ookawa, A.: J. Crystal Growth, 1977, 42, 41.
[36] Kumar C. and Estrin, J.: J. Crystal Growth, 1981, 51, 323
[37] Narayanan, H. G., Youngquist, R. and Estrin, J.: J. Colloid Interface Sci., 1982, 85, 319
[38] Ovrutskii, A. M. and Chuprina, L. M.: Sov. Phys. Crystal., 1977, 22, 393
[39] Ovrutskii, A. M.: Sov. Phys. Crystal., 1978, 23, 522
[40] Ovrutskii, A. M.: Sov. Phys. Crystal., 1979, 24, 327
[41] Chernov, A. A. and Nishinaga, T., in: Morphology of Crystals, Ed. Sunagawa, I., (Terra, Tokyo, 1987) 207
[42] Heermann, D. W.: Computer Simulation Methods in Theoretical Physics, (Springer, Berlin, 1986), and references therein
[43] Chernov, A. A. and Lewis, J.: J. Phys. Chem. Solids, 1967, 28, 2185
[44] Abraham, F. F.: Adv. Phys., 1986, 35, 1, and references therein
[45] Gilmer, G. H. and Bennema, P.: J. Appl. Phys., 1972, 43, 1347
[46] Glicksman, M. E., Singh, N. B. and Chopra, M., in: Materials Processing in the Reduced Gravity Environment of Space, Ed. Rindone, G. E. (Elsevier, Amsterdam, 1982) 461
[47] Witten, T. A. and Sander, L. M.: Phys. Rev., 1983, B27, 5686
[48] On Growth and Form, Eds. Stanley, H. E. and Ostrowsky, N. (Nijhoff, Dordrecht, 1986)
[49] Random Fluctuations and Pattern Growth: Experiments and Models, Eds. Stanley, H. E. and Ostrowsky, N. (Kluwer, Dordrecht 1988)
[50] Vicsek, T.: Phys. Rev., 1985, A32, 3084
[51] Tao, R., Novotny, M. A. and Kaski, K.: Phys. Rev., 1988, A38, 1019
[52] Ball, R. C., Brady, R. M., Rossi, G. and Thompson, B. R.: Phys. Rev. Lett., 1985, 55, 1406.
[53] Meakin, P., Chen, Z. Y. and Evesque, P.: J. Chem. Phys., 1987, 87, 630.
[54] Tang, C.: Phys. Rev., 1985, A31, 1977
[55] Nittmann, J. and Stanley, H. E.: Nature, 1986, 321, 663
[56] Ball, R. C.: Physica, 1986, A140, 62
[57] Kertesz, J.: Phil. Mag., 1987, B 56, 729
[58] Xiao, R.-F., Alexander, J. I. D. and Rosenberger, F.: Phys. Rev., 1988, A38, 2447
[59] Xiao, R.-F., Alexander, J. I. D. and Rosenberger, F.: Phys. Rev., 1989, A39, 6397
[60] Xiao, R.-F., Alexander, J. I. D. and Rosenberger, F.: J. Crystal Growth (in press)
[61] Xiao, R.-F.: Ph. D. Thesis, University of Utah, Salt Lake City, Utah, 1988
[62] Saito, Y. and Ueta, T.: Phys. Rev., 1989, A40, 3408
[63] Interfacial Aspects of Phase Transformations, Ed. Mutaftschiev, B., (Reidel, Dordrecht, 1982)
[64] Burton, W. K., Cabrera, N. and Frank, F. C.: Phil. Trans. Roy. Soc., 1951, A243, 299
[65] Weeks, J. D., in: Ordering in Strongly Fluctuating Condensed Matter, Ed. Riste, T. (Plenum, New York, 1980) 293, and references therein

[66] Van Beijeren, H. and Nolden, I., in: Structure and Dynamics of Interfaces, II, Eds. Schommers, W. and Van Blanckenhagen, P. (Springer, Berlin 1987)
[67] Gilmer, G. H. and Jackson, K. A., in: Current Topics in Materials Science, Ed. E. Kaldis (North-Holland, Amsterdam, 1977), 2, 79
[68] Esin, V. O. and Tarabaev, L. P.: Phys. Stat. Sol. (a), 1985, 90, 425
[69] Elwenspoek, M. and van der Eerden, J. P.: J. Phys. A: Math. Gen., 1987, 20, 669
[70] Miller, C. E.: J. Crystal Growth, 1977, 42, 357
[71] Peteves, S. D. and Abbaschian, G. J.: J. Crystal Growth, 1986, 79, 775
[72] Dougherty, A. and Gollub, J. P.: Phys. Rev., 1988, A38, 3043
[73] Gallet, F., Balibar, S. and Rolley, E., J. Physique, 1987, 48, 369
[74] Temkin, D. E., in: Crystallization Processes, Eds. Sirota, N. N., Gorskii, F. K. and Varikash, V. M. (Consultants Bureau, New York, 1969) 15